Semi-Annual Progress Report No. 8

to the

NATIONAL SCIENCE AND SPACE ADMINISTRATION

in connection with

NASA Grant NGR 47-004-006

[redacted]

Final Report

V.P.I. Project 313099

A METHOD FOR CALCULATING LAMINAR AND TURBULENT CONVECTIVE HEAT TRANSFER OVER BODIES AT AN ANGLE OF ATTACK

by

Fred R. DeJarnette
Tsze C. Tai

Virginia Polytechnic Institute
Blacksburg, Virginia

March, 1969

I. SUMMARY

The axisymmetric analogue (small cross flow approximation) is employed to develop methods for calculating laminar and turbulent heat-transfer over bodies of revolution at angles of attack. These methods are restricted to hypersonic flows over bodies with highly cooled walls.

A method is presented for determining the surface inviscid streamline geometry and coordinate scale factors, which are required in the axisymmetric analogue. This method requires the surface pressure distribution to be known, whether theoretical or experimental. A theoretical pressure distribution is developed using combinations of Modified Newtonian pressures, Prandtl-Meyer relations, and the second-order shock expansion method.

Results are presented for spheres, paraboloids, and spherically blunted cones at angles of attack. Surface pressures and streamline geometries were found to compare favorably with experimental data and the three-dimensional method of characteristics. Laminar heat-transfer results were also found to compare favorably with experimental data. The turbulent heating rates yielded results close to those of Vaglio-Laurin's method.

It was found that the surface pressure distribution affected laminar heating rates more than the inviscid streamline geometry. The choice of reference conditions and the exponent in the viscosity-temperature relationship highly affected the turbulent heating rates.

II. TABLE OF CONTENTS

III. LIST OF FIGURES AND TABLES

FIGURE PAGE

IV. LIST OF SYMBOLS

A	function of x^*, used in Eq. (56)
A_∞	a constant in Eq. (B-3b)
a_o	function determined by Eq. (B-1)
B	function of x^*, used in Eq. (56)
B_∞	an arbitrary constant in Eq. (B-3d)
b	function determined by Eq. (B-4)
C	$= 1 - P_\infty/P_o$
C_f	local skin friction coefficient
$C_f{}^*$	local incompressible skin friction coefficient
C_k	$= P_\infty/P_o$
C_ℓ	$= 1 - 2/(\gamma_\infty-1)M_\infty^2$
C_p	pressure coefficient
C_q	function determined by Eq. (C-3b)
C_{qr}	function determined by Eq. (C-16a)
C_{qt}	function determined by Eq. (C-12a)
E	function of x^*, used in Eq. (56)
F	$F \equiv \sqrt{1 + f'^2}$
f, f', f''	local body radius, and its first and second derivatives with respect to x^*
G	function determined by Eq. (11)
g	$= (\bar{\gamma}-1)/\bar{\gamma}$
H	stagnation enthalpy
H_f	form factor, $H_f = \Delta^*/\Theta$

h	static enthalpy
h_1, h_2	scale factors for curvilinear coordinates ξ and β, respectively
$\overline{h}_2$	$\overline{h}_2 = h_2/R_o$
I	integral defined by Eq. (A-5)
K	a constant used in Eq. (28)
ℓ	distance along the surface of a flat plate
M	Mach number
n	function determined by Eq. (54b)
Nu	Nusselt number, $Nu = q_w R_o Pr/\mu_o (H_e - h_w)$
Nu_ℓ	Nusselt number, $Nu_x = q_w \ell Pr/\mu_e (H_e - h_w)$
Pr	Prandtl number
P_r	static pressure as a function of local body radius at $\alpha = o$, used in Eq. (52)
P	static pressure
Q	function determined by Eq. (54d)
q	heat transfer rate
Re	Reynolds number, $Re = \rho_o H_e^{1/2} R_o/\mu_o$
Re_ℓ	Reynolds number, $Re_\ell = \rho_e u_e \ell/\mu_e$
Re_Θ	Reynolds number based on momentum thickness, $Re_\Theta = \rho_e u_e \Theta/\mu_e$
R	universal gas constant
R_o	nose radius
r	body radius measured from axis of symmetry
S	distance along a streamline measured from the stagnation point

$\bar{S}$	$= S/R_o$
St	Stanton number
T	temperature, °R
u,w	inviscid velocity components in (x,ϕ) coordinates
u_e	velocity at the edge of boundary layer
V_∞	freestream velocity
V_1, V_2, V_3	velocity components in curvilinear coordinates ξ, β, z
W	function determined by Eq. (C-3b)
x	coordinate measured along body meridian line
$\bar{x}$	$= x/R_o$
x*	coordinate measured along body axis of symmetry
$\bar{x}^*$	$= x^*/R_o$
Z	function defined by Eq. (16)
α	angle of attack
γ_∞	ratio of specific heats for freestream condition
$\bar{\gamma}$	effective ratio of specific heats after shock
Δ	boundary layer thickness
δ	angle between the body tangent and axis of symmetry
Δ^*	boundary layer displacement thickness
ε	$= x_i^* - x_o^*$
ζ	$= x^* - x_j^*$
Θ	boundary layer momentum thickness
θ	angle between the tangent to a local streamline and the meridian line
μ	coefficient of viscosity

ν	Prandtl-Meyer angle
ν_r	kinematic viscosity coefficient at reference condition
ξ, β, z	streamline-oriented, orthogonal, curvilinear coordinates
ρ	density
τ	shear stress
ϕ	azimuthal angle
ψ	angle between the body tangent and freestream velocity
Ω	function determined by Eq. (54e)
ω	exponent in viscosity-temperature relation

Subscripts

c	cone
comp	compressible
e	at the edge of boundary layer
i	initial conditions
incomp	incompressible
j	at juncture
o	stagnation conditions at the edge of boundary layer
q	matching point
r	reference conditions
∞	undisturbed, free stream condition

V. INTRODUCTION

Theoretical methods for predicting aerodynamic heat transfer to axisymmetric bodies at an angle of attack and asymmetric lifting bodies are currently required for the proper design of high velocity heat protection systems. A review of the literature (see, for instance, refs. 1 through 5) reveals that previous analyses were generally restricted to limited conditions such as axisymmetric bodies at small or zero angle of attack, or yawed cones and infinite cylinders. A simple method for computing laminar heating rates over bodies at moderate angles of attack has recently been developed by DeJarnette (ref. 6). In this method the direction of a surface inviscid streamline is assumed to be the direction of the free-stream velocity minus its normal component at every point on the body. However, ref. 6 uses the modified Newtonian pressure distribution which is not highly accurate for positions away from the stagnation region.

In order to determine convective heating rates over asymmetric bodies and axisymmetric bodies at an angle of attack, one must solve both the inviscid and the viscous flow fields. The complexity of the partial differential equations governing these three dimensional flow-fields makes the use of simplifying approximations desirable so that tractable solutions may be obtained. A substantial simplification to the viscous flow-field equations may be achieved through the "axisymmetric analogue", or small cross flow assumption, as used in refs. 6, 7 and 8. The cross flow is the component of boundary layer flow normal to the direction of the inviscid streamline and along the body surface.

The axisymmetric analogue permits the heat transfer to be calculated over bodies at an angle of attack by any method applicable to a body of revolution at zero angle of attack provided the inviscid solution (pressure distribution and geometry of the surface inviscid streamlines) is known on the surface. The surface inviscid streamlines may be obtained from a known pressure distribution, whether theoretical or experimental, as will be demonstrated later.

In hypersonic flows, bodies are generally blunted to some extent and the wall temperature is small compared with the temperature at the edge of the boundary layer. If the total enthalpy at the edge of boundary layer is much higher than that at the wall, it is termed a highly cooled wall. The flow is also characterized by relatively low local Mach numbers at the edge of boundary layer and by a density at the wall much greater than that at the edge of boundary layer. As a consequence, the small cross flow assumption is valid for laminar as well as turbulent boundary layers (refs. 9 and 10). Most recently, the cross flow momentum equation was solved by Bradley (ref. 5) for a compressible turbulent boundary layer over a yawed, infinite cylinder. Based on a method by Sasman and Cresci (ref. 4), Bradley's cross flow solutions provide an indication of the applicability of the small cross flow postulate.

The compressible laminar boundary layer for two-dimensional and axisymmetric bodies at zero angle of attack has been investigated extensively in the past. Theoretical methods for predicting the heat transfer and boundary layer characteristics are well developed. In general, solutions are obtained by similar solutions with the aid of

Levy-Lees type transformation and by the integral form of the momentum and energy equations along with Reynolds' analogy. Results may also be achieved from the numerical schemes such as the one developed by Davis and Flugge-Lotz (ref. 11). For flows in the hypersonic range with a highly cooled surface, the theory of Lees (ref. 1) has proved successful and most convenient for estimating the laminar heat transfer over an axisymmetric body at zero angle of attack. The heating rates predicted by this method for thermodynamic equilibrium agree well with experimental data (refs. 6, 12 and 13). An even simpler method for estimating the heating rates may be obtained by extending classical incompressible methods to the compressible case by introducing reference fluid properties (refs. 3 and 14). Although this simple theory is remote from more rigorous considerations, it yields good agreement with experimental data.

The laminar boundary-layer may change to the turbulent one in the downstream region of some flow fields. The point at which this change takes place is called the transition point. It is mainly determined by the experimental observations; therefore, no attempt is made here to treat this difficult problem theoretically.

The existence of apparent turbulent shear and heat flux, and the effects of Mach number and wall temperature make the compressible turbulent boundary layer difficult for analytical treatment. Even semi-empirical theories suffer from incompleteness due to the contradiction of experimental results from one case to another (ref. 15). In general, theoretical approaches frequently used for turbulent boundry layers involve one or more of the following: (a) introducing a reference condition for fluid properties (refs. 16 and 17), (b) use of Prandtl's mixing length theory or von Karman's similarity hypothesis (ref. 18), and (c) using transformation of coordinates (ref. 15). The idea of using reference quantities was first introduced by von Karman (ref. 16) with the assumption that the skin friction laws of incompressible flow remain valid in the case of compressible flow if the fluid properties are evaluated at some reference condition. von Karman used the wall temperature as reference temperature for an adiabatic wall. For bodies with heat transfer, one has to take account of large and small values of temperature in evaluating the reference condition, as suggested by Eckert (ref. 17). Therefore, turbulent heating rates may be estimated by using an incompressible skin friction law along with Reynolds' analogy.

Prandtl's mixing length theory was used by van Driest (ref. 18) for the compressible turbulent boundary layer over a flat plate with and without heat transfer. The approach of transforming the compressible turbulent boundary layer equations into the incompressible form was first performed by Mager (ref. 15). This transformation is essentially the same as the laminar one, given by Stewartson, except the stream function is modified and the apparent turbulent shear is postulated to remain invariant.

In the case of axisymmetric flow, the integral form of the momentum and energy equations has been used by Reshotko and Tucker (ref. 19) and Cohen (ref. 20) along with the Illingworth-Stewartson transformation. The use of the momentum integral and moment of momentum integral equations with a Mager type transformation was developed by Sasman and Cresci (ref. 4).

For hypersonic flows with a highly cooled wall, the effect of Mach number at the edge of boundary layer is small (ref. 2). This provides a partial reasoning for one to correlate the incompressible result with the compressible case. In ref. 2 Rose, Probstein, and Adams showed that the hypersonic turbulent heating rates could be reasonably predicted by the incompressible skin friction coefficient and Reynolds' analogy modified for the Prandtl number dependence (with the Lewis number equal to unity).

Vaglio-Laurin (ref. 9) derived a more sophisticated method for estimating turbulent heat transfer by the extension of Mager's transformation to the hypersonic case (in the presence of pressure gradient and heat transfer at the wall). The boundary layer equations were written in an orthogonal curvilinear coordinate system with the streamlines of the inviscid flow as one family of coordinate lines, and the cross flow and Reynolds stresses were neglected. Satisfactory agreement with experimental data at zero angle of attack was obtained.

The most obvious difficulty in applying the axisymmetric analogue is the determination of the inviscid solution on the body surface. In the literature, few analyses have been developed to determine the inviscid streamline geometry from experimental or theoretical pressure distributions (refs. 10, 21 and 22). However, a valid and applicable three-dimensional inviscid solution is still in demand. The need of such a method is evidenced by the recent works of Bradley (ref. 5) and Fannelop (ref. 23). A very simple method for determining the inviscid surface streamline geometry, independent of pressure distribution, was developed in ref. 6 as mentioned previously.

In the present report, the axisymmetric analogue is applied to both laminar and turbulent boundary layers for bodies at an angle of attack and with highly cooled walls. The methods of Lees (ref. 1) and Vaglio-Laurin (ref. 9) are utilized for the laminar and turbulent heating rates, respectively, at zero angle of attack. In addition, a relatively simple expression for estimating the turbulent heating rates is derived for comparison. Radiative heat transfer and surface ablation are not considered. A general method for determining the inviscid streamline geometry and coordinate scale factor from known surface pressure distributions, whether theoretical or experimental, is developed.

The surface pressure distribution may be calculated approximately by the modified Newtonian theory near the stagnation region and then by the Prandtl-Meyer relation from the "matching point" to the shoulder of the body. For the region beyond the shoulder where the inclination of body surface is constant, the second order shock expansion method is employed. Since the Prandtl-Meyer relation and second order shock expansion method are applicable only along the streamlines in the plane of symmetry, the peripheral pressure distributions are obtained through interpolation formulas given by refs. 13 and 24. However, experimental pressures can be used when available.

The present method is applied to a sphere, spherically blunted cones, and a paraboloid in hypersonic flows at angles of attack. However, the basic method is applicable to any three dimensional or axisymmetric body at an angle of attack. The procedure for the numerical computation of heating rates on spherically blunted cones is illustrated and the associated computer program is attached. The calculated surface inviscid streamline patterns are compared with those obtained from the method of characteristics (ref. 25), the simplified method of refs. 6 and 26, and the geometric solution. Heating rates are compared with theoretically predicted results using the simplified method (ref. 26) and measured data of Zakkay (ref. 13) and Cleary (ref. 27).

VI. ANALYSIS

6.1 Axisymmetric Analogue

In order to investigate the heating rates over a general three dimensional body or a body of revolution at an angle of attack, it is convenient to write the boundary layer equations in a streamline-oriented, orthogonal, curvilinear, coordinate system. As shown in Fig. 1, the coordinate direction ξ coincides with the local external inviscid streamline projected in the plane tangent to the surface; β is also in the tangent plane and normal to ξ; and z is measured from the surface along a straight line normal to the tangent plane. The metric is

$$dL^2 = (h_1 d\xi)^2 + (h_2 d\beta)^2 + dz^2$$

where $h_1 d\xi = dS$ and dS is the length element along a streamline in the boundary layer; $h_1(\xi,\beta)$ and $h_2(\xi,\beta)$ are the scale factors for the ξ and β directions, respectively.

In this coordinate system, the equations governing the steady laminar boundary layer flow of a homogeneous gas, in the absence of body forces and heat sources, may be written as (Ref. 28)

Continuity:

$$\frac{\partial}{\partial \xi}(h_2 \rho V_1) + \frac{\partial}{\partial \beta}(h_1 \rho V_2) + \frac{\partial}{\partial z}(h_1 h_2 \rho V_3) = 0 \qquad (1)$$

ξ-momentum:

$$\frac{V_1}{h_1}\frac{\partial V_1}{\partial \xi} + \frac{V_2}{h_2}\frac{\partial V_1}{\partial \beta} + V_3\frac{\partial V_1}{\partial z} + \frac{V_1 V_2}{h_1 h_2}\frac{\partial h_1}{\partial \beta} - \frac{V_2^{\,2}}{h_1 h_2}\frac{\partial h_2}{\partial \xi}$$

$$= -\frac{1}{\rho h_1}\frac{\partial P}{\partial \xi} + \frac{1}{\rho}\frac{\partial}{\partial z}\left(\mu \frac{\partial V_1}{\partial z}\right) \qquad (2a)$$

β-momentum:

$$\frac{V_1}{h_1}\frac{\partial V_2}{\partial \xi} + \frac{V_2}{h_2}\frac{\partial V_2}{\partial \beta} + V_3\frac{\partial V_2}{\partial z} + \frac{V_1 V_2}{h_1 h_2}\frac{\partial h_2}{\partial \xi} - \frac{V_1^2}{h_1 h_2}\frac{\partial h_1}{\partial \beta}$$

$$= -\frac{1}{\rho h_2}\frac{\partial P}{\partial \beta} + \frac{1}{\rho}\frac{\partial}{\partial z}\left(\mu\frac{\partial V_2}{\partial z}\right) \quad (2b)$$

z-momentum:

$$\frac{\partial P}{\partial z} = 0 \quad (2c)$$

Energy:

$$\frac{V_1}{h_1}\frac{\partial H}{\partial \xi} + \frac{V_2}{h_2}\frac{\partial H}{\partial \beta} + V_3\frac{\partial H}{\partial z} = \frac{1}{\rho}\frac{\partial}{\partial z}\left[\mu\left(\frac{\partial H}{\partial z} + \frac{1-Pr}{Pr}\frac{\partial h}{\partial z}\right)\right] \quad (3)$$

The boundary conditions are

$$\begin{array}{lll} z = 0, & V_1 = V_2 = V_3 = 0, & H = H_w = h_w \\ z \to \Delta & V_1 \to u_e,\ V_2 \to 0 & H \to H_e \end{array} \quad (4)$$

where Δ is the boundary layer thickness.

It is shown in Refs. 5, 9, and 10 that the small crossflow approximation is valid for an arbitrary streamline when the quantity $[(V_1/u_e)^2 - \rho_e/\rho]$ is small. This quantity is small for highly cooled walls, which generally exists for hypersonic conditions. Setting $(V_1/u_e)^2 - \rho_e/\rho = 0$, the β-direction momentum equation is homogeneous in V_2 and has homogeneous boundary conditions; thus, the small crossflow assumption reduces this equation to simply

$$V_2 = 0 \text{ (inside the boundary layer)} \quad (5)$$

Then Eqs. (1) to (3) can be written as

Continuity:

$$\frac{1}{h_1}\frac{\partial}{\partial \xi}(h_2 \rho V_1) + \frac{\partial}{\partial z}(h_2 \rho V_3) = 0 \tag{6}$$

ξ-momentum:

$$\frac{V_1}{h_1}\frac{\partial V_1}{\partial \xi} + V_3 \frac{\partial V_1}{\partial z} = -\frac{1}{\rho h_1}\frac{\partial P}{\partial \xi} + \frac{1}{\rho}\frac{\partial}{\partial z}\left(\mu \frac{\partial V_1}{\partial z}\right) \tag{7a}$$

β-momentum:

$$V_2 = 0 \tag{7b}$$

z-momentum:

$$\frac{\partial P}{\partial z} = 0 \tag{7c}$$

Energy:

$$\frac{V_1}{h_1}\frac{\partial H}{\partial \xi} + V_3 \frac{\partial H}{\partial z} = \frac{1}{\rho}\frac{\partial}{\partial z}\left[\mu \left(\frac{\partial H}{\partial z} + \frac{1-Pr}{Pr}\frac{\partial h}{\partial z}\right)\right] \tag{8}$$

The boundary conditions are as follows:

$$\left.\begin{array}{lll} z = 0, & V_1 = V_3 = 0, & H = H_w = h_w \\ z \to \Delta, & V_1 \to u_e, & H \to H_e \end{array}\right\} \tag{9}$$

Equations (6) to (9) are identical to those governing the laminar boundary layer over an axisymmetric body at zero angle of attack if one replaces h_2 with the radial coordinate r and S is distance along a streamline, where again $dS = h_1 \, d\xi$.

The analogue in the governing equations permits the heating rates to be calculated by any method applicable to a body of revolution at zero angle of attack provided the streamline geometry and the scale factor, h_2, are known from the inviscid solution on the surface of the body in question.

For the turbulent boundary layer at hypersonic speeds, the equations governing the mean motion of turbulent flow in three dimensions are also analogous to those for axisymmetric flows, as indicated by Vaglio-Laurin (Ref. 9). Thus, the axisymmetric analogue holds for the turbulent as well as the laminar boundary layer for hypersonic flows over bodies with a cool wall.

6.2 Calculation of Laminar and Turbulent Heating Rates

6.2.1 Laminar Heating Rate Expression

For the calculation of laminar heating rates, the method of Lees (Ref. 1), developed for the flow over blunted bodies of revolution at zero angle of attack and at hypersonic speeds, may be used in the axisymmetric analogue. Lees gives

$$\frac{\dot{q}_w}{\dot{q}_{w_o}} = \frac{\frac{p}{p_o}\,\frac{u_e}{V_\infty}\, r R_o^{\,1/2}}{\left[\int_o^S \frac{p}{p_o}\,\frac{u_e}{V_\infty}\, r^2 dS\right]^{1/2} 2G} \tag{10}$$

Lees also shows that the modified Newtonian pressure distribution combined with the assumption of isentropic flow along the body surface yields

$$G = \left[\frac{1}{V_\infty}\left(\frac{du_e}{d\delta}\right)_o\right]^{1/2} = \left[\frac{\bar{\gamma}-1}{\bar{\gamma}}\left(1 + \frac{2}{(\gamma_\infty-1)M_\infty^2}\right)\left(1 - \frac{1}{\gamma_\infty M_\infty^2}\right)\right]^{1/4} \tag{11}$$

Note that "G" is used only in the expression for the heating rate at the stagnation point where the modified Newtonian pressure distribution is valid.

According to the axisymmetric analogue, Eqs. (10) and (11) are also applicable to any inviscid surface streamline on a three-dimensional body at an angle of attack if S is the distance measured along the streamline and r is replaced by the scale factor, h_2, corresponding to the coordinate β measured along the body surface and perpendicular to the streamline. (β is constant along a given streamline.)

6.2.2 Turbulent Heating Rate Expressions

For turbulent heating rates, two expressions are used along with the axisymmetric analogue. After investigating several methods for computing the turbulent heating rates on axisymmetric bodies at zero angle of attack, it was found that the method of Vaglio-Laurin (Ref. 9) gives more accurate results than the others. As mentioned previously, it was developed for hypersonic flows with highly cooled walls and pressure gradients. However, a new and relatively simple expression is derived here for comparison purposes. From now on, the former is designated as Expression I, and the latter as Expression II.

(a) Expression I

Vaglio-Laurin (Ref. 9) gives

$$\dot{q}_w = 0.5\ Pr^{-2/3}\ (H_e - H_w)\ \left(\frac{\mu_e}{\mu_r}\right)\ \rho_e u_e C_f^* \tag{12}$$

where C_f^* is determined by

$$\ln C_f^* + \ln\left[2.62\ \frac{H_e^{1/2}}{\nu_r}\ \frac{1}{h_2} \int_o^S \frac{u_e}{H_e^{1/2}}\ \frac{\rho_e \mu_e}{\rho_r \mu_r}\ h_2 dS\right] = 0.4\ \sqrt{2}\ C_f^{*\,-1/2} \tag{13}$$

Equations (12) and (13) are already written in the streamline coordinate system. The quantities with subscript "r" refer to a reference condition which may be evaluated at the stagnation state of the external flow or by the expression

$$\frac{T_r}{T_o} = 0.5\,\frac{T_e}{T_o} + 0.5\,\frac{T_w}{T_o} + 0.22\,\sqrt[3]{Pr}\,\frac{\bar{\gamma}-1}{2}\,M_e^{\,2}\,\frac{T_e}{T_o} \tag{14a}$$

or its equivalent

$$\frac{h_r}{H_e} = 0.5\,\frac{h_e}{H_e} + 0.5\,\frac{h_w}{H_e} + 0.22\,\sqrt[3]{Pr}\,\frac{\bar{\gamma}-1}{2}\,M_e^{\,2}\,\frac{h_e}{H_e} \tag{14b}$$

as suggested by Eckert (ref. 17). However, according to ref. 9, a choice of the reference conditions based on Eq.(14)leads to heating rates higher than the measured values.

In practical applications it is convenient to calculate the ratio of the local heating rate to the heating rate at the stagnation point. Using the result of Lees (ref. 1) for the stagnation point heating rate (laminar) and the condition of a highly cooled wall, ($H_e >> H_w$) Eq. (12) is recast as

$$\frac{\dot{q}_w}{\dot{q}_{w_o}} = \frac{R_o^{\,1/2}\rho_e\mu_e u_e C_f{}^*}{\sqrt{2}\;\mu_r\sqrt{\rho_o\mu_o V_\infty}\,G} \tag{15}$$

The implicit expression for $C_f{}^*$ in Eq. (13) requires an iteration process, and this process generally converges very slowly. Therefore, a simpler means for evaluating $C_f{}^*$ becomes desirable. Let

$$Z = \ell n\left[\frac{2.62H_e^{\,1/2}}{\nu_r h_2}\int_o^S \frac{\rho_e}{\rho_r}\,\frac{u_e}{H_e^{\,1/2}}\,\frac{\mu_e}{\mu_r}\,h_2 dS\right] \tag{16}$$

then Eq. (13) becomes

$$\ell n C_f{}^* + Z = 0.4\sqrt{2}\, C_f{}^{*-1/2} \tag{17}$$

and $C_f{}^*$ is calculated by iteration from Eq. (17) for a given Z. The range of variation of Z is $2 \leq Z \leq 14$ for a possible turbulent flow; and it is found that the following fifth order polynomial in inverse powers of Z yields $C_f{}^*$ approximately,

$$C_f{}^* = a_o + \frac{a_1}{Z} + \frac{a_2}{Z^2} + \frac{a_3}{Z^3} + \frac{a_4}{Z^4} + \frac{a_5}{Z^5} \tag{18}$$

where $a_o \ldots a_5$ are determined from iterated results of Eq. (17). Their values are given in Eq.(C-14) of Appendix C for $2 \leq Z \leq 14$, and the graph of Eq. (18) is shown in Fig. 33.

(b) Expression II

This method is new and basically similar to that of Rose, Probstein, and Adams (Ref. 2) except a different transformation is used and the pressure gradient effect is considered. For incompressible flow over a flat plate one may use the 1/7 power law velocity distribution to obtain the modified Blasius formula for the local skin friction coefficient of a turbulent boundary layer. This expression is given by Schlichting (Eq. 21.12 of Ref. 29) as

$$(\tfrac{1}{2}C_f)_{incomp} = 0.0296(Re_\ell)^{-0.2} \tag{19}$$

where $Re_\ell = \rho_e u_e \ell/\mu_e$ and ℓ is the distance along a flat plate.

To apply the above formula to compressible turbulent boundary layers, Mager (Ref. 15) found the transformation between skin friction coefficients and Reynolds numbers as

$$(C_f)_{comp} = (\frac{\mu_e}{\mu_o})\ (C_f)_{incomp} \qquad (20)$$

$$(Re_\ell)_{comp} = (\frac{\mu_o}{\mu_e})^2\ (Re_\ell)_{incomp} \qquad (21)$$

With these relations, Eq. (19) may be written as

$$\frac{1}{2}C_f = 0.0296(Re_\ell)^{-0.2}\ (\frac{\mu_e}{\mu_o})^{0.6} \qquad (22)$$

for a flat plate. Equation (22) is valid up to $Re_\ell = 10^7$ as indicated in ref. 15. Substituting this result into the modified Reynolds' analogy for turbulent flow

$$St = \frac{C_f}{2}\ Pr^{-2/3} \qquad (23a)$$

or

$$Nu_\ell = \frac{1}{2}C_f\ \sqrt[3]{Pr}\ Re_\ell \qquad (23b)$$

(as given in ref. 29), one obtains

$$Nu_\ell = 0.0296\ \sqrt[3]{Pr}\ Re_\ell^{0.8}(\frac{\mu_e}{\mu_o})^{0.6} \qquad (24)$$

where Nu_ℓ is the local Nusselt number, defined by

$$Nu_\ell = \frac{\dot{q}_w \ell Pr}{\mu_e(H_e - h_w)}$$

In turn, Eq. (24) can be written as

$$\dot{q}_w = 0.0296\ Pr^{-2/3}\ (H_e - h_w)\ \frac{\mu_e^{0.2}(\rho_e u_e)^{0.8}}{\ell^{0.2}}\ (\frac{\mu_e}{\mu_o})^{0.6} \qquad (25)$$

for a flat plate.

In order to take account of the pressure gradient and the variation of fluid properties at the edge of boundary layer (in axisymmetric flow), the characteristic length ℓ in Eq. (25) should be stretched by a further transformation (ref. 9). Following the well known and verified approximation that the same flow mechanism holds locally on axisymmetric bodies as on two-dimensional bodies (see, for example, refs. 2 and 9), the expression for ℓ is obtained by transforming the solution of the integral momentum equation for a flat plate to that for axisymmetric flow. The general integral momentum equation is (ref. 30)

$$\frac{\tau_w}{\rho_e u_e^2} = \frac{C_f}{2} = \frac{d\Theta}{dx} + \Theta\left(\frac{2+H_f}{u_e}\frac{du_e}{dx} + \frac{1}{\rho_e}\frac{d\rho_e}{dx} + \frac{1}{r}\frac{dr}{dx}\right) \tag{26}$$

where H_f is the form factor,

$$H_f = \frac{\Delta^*}{\Theta}$$

and Δ^* and Θ are the boundary-layer displacement thickness and momentum thickness, respectively.

In the case of a flat plate, Eq. (26) reduces to the form,

$$\frac{\tau_w}{\rho_e u_e^2} = \frac{d\Theta}{d\ell} \tag{27}$$

The solution to Eq. (27) is obtained by using the semi-empirical relation given by Schlichting (ref. 29)

$$\frac{\tau_w}{\rho_e u_e^2} = \frac{K}{\left(\frac{u_e\Theta}{\nu_r}\right)^{1/4}} \tag{28}$$

where K is a constant. Substitution of Eq. (28) into Eq. (27) and integration yield

$$\Theta = [\frac{5}{4}K\ (\frac{\nu_r}{u_e})^{1/4}\ell]^{4/5} \tag{29}$$

By the foregoing approximation that the same flow mechanism holds locally on axisymmetric bodies as on two-dimensional bodies, expression (28) is also valid for the left hand side of Eq. (26); and according to Lees (Ref. 1) and Vaglio-Laurin (Ref. 9), $H_f = -1$ for hypersonic flows with highly cooled walls. Hence, Eq. (26) becomes

$$\frac{K}{(\frac{u_e\Theta}{\nu_r})^{1/4}} = \frac{d\Theta}{dx} + \Theta(\frac{1}{u_e}\frac{du_e}{dx} + \frac{1}{\rho_e}\frac{d\rho_e}{dx} + \frac{1}{r}\frac{dr}{dx})$$

or

$$(\Theta\rho_e u_e r)^{1/4} d(\Theta\rho_e u_e r) = K\rho_e{}^{5/4}u_e\nu_r{}^{1/4}r^{5/4}dx$$

which integrates to

$$\Theta = \frac{1}{\rho_e u_e r}[\frac{5}{4}K\int_o^x \rho_e{}^{5/4}u_e\nu_r{}^{1/4}r^{5/4}dx]^{4/5} \tag{30}$$

Equating Eqs. (29) and (30) one obtains

$$\ell = \frac{1}{\rho_e{}^{5/4}u_e\nu_r{}^{1/4}r^{5/4}}\int_o^x \rho_e{}^{5/4}u_e\nu_r{}^{1/4}r^{5/4}dx \tag{31}$$

Using this result in Eq. (25) and replacing r by h_2 and x by S, the local turbulent heating rate at the wall on a body at an angle of attack becomes

$$\dot{q}_w = \frac{0.0296Pr^{-2/3}(H_e-h_w)\rho_e{}^{1.05}\mu_e{}^{0.8}u_e\nu_r{}^{0.05}h_2{}^{1/4}}{\mu_o{}^{0.6}[\int_o^S\rho_e{}^{5/4}u_e\nu_r{}^{1/4}h_2{}^{5/4}dS]^{1/5}} \tag{32}$$

As done for Expression I, Eq. (32) is recast into the form of the ratio of the local heating rate to the heating rate at the stagnation point,

$$\frac{\dot{q}_w}{\dot{q}_{w_o}} = \frac{0.0417\rho_e^{1.05}\mu_e^{0.8}u_e\nu_r^{0.05}h_2^{1/4}R_o^{1/2}}{G(\rho_o V_\infty)^{0.5}\mu_o^{1.1}[\int_o^S \rho_e^{5/4}u_e\nu_r^{1/4}h_2^{5/4}dS]^{1/5}} \tag{33}$$

Again, the reference quantities can be evaluated with the aid of Eq. (14).

In applying the axisymmetric analogue, the difficulty lies in the determination of the surface inviscid streamline geometry, scale factor (h_2), and the surface pressure distribution; also, for the turbulent boundary layer, the transition point is not known.

6.2.3 The Transition Point

The difficulty of determining the transition point (transition from laminar to turbulent boundary layer) is well known. Analyses concerning the criteria of the transition point are mainly based on experimental observations (refs. 12, 14, 31, and 32). For a body at an angle of attack, the transition criteria for axisymmetric flow should be equally applicable to the same body at an angle of attack, if the meridian line in the former is replaced by the streamline in the latter. Using shock tube observations, Stetson (ref. 31) showed that transition first occurred in the sonic region and that the transition Reynolds number (based on local fluid properties at the edge of boundary layer and the momentum thickness) varied from roughly 200 to 600, depending on the freestream conditions and the body shape history. This result was verified by Cresci, Mackenzie and Libby (ref. 12) qualitatively and was also accepted by Zakkay and Callahan (ref. 14) and Bloxsom (ref. 32). In connection with the calculation of momentum thickness Reynolds number, Ref. 12 gives, (according to the theory of Lees),

$$Re_\Theta = \frac{0.66[\int_o^S \rho_e \mu_e u_e r^2 dS]^{1/2}}{\mu_e r} \quad (34)$$

The above equation has been recast and written in the present notation, where

$$Re_\Theta = \frac{\rho_e u_e \Theta}{\mu_e}$$

To evaluate the transition behavior of the boundary layer over bodies at an angle of attack, the integration of Eq. (34) should be carried out along a streamline with r replaced by the scale factor, h_2, based on the previous arguments. However, the transition Reynolds number given by Eq. (34) yields only a possible range in which the transition might occur. The true transition point (within the range Re_Θ from 200 to 600, roughly) depends on the freestream conditions, body shape, wall to stagnation enthalpy ratio and surface roughness. Apart from making rough assumptions, no definite criteria can be made in this regard. Therefore, both laminar and turbulent heating rates are calculated simultaneously; and to indicate the region of possible transition points, Eq. (34) is used along with the criteria observed in Refs. 12 and 31, i.e., Re_Θ varies from 200 to 350 for a blunt cap, 200 to 500 for a conical afterbody, and 200 to 600 for a cylinder.

6.3 Calculation of Streamlines and Scale Factors

Previous analyses on the calculation of surface streamline geometry and scale factor require cumbersome computations (Refs. 10 and 22).

Thus, a simpler, but rigorous, method becomes desirable.

For the flow over a body of revolution at an angle of attack, the inviscid momentum equations along the surface (from ref. 28) are:

x^*-momentum:

$$\frac{u}{\sqrt{1+f'^2}}\frac{\partial u}{\partial x^*} + \frac{w}{f}\frac{\partial u}{\partial \phi} - \frac{w^2 f'}{f\sqrt{1+f'^2}} + \frac{1}{\rho\sqrt{1+f'^2}}\frac{\partial p}{\partial x^*} = 0 \qquad (35a)$$

ϕ-momentum:

$$\frac{u}{\sqrt{1+f'^2}}\frac{\partial w}{\partial x^*} + \frac{w}{f}\frac{\partial w}{\partial \phi} + \frac{wuf'}{f\sqrt{1+f'^2}} + \frac{1}{\rho f}\frac{\partial p}{\partial \phi} = 0 \qquad (35b)$$

where x^* is the distance along the body axis of symmetry ($dx^* = (1+f'^2)^{-1/2}dx$) and ϕ is the azimuthal angle measured from the windward line (see Fig. 1). The velocity components u and w are measured along the surface in the x and ϕ directions, respectively, as shown in Fig. 1. The body radius is $f = f(x^*)$, measured from the axis of symmetry.

The geometry of any streamline emanating from the stagnation point may be expressed as $\phi = \phi(x^*, \beta)$, where again β is constant along a given streamline. The coordinates are related to the velocity components through the relation

$$f\left(\frac{\partial \phi}{\partial x}\right)_\beta = \frac{w}{u}$$

or

$$\frac{f}{\sqrt{1+f'^2}}\left(\frac{\partial \phi}{\partial x^*}\right)_\beta = \frac{w}{u}$$

Define $\frac{D}{Dx^*}$ as the substantial derivative, or derivative (with respect to x^*) along a streamline. Thus,

$$\left(\frac{\partial}{\partial x^*}\right)_\beta \equiv \frac{D}{Dx^*}$$

and the streamline equation becomes

$$\frac{D\phi}{Dx^*} = \frac{\sqrt{1+f'^2}}{f}\frac{w}{u} \tag{36}$$

Differentiate Eq. (36) with respect to x* to get

$$\frac{D^2\phi}{Dx^{*2}} = \frac{\sqrt{1+f'^2}}{f}\left[\frac{u\frac{Dw}{Dx^*} - w\frac{Du}{Dx^*}}{u^2}\right] + \frac{w}{u}\frac{D}{Dx^*}\left(\frac{\sqrt{1+f'^2}}{f}\right) \tag{37}$$

Since $u = u(x^*, \phi)$, then

$$Du = \frac{\partial u}{\partial x^*} Dx^* + \frac{\partial u}{\partial \phi} D\phi$$

and using Eq. (36), the above can be written as

$$\frac{Du}{Dx^*} = \frac{\partial u}{\partial x^*} + \frac{w}{u}\;\frac{1+f'^2}{f}\;\frac{\partial u}{\partial \phi}$$

Use this result in Eq. (35a) to get

$$\frac{Du}{Dx^*} = \frac{1}{u}\left[\frac{w^2 f'}{f} - \frac{1}{\rho}\left(\frac{\partial P}{\partial \phi}\right)_{x^*}\right] \tag{38a}$$

In a similar manner, Eq. (35b) becomes

$$\frac{Dw}{Dx^*} = -\frac{wf'}{f} - \frac{1+f'^2}{uf\rho}\left(\frac{\partial P}{\partial \phi}\right)_{x^*} \tag{38b}$$

Since

$$u^2 + w^2 = \frac{\bar{\gamma}M^2 P}{\rho} \tag{38c}$$

then

$$u^2 = \frac{\bar{\gamma}M^2 P}{\rho(1+w^2/u^2)} \tag{38d}$$

Substituting Eqs. (36) and (38) into Eq. (37) and simplifying, there results

$$\frac{D^2\phi}{Dx^{*2}} = \frac{F}{f}\left[1 + \frac{f^2}{1+f'^2}\left(\frac{D\phi}{Dx^*}\right)^2\right]\left[-\frac{f'}{F}\frac{D\phi}{Dx^*} - \frac{F}{f}\frac{1}{\bar{\gamma M}^2 P}\left(\frac{\partial P}{\partial\phi}\right)_{x^*}\right.$$

$$\left.+\frac{f}{F}\frac{D\phi}{Dx^*}\frac{1}{\bar{\gamma M}^2 P}\left(\frac{\partial P}{\partial x^*}\right)_{\phi}\right] + \frac{D\phi}{Dx^*}\frac{f}{F}\frac{D}{Dx^*}\left(\frac{F}{f}\right) \qquad (39)$$

where $F \equiv \sqrt{1+f'^2}$.

Now, introduce a new variable θ, the angle between the tangent of local streamline and body meridian line, i.e.,

$$\tan\theta = \frac{w}{u} = \frac{f}{F}\frac{D\phi}{Dx^*}$$

or

$$\frac{D\phi}{Dx^*} = \frac{F}{f}\tan\theta \qquad (40)$$

Differentiating this equation with respect to x* yields

$$\frac{D^2\phi}{Dx^{*2}} = \frac{f}{F}\frac{D\phi}{Dx^*}\frac{D}{Dx^*}\left(\frac{F}{f}\right) + \frac{1}{\cos^2\theta}\frac{F}{f}\frac{D\theta}{Dx^*}$$

Combining this result with Eq. (39) yields, with the aid of Eq. (40),

$$\frac{D\theta}{Dx^*} = \frac{\tan\theta}{\bar{\gamma M}^2 P}\left(\frac{\partial P}{\partial x^*}\right)_{\phi} - \frac{F}{f}\frac{1}{\bar{\gamma M}^2 P}\left(\frac{\partial P}{\partial\phi}\right)_{x^*} - \frac{f'\tan\theta}{f} \qquad (41)$$

Equations (40) and (41) are valid along a streamline (where β is constant), so they can be integrated simultaneously to determine the geometry of a chosen streamline, $\theta = \theta(x^*)$ and $\phi = \phi(x^*)$. However, the derivatives $\frac{D\phi}{Dx^*}$ and $\frac{D\theta}{Dx^*}$ in Eqs. (40) and (41) become infinite at the most forward point of the streamline where $\theta = 90°$. Of course, this occurs only for streamlines that move forward from the stagnation point (as shown in the sketch on the next page). In connection with these

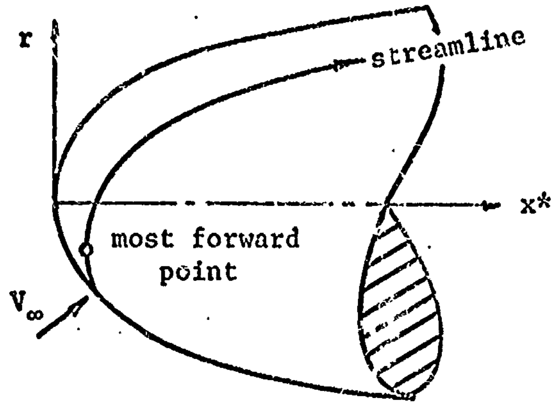

infinite derivatives, it is helpful to rewrite Eqs. (40) and (41) by using S, the distance measured along a streamline, as an independent variable instead of x*.

From the sketch shown below

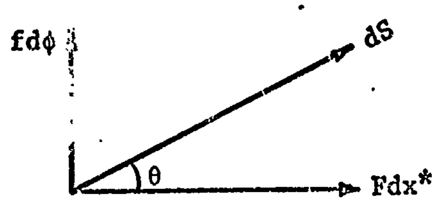

it is seen that

$$dS = \cos\theta \, Fdx^* + \sin\theta \, fd\phi$$

Now apply this result along a streamline to get

$$\frac{DS}{Dx^*} = \cos\theta F + \sin\theta f \frac{D\phi}{Dx^*}$$

and using Eq. (40) for $D\phi/Dx^*$, there results

$$\frac{DS}{Dx^*} = \frac{F}{\cos\theta}, \text{ or } \frac{Dx^*}{DS} = \frac{\cos\theta}{F} \tag{42}$$

Then Eqs. (40) and (41) may be written as

$$\frac{D\phi}{DS} = \frac{\sin\theta}{f} \tag{43}$$

and

$$\frac{D\theta}{DS} = \frac{1}{\gamma M^2 P}\left[\frac{\sin\theta}{F}\left(\frac{\partial P}{\partial x^*}\right)_\phi - \frac{\cos\theta}{f}\left(\frac{\partial P}{\partial \phi}\right)_{x^*}\right] - \frac{f'\sin\theta}{fF} \tag{44}$$

Equations (42), (43), and (44) constitute a set of simultaneous, first order, ordinary differential equations for determining the geometry of a chosen streamline from known pressure distribution. The integration with different initial conditions gives different streamlines. The evaluation of initial conditions will be presented in Appendix B.

The next task is to determine the equation for the scale factor, h_2, along a streamline. At a general point on the surface of the body, the sketch shown below holds. For this analysis consider

$$\phi = \phi(\xi,\beta) \text{ and } x = x(\xi,\beta);$$

From the sketch it follows that

$$\frac{\partial x}{\partial \xi} = h_1 \cos\theta \qquad \frac{\partial x}{\partial \beta} = - h_2 \sin\theta$$

$$\frac{\partial \phi}{\partial \xi} = \frac{h_1 \sin\theta}{f} \qquad \frac{\partial \phi}{\partial \beta} = \frac{h_2 \cos\theta}{f}$$

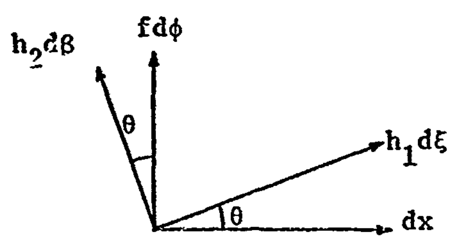

Since $x = x(\xi,\beta)$ and $\phi = \phi(\xi,\beta)$

then

$$\frac{\partial^2 x}{\partial\beta\partial\xi} = \frac{\partial^2 x}{\partial\xi\partial\beta} \tag{45a}$$

$$\frac{\partial^2 \phi}{\partial\beta\partial\xi} = \frac{\partial^2 \phi}{\partial\xi\partial\beta} \tag{45b}$$

For Eq. (45a)

$$\frac{\partial}{\partial \xi}\left(\frac{\partial x}{\partial \beta}\right) = \frac{\partial}{\partial \xi}(- h_2 \sin\theta) = - h_2 \cos\theta \frac{\partial \theta}{\partial \xi} - \sin\theta \frac{\partial h_2}{\partial \xi}$$

and

$$\frac{\partial}{\partial \beta}\left(\frac{\partial x}{\partial \xi}\right) = \frac{\partial}{\partial \beta}(h_1 \cos\theta) = \cos\theta \frac{\partial h_1}{\partial \beta} - h_1 \sin\theta \frac{\partial \theta}{\partial \beta}$$

Equating the right sides of the above two equations gives

$$\frac{1}{h_2}\frac{\partial h_2}{h_1\partial\xi}=\frac{1}{h_2}\frac{\partial\theta}{\partial\beta}-\cot\theta\,\frac{1}{h_1}\frac{\partial\theta}{\partial\xi}-\frac{\cot\theta}{h_1h_2}\frac{\partial h_1}{\partial\beta} \tag{46}$$

For Eq. (45b),

$$\frac{\partial}{\partial\xi}\left(\frac{\partial\phi}{\partial\beta}\right)=\frac{\partial}{\partial\xi}\left(\frac{h_2\cos\theta}{f}\right)=\frac{\cos\theta}{f}\frac{\partial h_2}{\partial\xi}-\frac{h_2\sin\theta}{f}\frac{\partial\theta}{\partial\xi}-\frac{h_2\cos\theta}{f^2}\frac{\partial f}{\partial\xi}$$

and

$$\frac{\partial}{\partial\beta}\left(\frac{\partial\phi}{\partial\xi}\right)=\frac{\partial}{\partial\beta}\left(\frac{h_1\sin\theta}{f}\right)=\frac{\sin\theta}{f}\frac{\partial h_1}{\partial\beta}+\frac{h_1\cos\theta}{f}\frac{\partial\theta}{\partial\beta}+\frac{f'h_1h_2\sin^2\theta}{f^2F}$$

Equating the right sides of the above two equations gives

$$\frac{\partial h_1}{\partial\beta}=\cot\theta\,\frac{\partial h_2}{\partial\xi}-h_2\frac{\partial\theta}{\partial\xi}-\frac{h_2\cot\theta}{f}\frac{\partial f}{\partial\xi}-h_1\cot\theta\,\frac{\partial\theta}{\partial\beta}-\frac{f'h_1h_2\sin\theta}{fF} \tag{47}$$

Substituting Eq. (47) into (46) and simplifying, one obtains

$$\frac{1}{h_1h_2}\frac{\partial h_2}{\partial\xi}=\frac{1}{h_2}\left(\frac{\partial\theta}{\partial\beta}\right)_\xi+\frac{f'\cos\theta}{fF}$$

Since $h_1 d\xi = dS$, the above equation may be written along a streamline as

$$\frac{Dh_2}{DS}=\left(\frac{\partial\theta}{\partial\beta}\right)_\xi+\frac{h_2f'\cos\theta}{fF} \tag{48}$$

The term $\left(\frac{\partial\theta}{\partial\beta}\right)_\xi$ in Eq. (48) is obtained by differentiating Eq. (44) with respect to β and letting

$$\frac{\partial^2\theta}{\partial\beta\partial\xi}=\frac{\partial^2\theta}{\partial\xi\partial\beta}$$

The result is the following:

$$\frac{D}{DS}\left(\frac{\partial\theta}{\partial\beta}\right) = \left[\frac{1}{\bar{\gamma}M^2P}\left(\frac{\cos\theta}{F}\frac{\partial P}{\partial x^*} + \frac{\sin\theta}{f}\frac{\partial P}{\partial\phi}\right) - \frac{f'\cos\theta}{fF}\right]\frac{\partial\theta}{\partial\beta}$$

$$+ \frac{h_2\sin^2\theta}{F}\frac{\partial}{\partial x^*}\left(\frac{f'}{fF}\right) - h_2\frac{D\theta}{DS}\left(\frac{D\theta}{DS} + \frac{f'\sin\theta}{fF}\right)$$

$$+ \frac{h_2}{\bar{\gamma}M^2}\left\{-\frac{\sin^2\theta}{F}\frac{\partial}{\partial x^*}\left(\frac{1}{PF}\frac{\partial P}{\partial x^*}\right) + \frac{\sin\theta\cos\theta}{fF}\frac{\partial}{\partial\phi}\left(\frac{1}{P}\frac{\partial P}{\partial x^*}\right) + \frac{\sin\theta\cos\theta}{F}\frac{\partial}{\partial x^*}\left(\frac{1}{Pf}\frac{\partial P}{\partial\phi}\right)\right.$$

$$\left. - \frac{\cos^2\theta}{f}\frac{\partial}{\partial\phi}\left(\frac{1}{Pf}\frac{\partial P}{\partial\phi}\right) + \left(\frac{D\theta}{DS} + \frac{f'\sin\theta}{fF}\right)\left[\frac{\sin\theta}{F}\frac{\partial}{\partial x^*}(\bar{\gamma}M^2) - \frac{\cos\theta}{f}\frac{\partial}{\partial\phi}(\bar{\gamma}M^2)\right]\right\} \quad (49)$$

Equations (48) and (49) are to be solved simultaneously along with Eqs. (42), (43), and (44) for the desired streamline geometry $\phi = \phi(S,\beta)$ and scale factor $h_2 = h_2(S,\beta)$. These equations, in turn, require the pressure distribution along the surface.

6.4 Estimation of Surface Pressure Distribution

6.4.1 Theoretical Methods

As indicated in the previous analysis, a known surface pressure distribution is required for calculating the inviscid streamline geometry and scale factor as well as heating rates. It is well known that the pressure distribution over blunted bodies is predicted fairly accurately by the modified Newtonian pressure distribution near the nose region and is written as

$$\frac{P}{P_o} = \left(1 - \frac{P_\infty}{P_o}\right)\cos^2\psi + \frac{P_\infty}{P_o} = \left(1 - \frac{P_\infty}{P_o}\right)(\cos\alpha\sin\delta + \sin\alpha\cos\delta\cos\phi)^2 + \frac{P_\infty}{P_o}$$

where ψ and δ are the local surface inclinations with respect to the freestream velocity and body axis of symmetry, respectively. Since

$$\sin\delta = \frac{f'}{\sqrt{1+f'^2}} \quad \text{and} \quad \cos\delta = \frac{1}{\sqrt{1+f'^2}}$$

it follows that

$$\frac{p}{p_o} = (1 - \frac{p_\infty}{p_o}) \frac{(f'\cos\alpha + \sin\alpha \cos\phi)^2}{1 + f'^2} + \frac{p_\infty}{p_o} \tag{50}$$

where $\frac{p_\infty}{p_o}$ is given in ref. 33 for a perfect gas, with constant ratio of specific heats $\bar{\gamma}$ after the normal shock, as

$$\frac{p_\infty}{p_o} = \left[\frac{2}{(\bar{\gamma}+1)M_\infty^2}\right]^{\frac{\bar{\gamma}}{\bar{\gamma}-1}} \left[\frac{2\bar{\gamma}M_\infty^2-(\bar{\gamma}-1)}{\bar{\gamma}+1}\right]^{\frac{1}{\bar{\gamma}-1}} \tag{51}$$

The modified Newtonian theory loses its accuracy where the slope of the surface with respect to the free stream velocity is small. It can be improved by employing the Prandtl-Meyer expansion downstream of the "matching point," i.e., where both pressures and pressure gradients calculated using both methods are equal, as suggested by Kurfman (ref. 24). The applicability of the Prandtl-Meyer relations to the three dimensional case was justified by Eggers, Savin, and Syvertson (ref. 34), if (a) disturbances originating on the surface are largely absorbed in the shock wave and (b) disturbances with the divergence of streamlines in tangent planes to the surface are of secondary importance compared to those associated with the curvature of streamlines in planes normal to the surface. However, the Prandtl-Meyer relations hold only along a streamline, and the pressure distribution must be known before the streamline can be calculated. The problem is resolved by utilizing the expression suggested by Kaattari (ref. 35):

$$\frac{p}{p_o} = \frac{\cos^2\phi}{2} \left[\frac{p_{r,o}}{p_o} + \frac{p_{r,180}}{p_o}\right]_{\alpha\neq o} + \frac{\cos\phi}{2} \left[\frac{p_{r,o}}{p_o} - \frac{p_{r,180}}{p_o}\right]_{\alpha\neq o}$$

$$+ \left(\frac{p_r}{p_o}\right)_{\alpha=o} \left(\frac{p_{0,180}}{p_o}\right)_{\alpha\neq o} \sin^2\phi \tag{52}$$

where $P_{r,o}$ and $P_{r,180}$ are pressures at a given r on the windward and leeward sides, respectively. P_r is the pressure as a function of r at zero angle of attack and $P_{0,180}$, the pressure at the most forward point of the body. Note that all these pressures are functions of x* except $P_{0,\ 180}$ is a constant for a given α.

Equation (52) permits one to determine pressure distributions over blunt bodies at angles of attack when the pressure in the vertical plane of symmetry is known at the angle of attack in question and also at zero angle of attack. The method holds up to $\alpha = 40°$ as conservatively suggested by ref. 35. Since the vertical plane of symmetry of the body at an angle of attack contains the most windward and leeward streamlines, and the meridian lines of an axisymmetric body are actually streamlines at zero angle of attack, then the pressure estimation techniques of matching the modified Newtonian law and the Prandtl-Meyer relation is applicable to determine the required pressures on the right side of Eq. (52). It should be noted that Eq. (52) is an interpolation formula for the circumferential pressure distribution. Another interpolation formula is given in Section 6.4.2 for conical afterbodies.

Based on the above argument, Eq. (52) is employed for pressure distributions downstream of the matching point for the streamlines in the plane of symmetry. The differential equation governing the Prandtl-Meyer relation is

$$\frac{d}{d\nu}\left(\frac{P}{P_o}\right) = -\frac{\bar{\gamma}M^2}{\sqrt{M^2-1}}\frac{P}{P_o} \qquad (53a)$$

where ν is the Prandtl-Meyer angle. To facilitate the integration along a streamline, the above equation is recast by using S, the arc length along a streamline, as the independent variable. This is done as follows,

$$\frac{D}{DS}\left(\frac{P}{P_o}\right) = \frac{Dx^*}{DS}\frac{d}{dx^*}\left(\frac{P}{P_o}\right) = \frac{Dx^*}{DS}\frac{d\nu}{dx^*}\frac{d}{d\nu}\left(\frac{P}{P_o}\right)$$

Since $\nu = \text{constant} - \text{Arctan}(f')$

$$\frac{d\nu}{dx^*} = -\frac{f''}{1 + f'^2} = -\frac{f''}{F^2}$$

and from Eq. (42)

$$\frac{Dx^*}{DS} = \frac{\cos\theta}{F}$$

For the streamlines in the plane of symmetry, $\cos\theta = 1$. Therefore, Eq. (53a) becomes

$$\frac{D}{DS}\left(\frac{P}{P_o}\right) = \frac{f''}{F^3}\frac{\bar{\gamma}M^2}{\sqrt{M^2-1}}\frac{P}{P_o} \tag{53b}$$

Note, however, that this expression yields constant pressure on surfaces of constant slope ($f'' = 0$).

For the region beyond the shoulder of a blunted cone, where the slope of the surface is constant, it was found that the second order shock expansion theory developed by Syvertson and Dennis (ref. 36) is appropriate. The second order shock expansion theory gives the pressure distribution along the cone surface (in the plane of symmetry) as

$$\frac{P}{P_o} = \frac{P_c}{P_o} - \left(\frac{P_c}{P_o} - \frac{P_1}{P_o}\right)e^{-n} \tag{54a}$$

where P_c is the pressure on the cone surface. For a cone at an angle of attack, the value of P_c on the windward and leeward lines may be obtained from the cone solution at zero angle of attack (such as ref. 37 or 38) if the cone half-angle is replaced by the surface inclination angle measured with respect to the free stream velocity. The term P_j is the pressure immediately after the juncture of a blunted cone, and

$$n = \left(\frac{\partial P}{\partial x^*}\right)_j \frac{x^* - x_j^*}{P_c - P_j} \tag{54b}$$

$$\left(\frac{\partial P}{\partial x^*}\right)_j = \frac{Q_j \cos\delta_c}{r_j} \left(\frac{\Omega_1}{\Omega_j} \sin\delta_1 - \sin\delta_j\right) + \frac{Q_j}{Q_1} \frac{\Omega_1}{\Omega_j} \left(\frac{\partial P}{\partial x^*}\right)_1 \tag{54c}$$

$$Q = \frac{\bar{\gamma} M^2 P}{2(M^2-1)} \tag{54d}$$

$$\Omega = \frac{1}{M} \left[\frac{1 + \left(\frac{\bar{\gamma}-1}{2}\right) M^2}{\frac{\bar{\gamma}+1}{2}}\right]^{\frac{\bar{\gamma}+1}{2(\bar{\gamma}-1)}} \tag{54e}$$

Here the subscript "j" implies the quantities evaluated just aft of the juncture, and "1" evaluated at one length segment before the juncture. The local surface inclination with respect to the body axis of symmetry is δ.

Equations (54) estimate the surface pressure in the form of an exponential decay if $P_j > P_c$. Recompression of the surface pressure occurs when $P_j < P_c$. In any event, both cases satisfy the boundary conditions exactly at the juncture and at the end of an infinitely long cone. In case the cone surface inclination with respect to the free stream velocity is larger than the "matching" slope for the Prandtl-Meyer relation, then it is more appropriate to use the modified Newtonian pressure law. Note that Eqs. (54) are used only along the windward and leeward streamlines. For bodies at an angle of attack, the circumferential pressure distribution is obtained from an interpolation formula such as Eq. (52) or Eq. (56) in the next section.

In summary, the surface pressure distribution over the body in question is first predicted by the modified Newtonian pressure distribution near the stagnation region; then by the Prandtl-Meyer relation beyond the "matching point," and finally by the second-order shock expansion method over the cone surface. The latter two must be applied along the windward and leeward lines; and thus, an interpolation formula is needed for circumferential pressure distributions. These methods are not only simple and fairly accurate for estimation of pressures, but also yield derivatives of the pressure for rapid computation of the streamline geometry and scale factors.

The surface pressure distribution required by the present method can also be obtained from the experimentally measured values or those from more sophisticated methods. This is particularly desirable for bodies with a blunt front surface and a rounded shoulder (Apollo-type reentry bodies). This type of body, while traveling at hypersonic speeds, will have the forward blunt surface in the subsonic region and the fluid properties are strongly influenced by the sharply rounded shoulder. The surface pressures predicted by the modified Newtonian law deviate from the experimental values up to 15% (ref. 39). Other cases where the surface pressures are not predicted accurately by the simple method described in the previous section is the case of a very long blunted cone. For this type of body, there may be a "pressure well" over the afterbody surface (ref. 25) which cannot be predicted by the second order shock expansion method. For these particular cases, the surface pressures should be obtained from experimental data or from more sophisticated methods, such as the method of characteristics.

6.4.2 Interpolation Formulas

In order to facilitate the calculation of streamlines, scale factors, and heating rates, it is necessary to have an interpolation formula from which the pressure derivatives may be obtained. For highly blunted bodies, Eq. (52) is appropriate. For long blunted cones, Zaakay (ref. 13) suggests the following interpolation formula,

$$\frac{P}{P_o} = A^o\alpha\cos\phi + B^o\alpha^2 + E^o\alpha^3\cos2\phi + \left(\frac{P_r}{P_o}\right)_{\alpha=o} \tag{55}$$

where A^o, B^o, and E^o are functions of x^* to be determined from known data, whether experimental or theoretical. Let

$$A = A^o\alpha, \quad B = B^o\alpha + \left(\frac{P_r}{P_o}\right)_{\alpha=o} \quad \text{and} \quad E = E^o\alpha^3$$

Eq. (55) is then simplified to

$$\frac{P}{P_o} = A\cos\phi + B + E\cos2\phi \tag{56}$$

where A, B, and E are also functions of x^* that can be determined as shown in Appendix C.

If experimental pressures are available, Eqs. (52) and (56) may also be used to determine the circumferential pressure variation. In order to obtain longitudinal pressure derivatives, an interpolation formula for the longitudinal pressures is needed. This may be accomplished by using a polynomial fit with the aid of the method of least squares.

For other types of blunt bodies, the simple theoretical methods given in the previous section should yield fairly accurate surface pressures. In general, it is adequate to use Eq. (52) for the forward blunted surface region and Eq. (56) for conical afterbodies.

6.5 Application and Method of Computation

The method developed in the previous sections is applied to a sphere, a spherically blunted cone and a paraboloid traveling at hypersonic speeds and at an angle of attack. The sphere case is considered mainly for the purpose of comparing the results of streamline geometry and the scale factors calculated by the present method with those obtained from the exact geometric solution. The paraboloid is chosen to represent the general nature of other body shapes that may be treated by the present method.

For all of the above three cases, the streamline geometry and the scale factor, h_2, are determined by integrating the following set of simultaneous, first order, non-linear ordinary differential equations derived earlier:

$$\frac{Dx^*}{DS} = \frac{\cos\theta}{F} \tag{42}$$

$$\frac{D\phi}{DS} = \frac{\sin\theta}{f} \tag{43}$$

$$\frac{D\theta}{DS} = \frac{1}{\bar{\gamma}M^2 P}\left(\frac{\sin\theta}{F}\frac{\partial P}{\partial x^*} - \frac{\cos\theta}{f}\frac{\partial P}{\partial\phi}\right) - \frac{f'\sin\theta}{fF} \tag{44}$$

$$\frac{Dh_2}{DS} = \frac{\partial\theta}{\partial\beta} + \frac{h_2 f'\cos\theta}{fF} \tag{48}$$

$$\begin{aligned}\frac{D}{DS}\left(\frac{\partial\theta}{\partial\beta}\right) &= \left[\frac{1}{\bar{\gamma}M^2 P}\left(\frac{\cos\theta}{F}\frac{\partial P}{\partial x^*} + \frac{\sin\theta}{f}\frac{\partial P}{\partial\phi}\right) - \frac{f'\cos\theta}{fF}\right]\frac{\partial\theta}{\partial\beta}\\ &+ \frac{h_2\sin^2\theta}{F}\frac{\partial}{\partial x^*}\left(\frac{f'}{fF}\right) - h_2\frac{D\theta}{DS}\left(\frac{D\theta}{DS} + \frac{f'\sin\theta}{fF}\right)\\ &+ \frac{h_2}{\bar{\gamma}M^2}\left\{-\frac{\sin^2\theta}{F}\frac{\partial}{\partial x^*}\left(\frac{1}{PF}\frac{\partial P}{\partial x^*}\right) + \frac{\sin\theta\cos\theta}{fF}\frac{\partial}{\partial\phi}\left(\frac{1}{P}\frac{\partial P}{\partial x^*}\right) + \frac{\sin\theta\cos\theta}{F}\frac{\partial}{\partial x^*}\left(\frac{1}{Pf}\frac{\partial P}{\partial\phi}\right)\right.\\ &\left.- \frac{\cos^2\theta}{f}\frac{\partial}{\partial\phi}\left(\frac{1}{Pf}\frac{\partial P}{\partial\phi}\right) + \left(\frac{D\theta}{DS} + \frac{f'\sin\theta}{fF}\right)\left[\frac{\sin\theta}{F}\frac{\partial}{\partial x^*}(\bar{\gamma}M^2) - \frac{\cos\theta}{f}\frac{\partial}{\partial\phi}(\bar{\gamma}M^2)\right]\right\}\end{aligned} \tag{49}$$

With a set of given initial conditions, the solutions of the above equations is carried out by the fourth-order Runge-Kutta method of numerical integration (ref. 40) along a streamline. The evaluation of initial conditions is presented in Appendices A and B. The stagnation point is assumed to be the point where the surface inner normal vector coincides with the free stream velocity, i.e.,

$$f'_o = \cot \alpha$$

As discussed in ref. 41, it is exactly true for the case of a sphere or a spherically blunted cone with the sonic line lying on the spherical cap. For other cases it is only approximate.

For the region near the stagnation point, Eq. (50) is used for the pressure distribution and its derivatives. Downstream of the matching point, Eq. (53) along with Eq. (52) is employed. The use of these two pressure estimation techniques is distinguished by the locus of the matching points at $\alpha \neq 0$, as shown in the sketch below.

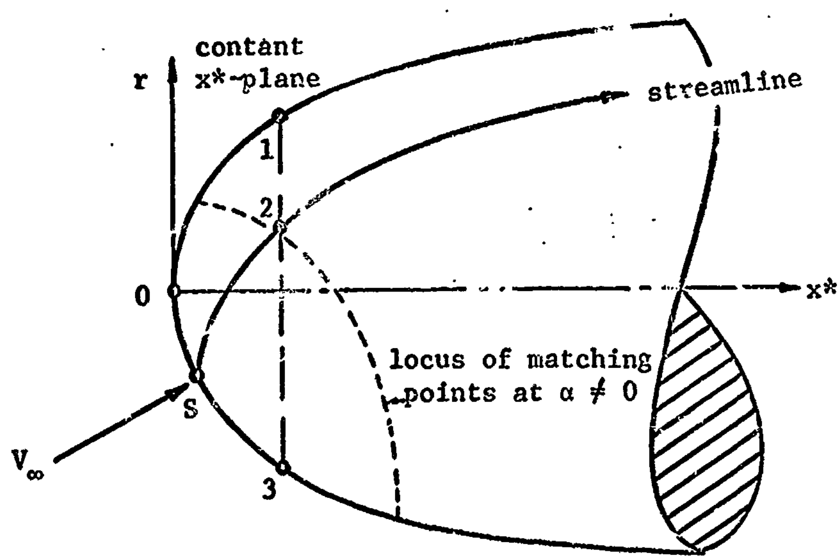

It is also seen in the sketch that the input pressures, $P_{0,180}$, $P_{r,180}$ and $P_{r,0}$ for Eq. (52) are the pressures at points 0, 1, and 3, respectively. The pressure P_r is the pressure at point 2 when $\alpha = 0$.

On a given streamline, the pressure beyond the matching point requires $P_{0,180}$, $P_{r,180}$, and $P_{r,o}$ as functions of x^*. For the region where these pressures fall within the Prandtl-Meyer domain, a relationship between the local M and the Prandtl-Meyer angle ν is desirable. An iteration technique suggested by Collar (ref. 42) is used here. Collar gives

$$M_{n+1}^2 = \frac{6}{\cos^2\left[\dfrac{\nu + \arccos M_n^{-1}}{\sqrt{6}}\right]} - 5 \tag{57}$$

where M_n and M_{n+1} are the assumed and improved Mach numbers for a given ν.

For a given x^* station, the Prandtl-Meyer angle along the leeward streamline is given by

$$\nu = \nu_q + \delta_q - \arctan f' + \alpha \tag{58a}$$

where ν_q and δ_q are the Prandtl-Meyer and surface inclination angles, respectively, at the matching point for $\alpha = o$. Simarily, the Prandtl-Meyer angle on the windward streamline is

$$\nu = \nu_q + \delta_q - \arctan f' - \alpha \tag{58b}$$

Since P_r is the pressure at given x^* station for $\alpha = o$, the ν corresponding to $\alpha = o$ is given by

$$\nu_{\alpha=o} = \nu_q + \delta_q - \arctan f' \tag{58c}$$

The matching point is determined by the method of ref. 24, which provides charts for obtaining Mach number and surface inclination angle at the matching point for a given P_∞/P_o. In order to facilitate digital computation, the result for M_q versus P_∞/P_o given in ref. 24 is transformed to the following third order polynomial

$$M_q = 1.3520894 + 1.2554079\left(\frac{P_\infty}{P_o}\right) + 12.451517\left(\frac{P_\infty}{P_o}\right)^2 - 162.76788\left(\frac{P_\infty}{P_o}\right)^3 \quad (59)$$

Equation (59) holds for $3 \leq M_\infty \leq 20$. As shown in Fig. 3, M_q is a weak function of P_∞/P_o.

To calculate laminar and turbulent heating rates, Eqs. (10), (16), and (33) are numerically integrated by Simpson's one-third rule along a streamline. The pressure distribution used here is the same as that for the streamline geometry and scale factors. As mentioned in Section 6.1.3, both the laminar and turbulent heating rates are calculated at the same time. To indicate the region of possible transition points, Reynolds numbers based on local external properties and the momentum thickness are also calculated along a streamline. The velocity ratio appearing in Eq. (10) is obtained from the pressure assuming an isentropic expansion along a streamline from the stagnation point to the point in question. To take account of the real gas effects, an effective specific heat ratio is used. Other fluid properties in Eqs. (14), (15), (16), and (33), and (34) may also be evaluated approximately from the isentropic relations (ref. 14). Following Vaglio-Laurin's suggestion (ref. 9), the reference condition quantities in Eqs. (15) and (16) are evaluated at the stagnation state of the external flow. But those in Eq. (33) are obtained using Eq. (14). In addition, a power law relationship between μ and T, $\mu/\mu_o = (T/T_o)^{\omega}$, is used with $0.76 \leq \omega \leq 1.0$. The term r in Eq. (10) is replaced by h_2, which is calculated from Eq. (48). In calculating the turbulent heating rate, the value of Z from Eq. (16) is fed into Eq. (18) and the resulting C_f* into Eq. (15).

The above procedure is applicable to a general blunted body. However, particular steps should be taken for certain body shapes. These are illustrated as follows.

6.5.1 Application to a Sphere

For the case of a sphere, the procedures for calculating the streamline geometry, scale factors, and laminar and turbulent heating rates are the same as described above. The body shape is written as

$$f/R_o = \sqrt{2\bar{x}^* - \bar{x}^{*2}} \tag{60}$$

The initial conditions, evaluated at a point generally one step size away from the stagnation point, are determined from geometric solutions developed in Appendix A. These are

$$\bar{x}_i = \text{Arccos}(\cos\alpha\cos\bar{S}_i - \sin\alpha\sin\bar{S}_i\cos\beta) \tag{61a}$$

$$\bar{x}^*_i = 1 - \cos\bar{x}_i \tag{61b}$$

$$\phi_i = \text{Arcsin}(\sin\bar{S}_i\sin\beta/\sin\bar{x}_i) \tag{61c}$$

$$\theta_i = \text{Arcsin}(\sin\alpha\sin\beta/\sin\bar{x}_i) \tag{61d}$$

$$\bar{h}_{2_i} = \sin\bar{S}_i \tag{61e}$$

$$\left(\frac{\partial\theta}{\partial\beta}\right)_i = \frac{\bar{h}_{2_i}\sin\theta_i\tan\theta_i}{\tan\bar{x}_i} + \frac{\sin\alpha\cos\beta}{\sin\bar{x}_i\cos\theta_i} \tag{61f}$$

The barred quantities are normalized by the radius of the sphere. The subscript "i" implies the initial values; S_i is the distance measured from the stagnation to initial point along a streamline and β defines a particular streamline as shown in Fig. 2.

The numerical procedure is programmed in Fortran IV language on the IBM 7040 digital computer. The average execution time for each increment in S (including integration of the heating rate equations and simultaneous differential equations for streamline and scale factor) is 0.17 second. If a step size of 0.01 is used, an average of 150 increments is required for one streamline from the stagnation point to $x^*/R_o=1$; then the execution time is 26 seconds up to that point. A typical body may require heating rates along 20 different streamlines, which results in a total computing time of approximately 9 minutes on the IBM 7040.

6.5.2 Application to a Spherically Blunted Cone

In hypersonic flows a typical body shape frequently considered in the literature is the spherically blunted cone. However, few investigations have been made for cases at an angle of attack. In applying the present method to this body, the numerical procedure for calculating the streamline geometry, scale factor, and the laminar and turbulent heating rates is similar to that of the sphere. The only difference is that the second order shock expansion method is used for estimating the pressure in the plane of symmetry over the cone surface. To illustrate a typical application of the present method, the complete and detailed computational procedure and the corresponding Fortran source program are presented in Appendices C and D, respectively.

The average computer execution time is also the same as in the case of a sphere, i.e., 0.17 second for each increment in S (including integration of the heating rate equations and simultaneous differential equations for streamline and the scale factors). A step size of 0.01 is used for the spherical cap region and 0.1 for the conical afterbody. An average of 230 increments is required for one streamline from the stagnation point to $x^*/R_o = 10$; thus, the execution time is 40 seconds up to that point. Also, a typical body may require heating rates along 20 different streamlines, which results in a total computing time of approximately 14 minutes on the IBM 7040.

6.5.3 Application to a Paraboloid

In order to compare the present method with that of refs. 6 and 26, an $f = \sqrt{1.3x^*}$ paraboloid is considered. The computational procedure for the case of a paraboloid is the same as that for a sphere, except the initial conditions are evaluated from Eqs. (B-3) in Appendix B.

In Eqs. (B-3), the initial quantities x^*_i, ϕ_i, θ_i, h_{2_i} and $(\partial\theta/\partial\beta)_i$ are given in terms of ε, A_∞ and B_∞ for a given angle of attack. Care must be exercised in selection of these values. Physically, ε determines the location of the initial point and A_∞ specifies a particular streamline at its initial point. The term B_∞ is an arbitrary constant. In the computation, a range of 20 to 200 is used for A_∞; ε is chosen as small as 10^{-6} to 5×10^{-6} and B_∞ may be set to unity. These quantities are shown in Fig. 4.

The remainder of the computational procedure is identical to that for the case of a sphere.

VII. RESULTS AND DISCUSSION

A series of programs have been computed on the IBM 7040 computer at the Virginia Polytechnic Institute to determine the inviscid streamline geometry, scale factors, and both laminar and turbulent heating rates over the following bodies and flow conditions:

(1) Sphere at $\alpha = 15°$ and $30°$, $M_\infty = 8.0$.

(2) Spherically blunted cone with 9° half-angle at $\alpha = 10°$, $M_\infty = 18$.

(3) Spherically blunted cone with 20° half-angle at $\alpha = 15°$, $M_\infty = 6.0$.

(4) Spherically blunted cone with 15° half-angle at $\alpha = 10°$, and $20°$, $M_\infty = 10.6$.

(5) Spherically blunted cone with 30° half-angle at $\alpha = 10°$ and $20°$, $M_\infty = 10.6$.

(6) Paraboloid $f = \sqrt{1.3x^*}$ at $\alpha = 15°$, $M_\infty = 8.0$.

The flow conditions have been chosen the same as those used in several theoretical and/or experimental investigations which are available for comparison purposes. All the cases above were computed with $\gamma_\infty = \bar{\gamma} = 1.4$. The results are presented in graphical form in Figures 5 to 32.

7.1 Streamline Geometry and Scale Factors

For the case of a sphere, the calculated streamlines and scale factors at $M_\infty = 8.0$ and $\alpha = 15°$ are shown in Figures 5 and 6 and compared with those obtained from the known geometric solutions. In the region where the modified Newtonian pressure distribution theory is valid, the accuracy of the results for both streamline location $\phi(x^*,\beta)$ and scale factor, h_2, is within 0.5%. A comparison of the results is also made for the region from the "matching point" to the position $x^*/R_o = 0.74$. In this region, the Prandtl-Meyer relation is used along with Eq. (52), and the accuracy of the calculated $\phi(x^*, \beta)$ and h_2 is within 1.5%.

Fig. 7 shows the calculated streamline direction, θ, over a sphere at angles of attack of 15° and 30°. The maximum deviation from the geometric solution is 0.3%.

Since the accuracy of the calculated streamline geometry and scale factors depends on the pressure distribution, the validity of the interpolation formula for pressure, Eq. (52), has been partially tested. The test was to compare the resultant pressures obtained by both Eqs. (50) and (52) near the stagnation region. In this region, if the input pressures along the windward, meridian (at α=o) and leeward lines for Eq. (52) were calculated by using Eq. (50), then the resultant pressure should agree with that obtained directly from Eq. (50). The results are shown in Fig. 8, and the agreement is very good.

In Fig. 12 the calculated streamline patterns for a spherically blunted 9° half-angle cone at $M_\infty = 18$ and $\alpha = 10°$ are compared with those obtained from the method of characteristics (ref. 25) and the Simplified Method of ref. 6. The β angles specify the individual streamlines. Two different pressure distributions were used for the present method. For Pressure-I, the hybrid pressure (Newtonian plus Prandtl-Meyer) was used for the spherical cap and the pressures from the method of characteristics were employed over the cone surface. Eq. (56) was used for interpolation. Pressure-II uses the same pressure as Pressure-I over the spherical cap, but the second order shock expansion in the plane of symmetry was used along with Eq. (52) for the cone surface. In general, the calculated streamlines from the present method agree very well with those from the method of characteristics. However, considerable deviation occurs for streamlines near the windward side; this can be attributed to the fact that Eq. (56) fails to yield appropriate pressures on the windward side region near and beyond $x^*/R_o = 13.54$ as indicated in Fig. 13. As done in the Simplified Method of ref. 6, the modified Newtonian pressure distribution may also be used throughout the whole body surface in the present method. However, the results (which are not shown in Fig. 12) deviates from the method of characteristics significantly. The deviation is also slightly larger than that of the Simplified Method of ref. 6.

Unfortunately no data for the scale factors can be found in the literature. However, by inductive reasoning based on the accuracy of the streamline geometry, one may presume that the present method should also yield correct scale factors. Figs. 19 and 20 illustrate the streamline patterns and scale factors, respectively, for a spherically capped 20° half-angle cone at $M_\infty = 6.0$ and $\alpha = 15°$.

These conditions are the same as those for the experiments in ref. 13. In the present calculations, the experimental pressure distribution of ref. 13 was employed along with the interpolation formula of Eq. (56). The streamline pattern follows a trend similar to that of the previous case. The graph of the scale factor reveals that its variation along a streamline is consistent with the movement of the streamline. This is evidenced by the fact that the scale factors are proportional to the spacing between two adjacent streamlines. The streamlines near the windward side wrap around the body a large amount producing a large spacing between them. Since only relative values of the scale factors are of practical interest, their streamwise variation shown in Fig. 20 agrees with the spacing between two adjacent streamlines as indicated in Fig. 19.

For the case of a paraboloid, there is no simple geometric solution for comparison like the sphere. However, in order to test the accuracy of Eq. (B-3) for evaluating the initial conditions, they were first applied to a sphere. Using $M_\infty = 8.0$ and $\alpha = 10°$, 20° and 30°, the calculated results along with those obtained from the known geometric solution are presented in Table I. Excellent agreement was obtained for small values of ε. Also, the initial data for the paraboloid, $f = \sqrt{1.3x^*}$ at $M_\infty = 8.0$ and $\alpha = 15°$ are compared with those of the Simplified Method of ref. 6, and the difference in θ obtained by both methods is within 0.3%. The calculated streamline geometry and scale factors are shown in Figs.14 and 15, respectively. The general trend of the results agrees reasonably well with the previous cases except for the scale factors of the two streamlines, $\beta = 154°$ and $174°$. The magnitude of the scale factor shown is its relative value times an arbitrary constant which was introduced in evaluating the initial data. Therefore, it is observed from the figure that the scale factors of these two streamlines still exhibit the correct trend.

7.2 Heat Transfer Distributions

The heat transfer distributions for the bodies considered were calculated in terms of the ratio of the heating rate at a local point to that at the stagnation point or in terms of Nusselt and Reynolds numbers. The surface pressure distributions used for calculating the heat transfer results were the same as those used for the streamline geometry and scale factors.

Figures 10 and 11 show the longitudinal and circumferential heating rate distribution over a sphere at $M_\infty = 8.0$ and $\alpha = 15°$. The present results are also compared with those obtained from the Simplified Method. In both methods the laminar heating rates (at $\alpha = 0$) of Lees, Eq. (10), were utilized, and the agreement of both methods is very good in the upstream region. The deviation downstream is obviously due to the use of modified Newtonian pressures in the Simplified Method, since the Prandtl-Meyer relation was used in the present method for this region. The two pressure distributions are shown in Fig. 9. The slightly low values of the Simplified Method along $\phi = 180°$ may be attributed to the numerical truncated error in ref. 26. If the meridian line of a sphere at zero angle of attack is replaced by the streamline at an angle of attack, then the heating rate result of Lees (ref. 1) for a sphere at zero angle of attack may be transformed into Fig. 10. As shown in Fig. 10, the heating rate results from the present method agrees with those from ref. 1 as well as the Simplified Method.

The dependency of the heat transfer results on the pressure distribution used is also supported by Fig. 16. For the case of the paraboloid $f = \sqrt{1.3x^*}$ at $M_\infty = 8.0$ and $\alpha = 15°$, the heating rates are shown in Figs. 17 and 18. Although the streamline geometry calculated by both the Simplified Method and the present method deviates from each other, the difference in heat transfer is mainly due to the pressure distributions. It is observed from the above results that the heating rates are directly affected by both pressure distribution and streamline geometry (which may be obtained independent of pressure distribution); the former is more sensitive than the latter.

In Figures 21 to 25 the heat transfer distribution over a spherically blunted 20° half-angle cone at $M_\infty = 6.0$ and $\alpha = 15°$ is presented. The body shape and flow conditions are the same as those used by Zakkay in ref. 13. In order to compare the results with the experimental measurements given in ref. 13, the heat transfer distributions were recast in terms of the ratio of Nusselt number, to the square root of the Reynolds number, where

$Nu = \dot{q}_w R_o Pr/\mu_o (H_e - h_w)$ and $Re = \rho_o H_e^{1/2} R_o/\mu_o$. In fact, $Nu/Re^{1/2}$ is a characteristic parameter for laminar heat transfer. To be consistent with ref. 13, the stagnation heat transfer value of Fay and Riddel (ref. 43) was used. Although the predicted stagnation point heat transfer from ref. 43 is approximately 10 to 15% higher than those of Lees (ref. 1), the variation of local heat transfer differs merely by a constant throughout.

Fig. 21 shows the heat transfer distribution along the most windward streamline together with the theoretical predictions of ref. 10 (method for streamline geometry) and experimental values of ref. 13. In both ref. 10 and the present method, the laminar heating rate solution given by Eq. (10) was employed. For positions away from the windward streamline, ref. 13 also provides measured heating rate data for comparison as shown in Figs. 22 to 25. It is observed that the heating rates calculated by the present method using pertinent experimental pressures of ref. 13 agree with the measured values more favorably than those using the hybrid pressure described in Section 6.3.

The present results are further compared with experimental data from the Ames Research Center, NASA (ref. 27) and theoretical values of the Simplified Method of ref. 6 as shown in Figures 26 to 29. Two spherically blunted cones with half-angles of 15° and 30° were considered. The angle of attack varied from 10 to 20 degrees for $M_\infty = 10.6$ using $\bar{\gamma} = \gamma_\infty = 1.4$. For brevity, the discussion of the results will be confined to those for 15° cone half-angle at $\alpha = 10°$, which are presented in Fig. 28. Two pressure distributions were used in the present method; namely, the hybrid pressure as given in Section 6.3 and the modified Newtonian pressure over the whole body surface. The latter was applied because it was utilized in the Simplified Method. In both methods, the laminar heat transfer expression given by Eq. (10) was used. It is observed that the heating rates predicted by the Simplified Method are close to those of the present method when Modified Newtonian Pressures are used. Also, the heating rates for the Simplified Method fall between those of the present method using the hybrid pressures and modified Newtonian pressures. Fairly close agreement with experimental values is found, except moderate deviation taking place near the shoulder region.

Near the shoulder the hybrid pressure of Section 6.3 predicted values higher than the measured values in all four cases of ref. 27. However, as shown in Figures 21 to 25 the theoretical results calculated by the same method employing the same hybrid pressure estimation technique are generally lower than the experimental data of ref. 13. The disagreement between these two sets of experimental results may be attributed to different test conditions such as free stream Mach number and wall to external total enthalpy ratio. It was found that the free stream Mach number and the mean specific heat ratio, $\bar{\gamma}$, affects the heating rate ratio very little as long as they are in the hypersonic range $(M_\infty \geq 5)$. The wall to external total enthalpy ratios, which were not indicated in any of these cases, may have played an influential role.

The experimental heating rates results of refs. 13 and 27 indicate that they correlate much better with the laminar than with the turbulent results. This implies that the laminar boundary layer is generally stable for hypersonic flows with highly cooled walls. Further verification of this argument is supported by the value of the Reynolds number based on local fluid properties at the edge of boundary layer and the momentum thickness, Re_θ. This is a parameter commonly used for determining boundary layer transition. As indicated in Fig. 28, the value of $Re_\theta = 151$ at $x^*/R_o = 16$ indicates that the boundary layer will remain laminar according to the criteria given in Section 6.2.3.

The local turbulent heat transfer was calculated using the two solutions given in Section 6.2.2 along with the present method for determining streamline geometry and scale factors. The heating rate results are presented in Figs. 28 and 29 for the most windward streamlines. Since the heat transfer parameters for turbulent flows are quite different from laminar ones, the freestream fluid properties come into the picture, i.e., the heating rate ratio depends upon the altitude at which the vehicle travels.

Figs. 28 and 29 are for an altitude of 150,000 feet, a wall to stagnation temperature ratio of 0.1, and $\omega = 0.76$. Very good agreement between the heating rates of Expressions I and II of Section 6.2.2 is obtained. Expression I used the stagnation conditions of the external flow as reference conditions, whereas Expression- II used Eckert's reference enthalpy method, Eq. (14).

In Figure 30, the effect of altitude on the turbulent heat transfer is shown. The turbulent heating rate ratio increases as the altitude decreases. It is observed that while other flow parameters remain the same, the turbulent heating rate ratio is influenced by the freestream pressure, temperature and coefficient of viscosity. The freestream fluid properties may be eliminated if the turbulent heat transfer expression is written in terms of $Nu/Re^{4/5}$.

Figure 31 indicates the effect of the relation between the viscosity and temperature on the turbulent heating rates. In the expression $\mu_e/\mu_o = (T_e/T_o)^\omega$, as the exponent ω decreases, the turbulent heating rate ratio increases. For most applications, the value of ω is usually chosen in the neighborhood of 0.76 to 1.0. However, inside the boundary layer, ω being unity was used by both references 1 and 9.

Also shown in Fig. 31 is the effect of the reference state on the turbulent heating rate of ref. 9 (Expression-I in Section 6.2.2). The results indicate that the predicted heating rates using the stagnation state of the external flow are considerably lower than those using Eckert's reference enthalpy method, Eq. (14).

It is observed in Figs. 30 and 31, as well as Figs. 28 and 29, that the results obtained from the presently derived expression for turbulent heating rates, Expression II, agree very favorably with those from ref. 9 (Expression I). Both solutions are influenced by the freestream properties and the viscosity-temperature relation in a similar pattern.

The method of ref. 9 (Expression I) was based on the highly cooled wall assumption and a crucial choice of reference state. Fig. 32 shows the effect of wall temperature on the turbulent heating rates using Eckert's reference enthalpy method. It is observed that the heating rates depend only slightly on the wall to stagnation enthalpy ratio. If the stagnation state of the outer flow is used for reference conditions, the heating rates are then independent of the wall to stagnation enthalpy ratio. This agrees with the experimental data discussed in ref. 9.

VIII. CONCLUSIONS

As a result of the present work, the following conclusions may be drawn:

(i) The "axisymmetric analogue" is applicable for the theoretical estimation of laminar and turbulent heat transfer over general three-dimensional bodies at an angle of attack in hypersonic flows with highly cooled walls. For flows over three dimensional bodies under conditions other than the above, it may be considered a first order approximation to the heat transfer.

(ii) A new method is rigorously developed for determining the inviscid streamline geometry and pertinent scale factors over axisymmetric bodies at an angle of attack. The method requires a known pressure distribution, which may be theoretical or experimental.

(iii) The suggested hybrid pressure estimation technique, which includes the modified Newtonian pressure law, the Prandtl-Meyer relation, and the second order shock expansion, yields fairly accurate results for both streamline geometry and heating rates. However, the Prandtl-Meyer relation and second order shock expansion must be applied in the vertical plane of symmetry for bodies at angles of attack, and also applied along the meridian line at zero angle of attack. The circumferential pressure variation is determined by an interpolation formula.

(iv) For bodies at an angle of attack, the streamline geometry and scale factors calculated by the present method agree very well with those obtained by the known geometric solution for the case of a sphere, and by the method of characteristics for the case of a spherically blunted cone. Favorable agreement in surface streamline patterns was obtained between the Simplified Method of reference 6 and the present method for the region near the stagnation point. However, significant differences between the two methods were noted downstream.

(v) The laminar heat transfer distributions calculated by the present method through the use of axisymmetric analogue compared favorably with available experimental measurements and other theoretical predictions.

(vi) A new expression for predicting turbulent heat transfer is derived by utilizing Mager's transformation between the incompressible and compressible skin friction coefficients and correlating the solutions of the momentum integral equations through Reynolds analogy. For highly cooled walls, it yields very favorable agreement with the solution of Vaglio-Laurin (ref. 9).

(vii) The ratio of local turbulent heat transfer rate to that at the stagnation point is affected considerably by the freestream fluid properties and viscosity-temperature relation, but only slightly by the wall to stagnation enthalpy ratio in the range of highly cooled walls. The predicted turbulent heating rate results with the reference conditions evaluated at the stagnation state of the external flow are considerably lower (about 25%) than those evaluated by Eckert's reference enthalpy method.

(viii) For hypersonic flows, both laminar and turbulent heating rates ratio are fairly insensitive to the freestream Mach number and the mean specific heats ratio after the normal shock.

(ix) The heat transfer distribution is affected by both pressure distribution and streamline geometry. However, the pressure has more effect than the streamline geometry.

IX. APPENDICES

Appendix A

Geometric Solution of Streamline Geometry and Scale Factor for a Sphere

The method for calculating the streamline geometry and the scale factors developed in Section 6.3 is applicable to general three-dimensional bodies at an angle of attack. For the particular case of a sphere traveling at an angle of attack with respect to its original axis of symmetry, a closed form geometric solution can be obtained by a simple transformation.

As shown in Fig. 2, the original axis of symmetry is x^*, and AC is a meridian line through the most forward point, A. Since any axis through the center of a sphere is a geometric axis of symmetry, then a new axis of symmetry, x_w^*, which coincides with the free stream velocity is formed. It may be referred to as the wind axis of symmetry. The streamlines emanating from the stagnation point, B, are then meridian lines with respect to the wind axis of symmetry, x_w^*. Hence, the streamline geometry is known for the case of a sphere.

To facilitate the calculation, the solution in the wind coordinates is transformed to the body coordinates as follows.

First, consider the spherical triangle, ABC. (See sketch below). For a given angle of attack α, specified streamline coordinate β, and arc length along of the streamline S, there results with the aid of ref. 44,

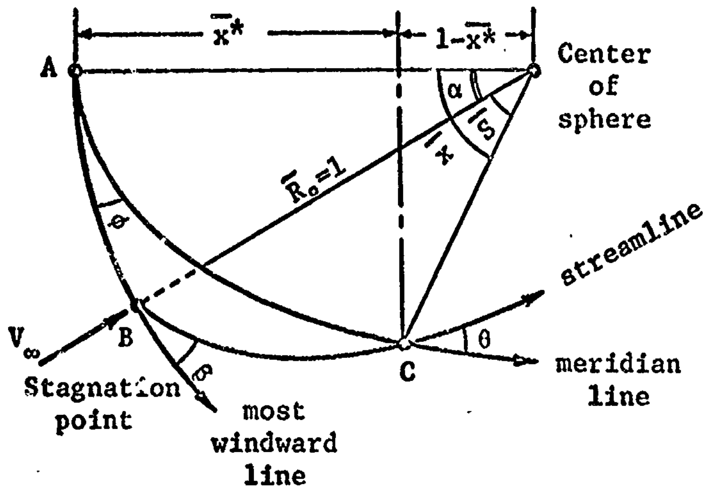

$$\bar{x} = \text{Arccos}(\cos\alpha\cos\bar{S} - \sin\alpha\sin\bar{S}\cos\beta) \tag{A-1}$$

$$\bar{x}^* = 1 - \cos\bar{x} \tag{A-2}$$

$$\phi = \text{Arcsin}\left(\frac{\sin\bar{S}\sin\beta}{\sin x}\right) \tag{A-3}$$

$$\theta = \text{Arcsin}\left(\frac{\sin\alpha\sin\beta}{\sin x}\right) \tag{A-4}$$

From Fig. 2,

$$\bar{h}_2 = \sin\bar{S} \tag{A-5}$$

where

$$\bar{x} = \frac{x}{R_o},\ \bar{x}^* = \frac{x^*}{R_o},\ \bar{S} = \frac{S}{R_o} \text{ and } \bar{h}_2 = \frac{h_2}{R_o}$$

Note that in spherical trigonometry, the sides normalized by the radius of the sphere are expressed in radians.

The above equations give the desired streamline geometry and scale factors. The quantity $(\frac{\partial\theta}{\partial\beta})$ is not needed here; however, it is required for spherically blunted bodies. Therefore, differentiating Eq. (A-4) with respect to β, one obtains

$$\cos\theta \frac{\partial\theta}{\partial\beta} = - \frac{\sin\alpha\sin\beta\cos\overline{x}}{\sin^2\overline{x}} \left(\frac{\partial\overline{x}}{\partial\beta}\right) + \frac{\sin\alpha\cos\beta}{\sin\overline{x}} \qquad \text{(A-6)}$$

Previously it was found in Section 6.3 that

$$\frac{\partial x}{\partial\beta} = - h_2 \sin\theta$$

Substituting this equation into Eq. (A-6) and simplifying yield

$$\frac{\partial\theta}{\partial\beta} = \frac{\overline{h}_2\sin\theta\tan\theta}{\tan\overline{x}} + \frac{\sin\alpha\cos\beta}{\sin\overline{x}\cos\theta} \qquad \text{(A-7)}$$

Appendix B

Evaluation of Initial Conditions for Calculating Streamline Geometry and Scale Factor over a Body of Revolution at an Angle of Attack

In order to integrate the simultaneous differential equations for calculating the streamline geometry and scale factor over a general three-dimensional body, as developed in Section 6.3, a set of initial conditions is required. The evaluation of these initial conditions for a body of revolution at an angle of attack is illustrated here.

With reference to Fig. 4, the initial point is determined by (x_i^* , ϕ_i). The subscript "i" denotes the quantities at the initial point. For a given x_i^*, let

$$\varepsilon = x_i^* - x_o^*$$

$$\phi_i = |\varepsilon|^{a_o}(A_{oo} + A_{o1}\varepsilon + A_{o2}\varepsilon^2 + \ldots) + |\varepsilon|^{a_1} (A_{10} + A_{11}\varepsilon + A_{12}\varepsilon^2 + \ldots)$$

$$+ |\varepsilon|^{a_2} (A_{20} + A_{21}\varepsilon + A_{22}\varepsilon^2 + \ldots) + \ldots$$

$$f_i = f_o + f_o'\varepsilon + f_o'' \frac{\varepsilon^2}{2} + \ldots$$

$$f_i' = f_o' + f_o''\varepsilon + f_o''' \frac{\varepsilon^2}{2} + \ldots$$

$$f_i'' = f_o'' + f_o''' \varepsilon + f_o^{IV} \frac{\varepsilon^2}{2}$$

$$\sin \phi_i = \phi_i - \frac{\phi_i^3}{3} + \ldots$$

$$\cos \phi_i = 1 - \frac{\phi_i^2}{2} + \ldots$$

where x_o^* is the distance from the most forward point of the body to the stagnation point along the axis of symmetry and a_o, $a_1 \ldots$ and A_∞, $A_{o1} \ldots$ are constants.

If the initial point x_i^* is chosen very close to the stagnation point (x_o^*), then $\varepsilon(= x_i^* - x_o^*)$ is a very small quantity. Hence, the above equations can be written, with $O(\varepsilon^2)$ terms dropped, as

$$\phi_i = A_\infty |\varepsilon|^{a_o}$$

$$f_i = f_o + f_o'\varepsilon$$

$$f_i' = f_o' + f_o''\varepsilon$$

$$f_i'' = f_o'' + f_o'''\varepsilon$$

$$\sin \phi_i = \phi_i$$

$$\cos \phi_i = 1$$

Using these equations in Eq. (38) along with Eq. (50) one obtains after a tedious munipulation,

$$a_o = -\frac{(1 + f_o'^2)}{f_o f_o''} \tag{B-1}$$

Note that the left-hand side of Eq. (B-1) is the ratio of two principal radii of curvature at the stagnation point and that A_∞ is a constant which distinguishes the different streamlines.

For a given angle of attack, α, and a body shape, $f = f(x^*)$, the quantities in Eq. (B-1) may be determined approximately by

$$f_o' = \cot \alpha \tag{B-2}$$

Eq. (B-2) implies that the vector normal to the body surface at the stagnation point coincides with the direction of the free stream velocity. This is exactly true for the case of a sphere (ref. 41).

With a_o found as above, there results

$$x_i^* = x_o^* + \varepsilon \tag{B-3a}$$

$$\phi_i = A_\infty |\varepsilon|^{a_o} \tag{B-3b}$$

and from Eq. (39)

$$\theta_i = \text{Arctan}\left(\frac{A_\infty a_o f_i \varepsilon^{a_o - 1}}{\sqrt{1 + f_i'^2}}\right) \tag{B-3c}$$

For the scale factor, let

$$h_{2_i} = B_\infty |\varepsilon|^b \tag{B-3d}$$

then

$$\left(\frac{\partial\theta}{\partial\beta}\right)_i = \left(\frac{Dh_2}{DS} - \frac{h_2 f' \cos\theta}{f\sqrt{1+f'^2}}\right)_i = \frac{B_\infty|\varepsilon|^b \cos\theta_i}{\sqrt{1+f_i'^2}} \quad \left(\frac{b}{\varepsilon} - \frac{f_i}{f_i}\right) \qquad \text{(B-3e)}$$

Substitution of Eqs. (B-3) into Eq. (49) yields after considerable munipulation

$$b = a_o \qquad \text{(B-4)}$$

and B_∞ can be an arbitrary constant.

The results of Eqs. (B-1) and (B-4) are exactly the same as those obtained from ref. 26 using the same procedure.

Appendix C

Computational Procedure for Case of Spherically Blunted Cone

The complete computational procedure for calculating the streamline geometry, scale factors and heating rates for spherically blunted cones traveling at hypersonic speeds at an angle of attack consists of three parts:

(1) Evaluation of the initial conditions and constants.

(2) Integration of the heating rate equations.

(3) Calculation of streamline geometry and the scale factors.

The first and second parts are written in a main program and the third part written in five separate subprograms corresponding to five sequential surface pressure conditions, as indicated in Section C-3.

C-1 Evaluation of the Initial Conditions and Constants

For a spherically blunted cone with half-angle δ_c traveling at a given freestream Mach number, altitude and at an angle of attack, the following are known quantities: M_∞, P_∞, T_∞, μ_∞, γ_∞, α and δ_c. Using S, the arc length measured from the stagnation point along a streamline, as the independent variable, the initial values for x^*_i, ϕ_i, θ_i, $(\frac{\partial\theta}{\partial\beta})_i$ and h_{2_i} are obtained from the geometric solution in Appendix A. The initial point is chosen one step size from the stagnation point, i.e., $S_i/R_\circ = 0.01$.

There are three kinds of constants in the program, i.e., (a) input constants which depend on the body shape, flight conditions and selected flow parameters, (b) functional constants which are calculated by the equations in Section VI from known input constants, and (c) defined constants which are defined for the purpose of simplifying the calculation.

The input constants are: M_∞, P_∞, T_∞, μ_∞, γ_∞, $\bar{\gamma}$, α, δ_c, R_g, Pr, T_w/T_o and ω.

The functional constants are: P_∞/P_o, x_o^*, f_o, f_o', f_o'', R_o, x_j^*, f_j, f_j', M_q, P_q/P_o, δ_q and ν_q.

The defined constants are: C, C_k, C_ℓ, g, C_q, C_{qr}, and C_{qt}.

C-2 Integration of the Heating Rate Equations

A.2.1 Laminar Heating Rates

Equation (10) of Section 6.2 is

$$\frac{\dot{q}_w}{\dot{q}_{w_o}} = \frac{\frac{P}{P_o}\frac{u_e}{V_\infty} h_2 R_o^{1/2}}{[\int_o^S \frac{P}{P_o}\frac{u_e}{V_\infty} h_2^2 \, dS]^{1/2} 2G} \tag{C-1}$$

where r is replaced by h_2. From the isentropic flow relation with an effective $\bar{\gamma}$, there results, according to Lees,

$$\frac{u_e}{V_\infty} = \sqrt{[1 + \frac{2}{(\gamma_\infty-1)M_\infty^2}][1 - (\frac{P}{P_o})^g]}$$

$$= C_\ell^{1/2} [1 - (\frac{P}{P_o})^g]^{1/2} \tag{C-2}$$

where

$$g = \frac{\bar{\gamma}-1}{\bar{\gamma}}, \quad C_\ell = 1 - \frac{2}{(\gamma_\infty-1)M_\infty^2}$$

G is given in Eq. (11) of Section 6.2. Using the defined constants, one has

$$G = (gC_\ell C)^{1/4} \quad \text{where} \quad C = 1 - P_\infty/P_o$$

After simplifying, the ratio of laminar heating rate at the surface to that at the stagnation point becomes

$$\frac{q_w}{q_{w_o}} = \frac{C_q W h_2}{[\int_o^S W h_2^2 \, dS]^{1/2}} \tag{C-3}$$

where

$$C_q = \frac{R_o^{1/2}}{2(Cg)^{1/4}} \tag{C-3a}$$

$$W = \frac{P}{P_o}\,[1 - (\frac{P}{P_o})^g]^{1/2} \tag{C-3b}$$

The denominator in Eq. (C-3) is integrated numerically by Simpson's one-third rule with h_2 obtained from a subprogram described in the next section. The initial value of the integral is obtained by using the same approach described in Appendix B, i.e., let

$$\varepsilon = x_1^* - x_o^*, \quad |\varepsilon| << 1$$

$$\phi_1 = A_\infty |\varepsilon|^{a_o}$$

$$h_2 = B_\infty |\varepsilon|^b$$

$$f_1 = f_o + f_o'\varepsilon$$

$$f_1' = f_o' + f_o''\varepsilon$$

$$f_1'' = f_o'' + f_o'''\varepsilon$$

$$dS = \sqrt{(dx)^2 + (fd\phi)^2}$$

$$= \sqrt{1 + f'^2 + A_\infty^2 a_o^2 f_i^2 |\varepsilon|^{2a_o-2}}\, d\varepsilon$$

then

$$I_i = \int_o^S W_i h_{2_i}^2 dS = \int_o^\varepsilon WB_\infty^2 |\varepsilon|^{2a_o} \sqrt{1 + f_i'^2 + A_\infty^2 a_o^2 f_i^2 |\varepsilon|^{2a_o-2}}\, d\varepsilon \qquad \text{(C-5)}$$

With the use of Eq. (50) for the surface pressure, it can be seen that

$$\frac{A_\infty^2 a_o^2 f_o^2}{1 + f_o'^2} |\varepsilon|^{2a_o-2} << 1$$

Hence,

$$I_i \simeq -B_\infty^2 g^{1/2} f_o'' \sin\alpha |\varepsilon|^{2a_o} \{\frac{\varepsilon^2}{2(a_o+1)} + \frac{K_1|\varepsilon|2a_o}{8a_o} - \frac{K_2}{2}[\frac{\varepsilon^4}{a_o+2} + \frac{K_1|\varepsilon|^{2a_o+2}}{4a_o+2}]\} \qquad \text{(C-6)}$$

where

$$K_1 = \frac{A_\infty^2 a_o^2 f_o^2}{1+f_o'^2}, \qquad K_2 = \frac{f_o''^2 \sin^2\alpha}{1+f_o'^2}$$

Since the value of the right-hand side is of order of ε^4, I_i is seen to be negligibly small compared with the value of the first integration from the initial point. (It requires two increments to perform one integration in using Simpson's one-third rule.) Hence, in practice, it is appropriate to assume that the heating rates ratio is very close to unity at the initial point,

$$\left(\frac{\dot{q}_w}{\dot{q}_{w_o}}\right)_i \simeq 0.999$$

then

$$I_i = \int_0^S W_i h_{2_i}^2 \, dS \simeq \left(\frac{C_q W_i h_{2_i}}{0.999}\right)^2 \tag{C-7}$$

Equation (C-7) is comparable with Eq. (C-6) since both W_i and h_{2_i} are of order of ε and thus $(W_i h_{2_i})^2 = O(\varepsilon^4)$.

C.2.2 Turbulent Heating Rates Expression I

Equations (15), (16), and (17) of Section 6.2.2 are:

$$\frac{\dot{q}_w}{\dot{q}_{w_o}} = \frac{\rho_e u_e \mu_e R_o^{1/2} C_f^*}{\sqrt{2\rho_o \mu_o V_\infty} G \mu_r} \tag{C-8}$$

$$\ln C_f^* + Z = 0.4\sqrt{2}\, C_f^{*-1/2} \tag{C-9}$$

$$Z \equiv \ln\left[\frac{2.62 H_e^{1/2}}{\nu_r h_2} \int_0^S \frac{\rho_e}{\rho_r} \frac{u_e}{H_e^{1/2}} \frac{\mu_e}{\mu_r} h_2 dS\right] \tag{C-10}$$

Using the energy equation

$$\frac{1}{2} V_\infty^2 + h_\infty = H_e$$

one obtains

$$H_e^{1/2} = \frac{V_\infty}{\sqrt{2}}\left[1 + \frac{2}{(\gamma_\infty - 1)M_\infty^2}\right]^{1/2} = \left(\frac{C_\ell}{2}\right)^{1/2} V_\infty$$

As mentioned in Section 6.2.2, it is appropriate to evaluate the reference condition quantities at the stagnation state of the external flow. Thus,

$$\frac{\rho_e \mu_e}{\rho_r \mu_r} = \frac{\rho_e \mu_e}{\rho_o \mu_o} = \left(\frac{P}{P_o}\right)^{\frac{1}{\gamma}+g\omega}, \quad \frac{V_\infty}{\nu_r} = \frac{V_\infty \rho_o}{\mu_o}$$

where

$$\frac{\mu_e}{\mu_o} = \left(\frac{T_e}{T_o}\right)^{\omega}$$

is used. Upon substitution of these equations, Eq. (C-10) becomes

$$Z = \ln\{2.62C_\ell^{1/2}\left(\frac{P_o V_\infty}{\mu_o}\right)\frac{1}{h_2} \times$$

$$\int_o^S \left(\frac{P}{P_o}\right)^{\frac{1}{\gamma}+g\omega}\left[1 - \left(\frac{P}{P_o}\right)^{g}\right]^{1/2} h_2 dS\} \qquad \text{(C-11)}$$

where Eq. (C-2) has been used for u_e/V_∞.

For Eq. (C-8),

$$\frac{\rho_e u_e \mu_e}{\mu_r} = \frac{\rho_e u_e \mu_e}{\mu_o} = \rho_o V_\infty \left(\frac{P}{P_o}\right)^{\frac{1}{\gamma}+g\omega} \frac{u_e}{V_\infty}$$

therefore, Eq. (C-8) becomes

$$\frac{\dot{q}_w}{\dot{q}_{w_o}} = C_{qt}\left(\frac{P}{P_o}\right)^{\frac{1}{\gamma}+g\omega} \frac{u_e}{V_\infty} C_f^* \qquad \text{(C-12)}$$

where

$$C_{qt} = \frac{1}{\sqrt{2}(CgC_\ell)^{1/4}}\left(\frac{\rho_o V_\infty R_o}{\mu_o}\right)^{1/2} \qquad \text{(C-13)}$$

For a known surface pressure distribution and scale factor, Z is readily evaluated from Eq. (C-11). Once Z is known, C_f^* is d[illegible]mined by Eq. (18) in Section 6.2.2. The constant coefficients are o[illegible]ned with the aid of Eq. (C-9) for $2 \leq Z \leq 14$

$$C_f^* = 0.001052 - \frac{0.05617}{Z} + \frac{1.5243313}{Z^2} - \frac{6.3495944}{Z^3}$$

$$+ \frac{90.863065}{Z^4} - \frac{268.7737}{Z^5} \qquad \text{(C-14)}$$

The plot of C_f* vs. Z is shown in Fig. 33. Finally, the right side of Eq. (C-8) is found upon substitution.

C.2.3 Turbulent Heating Rates Expression II

Eq. (33) of Section 6.2.3

$$\frac{\dot{q}_w}{\dot{q}_{w_o}} = \frac{0.0417\,\rho_e^{1.05} u_e \mu_e^{0.8} \nu_r^{0.05} h_2^{0.25} R_o^{0.5}}{G(\rho_o V_\infty)^{0.5} \mu_o^{1.1}} \frac{1}{[\int_o^S \rho_e^{1.25} u_e \nu_r^{0.25} h_2^{1.25} dS]^{0.2}} \tag{C-15}$$

The reference properties in the above equation are evaluated with the aid of Eq. (14) in Section 6.2. To be consistent with Lees' derivation of the expression for u_e/V_∞ (Eq. (C-8)), where

$$h = \frac{\bar{\gamma}}{\bar{\gamma}-1} \frac{P}{\rho}$$

one may assume that the fluid is a perfect gas by using an effective specific ratio, $\bar{\gamma}$. Hence, Eq. (14-a) is used in the program with an adoptive $\bar{\gamma}$, and thus,

$$\frac{T_e}{T_o} = (\frac{P}{P_o})^g$$

$$M_e^2 = \frac{2}{\bar{\gamma}-1}[(\frac{P}{P_o})^{-g} - 1]$$

Then Eq. (14-a) becomes

$$\frac{T_r}{T_o} = 0.5(\frac{P}{P_o})^g + 0.5\,\frac{T_w}{T_o} + 0.22\,\sqrt[3]{Pr}\,[1 - (\frac{P}{P_o})^g] \tag{C-16}$$

Following the same procedure as previously, one obtains

$$\frac{\dot{q}_w}{\dot{q}_{w_o}} = \frac{C_{qr}\left(\frac{P}{P_o}\right)^{\frac{1.05}{\bar{\gamma}} + 0.8g\omega}\left(\frac{T_r}{T_o}\right)^{0.05(\omega - \frac{1}{\bar{\gamma}-1})}\frac{u_e}{V_\infty}\, h_2^{\,0.25}}{\left[\int_o^S \left(\frac{P}{P_o}\right)^{\frac{1.25}{\bar{\gamma}}}\frac{u_e}{V_\infty}\left(\frac{T_r}{T_o}\right)^{0.25(\omega - \frac{1}{\bar{\gamma}-1})} h_2^{\,1.25}\, dS\right]^{0.2}} \qquad \text{(C-17)}$$

where

$$C_{qr} = \frac{0.0417 R_o^{\,0.5}}{(CgC_\ell)^{0.25}} \left(\frac{\rho_o V_\infty}{\mu_o}\right)^{0.3} \qquad \text{(C-18)}$$

C.2.3 Reynolds Numbers

The Reynolds number based on local properties at the edge of boundary layer and a distance along a streamline from the stagnation point is

$$Re_s = \frac{\rho_e u_e S}{\mu_e}$$

Following the same procedure as in the previous section, one obtains,

$$Re_s = \frac{\rho_o V_\infty}{\mu_o}\left(\frac{u_e}{V_\infty}\right)\left(\frac{P}{P_o}\right)^{\frac{1}{\bar{\gamma}} - g\omega} S \qquad \text{(C-19)}$$

The Reynolds number based on local properties at the edge of boundary layer and the laminar momentum thickness is given by Eq. (34) as

$$Re_\theta = \frac{0.66\left[\int_o^S \rho_e u_e \mu_e h_2^2 dS\right]^{1/2}}{\mu_e h_2} \qquad \text{(C-20)}$$

where r has been replaced by h_2. To be consistent with Lees' theory, one assumes

$$\frac{\rho_e \mu_e}{\rho_o \mu_o} = \frac{P}{P_o}$$

Thus, Eq. (C-20) becomes

$$Re_\theta = \frac{0.66(\frac{\rho_o V_\infty}{\mu_o})^{1/2}[\int_o^S \frac{P}{P_o}\frac{u_e}{V_\infty} h_2^2\, dS]^{1/2}}{(\frac{T_e}{T_o})^\omega h_2}$$

Using Eq. (C-1) to eliminate the integral and h_2, it becomes

$$Re_\theta = \frac{0.66C_q C_\ell^{1/4}(\frac{\rho_o V_\infty}{\mu_o})^{1/2}(\frac{P}{P_o})^{1 - g\omega}[1 - (\frac{P}{P_o})^g]^{1/2}}{(\frac{\dot{q}_w}{\dot{q}_{w_o}})_{laminar}} \tag{C-21}$$

These Reynolds numbers are calculated for the purpose of locating a possible transition region.

C.3 Calculation of Streamline Geometry and Scale Factors

The hybrid surface pressure estimation technique forces the calculation of streamline geometry and scale factors to proceed from one region to another, according to the applicability of different theories described in Section 6.4.1. In consquence, a typical streamline will flow through five successive regions as follows:

(1) Modified Newtonian Region (M.N.) - In this region, the streamline lies between the stagnation point and the "matching point." The modified Newtonian pressure law is used for estimating surface pressures.

(2) Modified Newtonian and Prandtl-Meyer Mixed Region I (M.N. & P-M I) - After the "matching point," an interpolation formula for pressure distribution, Eq. (52), should be used. In this region, the streamline lies between the "matching point," corresponding to axial axis x_q^*,

and a point on the body surface corresponding to axial axis, x_1^*, such that $(P_{r,180})_{\alpha\neq o}$ along the leeward line falls in the Prandtl-Meyer region while $(P_r)_{\alpha=o}$ along the meridian line and $(P_{r,o})_{\alpha\neq o}$ along the windward line still remain in the Newtonian region.

(3) Modified Newtonian and Prandtl-Meyer Mixed Region II (M.N. & P-M II) - In this region the streamline lies between two points corresponding to axial coordinates x_1^* and x_2^*, respectively. The surface pressures along the leeward and meridian lines fall in the Prandtl-Meyer region while the windward line still remains modified Newtonian.

(4) Prandtl-Meyer Region (P-M) - In this region the streamline lies between two points corresponding to axial coordinates x_2^* and x_j^*. The Prandtl-Meyer relations are then applied to all three (leeward, meridian and windward) lines.

(5) Second-Order Shock Expansion Over Conical Surface - Over the cone surface, the second-order shock expansion method, Eqs. (54) is used for estimating surface pressures along the leeward, meridian and windward lines. Eq. (56) is employed for interpolation. The functions A, B, and E in Eq. (56) are determined with pressures along the above three lines. The pressure along $\phi = 90°$ (meridian) line at an angle of attack is assumed to be that along the same line at zero angle of attack, as noted by ref. 13.

These regions are illustrated in the sketch on the next page.

The resulting expressions for pressure distribution and necessary differential equations for computation are shown in Charts C-1 and C-2. Note that the differential equations listed in Chart C-2 are also good

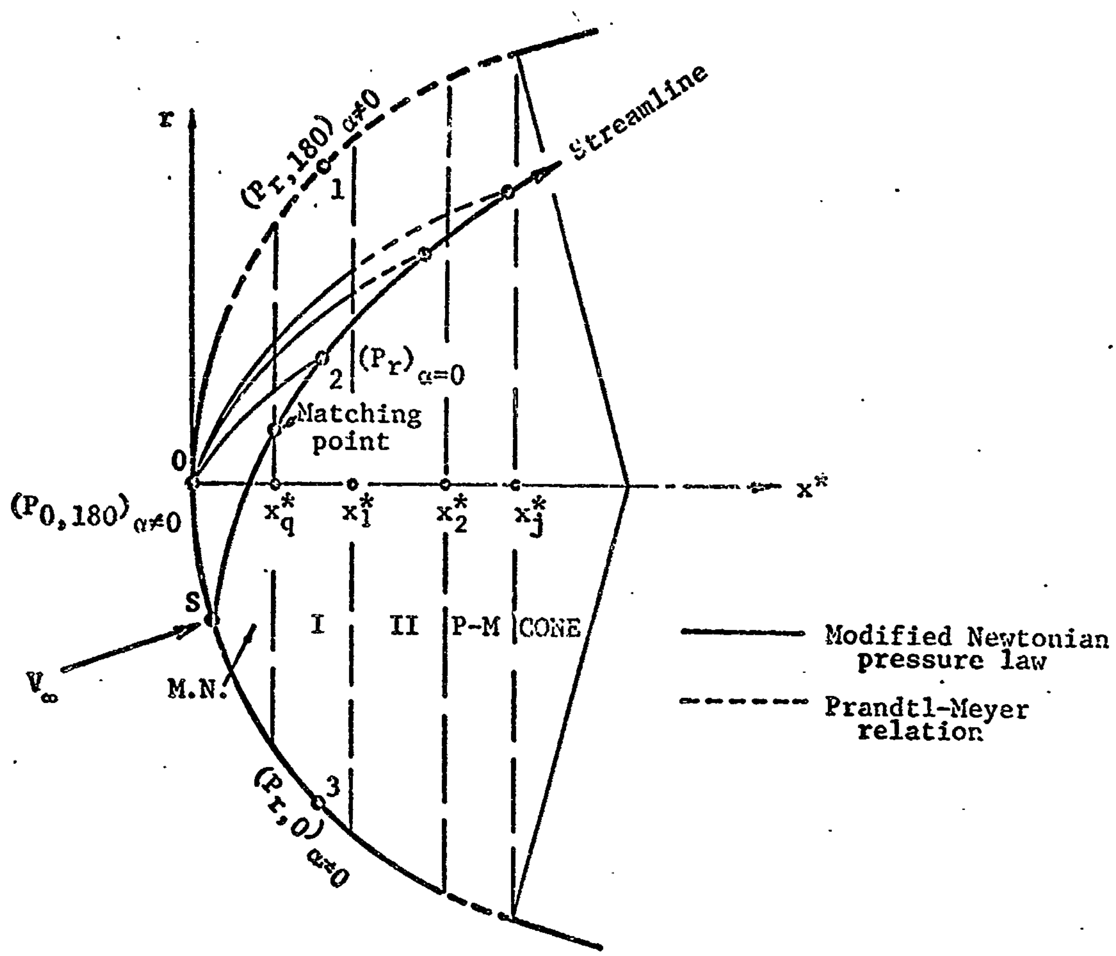

for a general body of revolution. The set of simultaneous differential equations is integrated along a streamline by fourth order Runge-Kutta method with the initial values determined by Eqs. (61). The significance of defining S_t, C_t and F's in Chart C-2 is twofold, i.e., to reduce the computer time drastically and to eliminate chances of making mistakes.

The above five regions with different pressure conditions result in five separate subprograms. As the streamline proceeds in the main program, one of the above subprograms is call according to the region the streamline will fall in.

The boundaries of each region, x_q^*, x_1^*, x_2^* vary with M_∞, α and body shape and differ from one streamline to another; nevertheless, they are determined solely by the matching criteria δ_q or $(P/P_o)_q$ along the streamline, or meridian or windward line.

Chart C-1 Basic equations for calculating streamline geometry and scale factor over a spherically blunted cone

Region	Body shape	Expression for pressure distribution	Differential equations used**
M.N.	$f = \sqrt{2x^* - x^{*2}}$	$\frac{P}{P_o} = \frac{C(f'\cos\alpha + \sin\alpha\cos\phi)^2}{1 + f'^2} + C_k$	(I),(II),(III),(IV),(V)
M.N. & P-M I	Same as above	$\frac{P}{P_o} = [\frac{C(f'\cos\alpha + \sin\alpha)^2}{1 + f'^2} + C_k]\frac{\cos^2\phi + \cos\phi}{2} + \frac{P_1}{P_o}\frac{\cos^2\phi - \cos\phi}{2} + P^\circ(\frac{Cf'}{1+f'^2} + C_k)\sin^2\phi$	(I),(II),(III),(IV),(V) (VI)
M.N. & P-M II	Same as above	$\frac{P}{P_o} = [\frac{C(f'\cos\alpha + \sin\alpha)^2}{1 + f'^2} + C_k]\frac{\cos^2\phi + \cos\phi}{2} + \frac{P_1}{P_o}\frac{\cos^2\phi - \cos\phi}{2} + P^\circ(\frac{P_2}{P_o})\sin^2\phi$	(I),(II),(III),(IV),(V) (VI),(VII)
P-M	Same as above	$\frac{P}{P_o} = \frac{P_1}{P_o}\frac{\cos^2\phi - \cos\phi}{2} + P^\circ(\frac{P_2}{P_o})\sin^2\phi + (\frac{P_3}{P_o})\frac{\cos^2\phi + \cos\phi}{2}$	(I),(II),(III),(IV),(V) (VI),(VII),(VIII)
CONE	$f = f_j + f'_j\zeta$	$\frac{P}{P_o} = A\cos\phi + B + E\cos 2\phi$	(I),(II),(III),(IV),(V)

** The corresponding equations are listed in Chart C-2

where

$A = 0.5(b_{03} - b_{01} + b_3 e^{-c_3\zeta} - b_1 e^{-c_1\zeta})$

$B = 0.25(b_{01} + 2b_{02} + b_{03} + b_1 e^{-c_1\zeta} + 2b_2 e^{-c_2\zeta} + b_3 e^{-c_3\zeta})$

$E = B - b_{02} - b_2 e^{-c_2\zeta}$

$\zeta = x^* - x^*_j \qquad P^\circ = C\cos^2\alpha + C_k$

$b_{0\sigma} = (\frac{P_c}{P_o})_\sigma, \quad \sigma = 1, 2, 3$

$b_\sigma = (\frac{P_j}{P_o} - \frac{P_c}{P_o})_\sigma, \quad \sigma = 1, 2, 3$

$c_\sigma = [(\frac{\partial P}{\partial x^*})_j \frac{1}{P_c - P_j}]_\sigma, \quad \sigma = 1, 2, 3$

Chart C-2 Differential equations for calculating streamline geometry and scale factor over a blunted cone

Equation number	Differential equations
(I)	$\frac{Dx^*}{DS} = \frac{C_t}{F}$
(II)	$\frac{D\phi}{DS} = \frac{S_t}{f}$
(III)	$\frac{D\theta}{DS} = \frac{F_e S_t - F_f C_t}{F_g} - \frac{f' S_t}{fF}$
(IV)	$\frac{Dh_2}{DS} = \frac{\partial\theta}{\partial\beta} + \frac{h_2 f' C_t}{fF}$
(V)	$\frac{D}{DS}\left(\frac{\partial\theta}{\partial\beta}\right) = -\frac{f' C_t}{fF}\left(\frac{\partial\theta}{\partial\beta}\right) + h_2\left[\frac{S_t^2(ff''-f'^2F)}{(fF)^2} - \frac{D\theta}{DS}\left(\frac{D\theta}{DS} + \frac{f'S_t}{fF}\right)\right]$ $+ \frac{1}{F_g}\left[(F_e C_t + F_f S_t)\frac{\partial\theta}{\partial\beta} - h_2\left(F_h S_t + \frac{F_k C_t^2}{f}\right)\right.$ $\left. + h_2 C_t S_t\left(\frac{F_i}{f} + F_j\right) - \frac{F_\ell}{F_g}(F_e S_t - F_f C_t)\right]$
(VI)	$\frac{D}{DS}\left(\frac{P_1}{P_o}\right) = \frac{f''}{F^3}\,\frac{\bar{\gamma}M_1^2}{\sqrt{M_1^2 - 1}}\left(\frac{P_1}{P_o}\right)$
(VII)	$\frac{D}{DS}\left(\frac{P_2}{P_o}\right) = \frac{f''}{F^3}\,\frac{\bar{\gamma}M_2^2}{\sqrt{M_2^2 - 1}}\left(\frac{P_2}{P_o}\right)$
(VIII)	$\frac{D}{DS}\left(\frac{P_3}{P_o}\right) = \frac{f''}{F^3}\,\frac{\bar{\gamma}M_3^2}{\sqrt{M_3^2 - 1}}\left(\frac{P_3}{P_o}\right)$

where

$F = \sqrt{1 + f'^2}$

$F_e = \frac{1}{PF}\frac{\partial P}{\partial x^*}$

$F_f = \frac{1}{Pf}\frac{\partial P}{\partial \phi}$

$F_g = \bar{\gamma}M^2$

$F_h = \frac{1}{F}\frac{\partial}{\partial x^*}\left(\frac{1}{PF}\frac{\partial P}{\partial x^*}\right)$

$F_i = \frac{\partial}{\partial\phi}\left(\frac{1}{PF}\frac{\partial P}{\partial x^*}\right)$

$F_j = \frac{1}{F}\frac{\partial}{\partial x^*}\left(\frac{1}{Pf}\frac{\partial P}{\partial\phi}\right)$

$F_k = \frac{\partial}{\partial\phi}\left(\frac{1}{Pf}\frac{\partial P}{\partial\phi}\right)$

$F_\ell = h_2\left[\frac{C_t}{f}\frac{\partial F_g}{\partial\phi} - \frac{S_t}{F}\frac{\partial F_g}{\partial x^*}\right]$

$M^2 = \frac{2}{\bar{\gamma}-1}\left[\left(\frac{P}{P_o}\right)^{-\frac{\bar{\gamma}-1}{\bar{\gamma}}} - 1\right]$

$S_t = \sin\theta$

$C_t = \cos\theta$

Appendix D

Computer Program for Calculating Streamline, Scale Factor, and Laminar and Turbulent Heating Rates over a Spherically Blunted Cone at an Angle of Attack

The complete computer program for calculating the streamline geometry, scale factors and laminar and turbulent heating rates over a spherically blunted cone is written very closely following the procedure described in Appendix C. The following correspondences are observed:

(1) "MAIN" program corresponds to

A.1 Evaluation of the initial conditions and constants, and

A.2 Integration of the heating rates equations.

(2) "RUN1" subprogram corresponds to

A.3.(1) Calculation of streamline geometry and scale factors in Modified Newtonian Region

(3) "RUN2" subprogram corresponds to

A.3.(2) Calculation of streamline geometry and scale factors in Modified Newtonian and Prandtl-Meyer Mixed Region I

(4) "RUN3" subprogram corresponds to

A.3.(3) Calculation of streamline geometry and scale factors in Modified Newtonian and Prandtl-Meyer Mixed Region II

(5) "RUN4" subprogram corresponds to

A.[illegible] Calculation of streamline geometry and scale factors in Prandtl-Meyer Region

(6) "RUN5" subprogram corresponds to

A.3.(5) Calculation of streamline geometry and scale factors over cone surface.

(7) "COLLAR" subprogram corresponds to the evaluation of initial pressure for integrating the Prandtl-Meyer relations, Eq. (57).

2065 T C TAI FORTRAN SOURCE LIST

ISN SOURCE STATEMENT

```
$IBFTC MAIN
C
C      PROGRAM FOR CALCULATING STREAMLINE, SCALE FACTORS, AND LAMINAR
C      AND TURBULENT HEATING RATES OVER A SPHERICALLY BLUNTED CONE AT
C      AN ANGLE OF ATTACK AT HIGH SPEEDS
C
      COMMON C,CK,CA,SA,GAM,G,H,PC,XJ,FJ,DFJ /BBC/BO1,BO2,BO3,
     1 B1,B2,B3,C1,C2,C3
      EXTERNAL NOLFUN
      DIMENSION SM(3), SM1(3), SM2(3)
   10 READ (5, 501) BO1, B1, C1, BO2, B2, C2, TMD
      READ (5, 501) BO3, B3, C3, ALPHA, CR1, CR2, RE
      READ (5, 501) FM, GAM, POO, TOO, PR, CM, TW, V
      READ (5, 505) K
      AL = ALPHA/57.2957795
      SA = SIN(AL)
      CA = COS(AL)
      G = (GAM  -1.)/GAM
      CG = 1./GAM - G*CM
      CK = (2./((GAM + 1.)*FM*FM))**(1./G)*((2.*GAM*FM*FM - GAM +1.)/
     1 (GAM + 1.))**(1./(GAM - 1.))
      C = 1. - CK
      FO = C*CA*CA + CK
      DFO = CA/SA
      FC = SA
      XO = 1. - CA
      DDFO = -1. /FO**3
      RS = 1.0
      A = 1.0
      TM = TMD/57.2957795
      XJ = 1. - COS(TM)
      FJ = SQRT(2.*XJ - XJ*XJ)
      DFJ = (1. - XJ) /FJ
      RMQ=1.3520894+1.2554079*CK+12.451517*CK*CK-162.76788*CK**3
      PQ = (2./(2. + (GAM - 1.)*RMQ*RMQ))**(1./G)
      DELQ = ARSIN(SQRT((PQ - CK)/C))
      CN = TAN(DELQ)
      CB = TAN(DELQ - AL)
      RNUQ = SQRT(( GAM+ 1.)/(GAM - 1.))*ATAN(SQRT((GAM - 1.)*
     1 (RMQ*RMQ - 1.) / (GAM + 1.)))- ATAN(SQRT(RMQ*RMQ - 1.))
   20 WRITE (6, 601) FM, GAM, POO, TOO, PR,      TW, V, ALPHA, XO, RS,
     1 FO, DFO, DDFO, A, CR1, CR2, RE, CM
      WRITE (6, 602)
      WRITE (6, 620) CK, RMQ, PQ, DELQ, RNUQ, TMD, XJ, FJ
C
C      LAMINAR HEAT TRANSFER BY LESTER LEES
      WF(Y) = Y* SQRT(1.  -Y**G)
      CQ = SQRT(RS)/(2.*(C*G)**0.25)
C
C      TURBULENT HEAT TRANSFER BY VAGLIO-LAURIN
      TRF(Y) = (CR1 - RECOV)*Y**G + RECOV + CR2*TW
      UF(Y) = SQCL*W/Y
      ZF(SINT, R) = ALOG(2.62*URM/R*SINT)
      CF1(ZR) = 0.00206219 - 0.02348014*ZR - 0.17993221*ZR*ZR +
     1 17.36162*ZR**3 - 49.932948*ZR**4 + 44.817625*ZR**5
```

```
312065           T  C  TAI                    FORTRAN SOURCE LIST MAIN
  ISN         SOURCE STATEMENT

              CF2(ZR) = 0.C01052 - C.05617*ZR + 1.5243313*ZR*ZR -
            1 6.3495944*ZR**3 + 90.863065*ZR**4 - 268.7737*ZR**5
              RG = 1717.55C65
              RECOV = RE   *PR**0.33333333
              CL = 1. + 5./FM**2
              SQCL = SQRT(CL)
              GG = 1./(GAM - 1.) - CM
              GR = 1./(GAM - 1.) + CM
              GP = 1./GAM + G*CM
              URM = 2.**(1.+CM) * PCC/( CK*V*SQRT(RG*TCC)*(G*CL)**(1. + CM)
            1 *1.4**(0.5 + CM) *FM**(1.+2.*CM))
              CQT = SQRT(RS*URM/2.) / (C*G*CL)**0.25
        C
        C     TURBULENT HEAT TRANSFER BY TRANSFORMATION
              G2 = 0.05*(CM - 1./(GAM - 1.))
              G4 = 0.25*(CM - 1./(GAM - 1.))
              GN = 1.05/GAM + C.8*G*CM
              GD = 1.25/GAM
              FNF(Y) = Y** GN * TR**G2 * U * R**0.25
              FDF(Y) = Y** GD * TR**G4 * U * R**1.25
              CQR =0.0417*SQRT(RS)*URM**0.2/(G*C*CL)**0.25
        C
              CREM = 0.66* CG*SQRT(CL**0.5*URM)
        C
              WRITE (6, 633) RECOV, CL, URM, CG, CQT, CQR, CREM
              DO 490 M = 1, K
              SM1(1) = 0.0
              SM2(1) = 0.0
              SIM1 = 0.0
              SIM2 = 0.0
           25 READ (5, 501) BD, H, XED, PED, FACTOR
              S = 0.01
           30 WRITE (6, 612)
              B = BD/57.2957795
              XS = ARCOS(CA*COS(S) + SA*SIN(S)*COS(B))
              X = 1. - COS(XS)
              P = ARSIN(SIN(S)*SIN(B)/SIN(XS))
              IF(BD.GT.90.) P =ARCOS(( COS(S)- COS(XS)*CA)/( SIN(XS)*SA))
              T = ARSIN(SA*SIN(B)/SIN(XS))
              IF(BD.LT.90.) T = ARCOS((CA- COS(S)* COS(XS))/( SIN(S)* SIN(XS)))
              R = SIN(S)
              TB = R* SIN(T)*TAN(T)/TAN(XS)-SA* COS(B)/SIN(XS)/ COS(T)
              PD = P * 57.2957795
              TD = T * 57.2957795
              WRITE (6, 610) H, BD
              WRITE ( 6, 616) S, X, PD, TD, R
              CALL RUN1   (X, P, T, R, TB,     XA,PA,TA,RA,TBA)
              X = X + XA
              P = P + PA
              T = T + TA
              R = R + RA
              TB = TB + TBA
              DF = (1. - X)/SQRT(2.*X - X*X)
              Y   = C*(DF*CA + SA*COS(P))**2/(1. + DF*DF) + CK
              W = WF(Y)
```

ISN SOURCE STATEMENT

```
      U = UF(Y)
      SM (1) = W*R*R
      Q = 0.999
      SIM = (CQ*W*R/Q)**2
      REYS = URM*Y**CO*U*S
      REYM = CREM*W/( Y**(G*CM)*Q)
      PD = P * 57.2957795
      TD = T * 57.2957795
      S = S + H
      WRITE(6, 616) S, X, PD, TD, R, Y, REYM, REYS, Q
      TT = ARSIN(SA*SIN(B)/SIN(TM))
      SS = 2.*ATAN(TAN((TM+AL)/2.)*COS((B+TT)/2.)/COS((B-TT)/2.)) -2.*H
      NN = SS/H/2.
      RNN = NN
      H = H + (SS - RNN*H*2.) / (2.*RNN)
      DO 39 L = 1, NN
      DO 36 N = 2, 3
      CALL RUN1   (X, P, T, R, TB,     XA,PA,TA,RA,TBA)
      X = X + XA
      P = P + PA
      T = T + TA
      R = R + RA
      TB = TB + TBA
      DF = (1. - X)/SQRT(2.*X - X*X)
      Y   = C*(DF*CA + SA*COS(P))**2/(1. + DF*DF) + CK
      W = WF(Y)
      U = UF(Y)
      TR = TRF(Y)
      SM (N) = W*R*R
      SM1(N) = U*Y**GP*R
      SM2(N) = FDF(Y)
   36 S = S + H
      PD = P * 57.2957795
      TD = T * 57.2957795
      SIM  = SIM  + H*(SM (1) + 4.*SM (2) + SM (3))/3.
      SIM1 = SIM1 + H*(SM1(1) + 4.*SM1(2) + SM1(3))/3.
      SIM2 = SIM2 + H*(SM2(1) + 4.*SM2(2) + SM2(3))/3.
      Q = CQ*W*R / SQRT(SIM)
      ZR = 1./ZF(SIM1, R)
      Q1 = CQT*Y**GP*U*CF1(ZR)
      Q2 = CQR*FNF(Y)/SIM2**0.2
      REYS = URM*Y**CO*U*S
      REYM = CREM*W/( Y**(G*CM)*Q)
      WRITE(6, 616) S, X, PD, TD, R, Y, REYM, REYS, Q, Q1, Q2
      SM (1) = SM (3)
      SM1(1) = SM1(3)
      SM2(1) = SM2(3)
   40 IF (Y  .LT. PQ) GO TO 50
   39 IF (X .GE. XJ) GO TO 400
   50 RNU = RNUO + DELO + AL - ATAN(DF)
      CALL COLLAR (GAM, G, RMO, RNU, PT)
      WRITE (6, 604)
      WRITE (6, 620) DF, PT, RNU, Y
      IF (DF.LE. CM) GO TO 92
      NN = NN - L
```

```
12065          T  C  TAI                    FORTRAN SOURCE  LST MAIN
  ISN        SOURCE STATEMENT

             DO 90 L = 1, NN
             DO 70 N = 2, 3
             CALL RUN2   (X, P, T, R, TB, PT,XA,PA,TA,RA,TBA, PTA)
             X = X + XA
             P = P + PA
             T = T + TA
             R = R + RA
             TB = TB + TBA
             PT = PT + PTA
             DF = (1. - X)/SQRT(2.*X - X*X)
             YA = SQRT(1. + DF*DF)
             CP = COS(P)
             Y        =(C*((DF*CA+SA)/YA)**2+CK)*(CP    **2 +CP     )/2. +  PT*
            1 (CP    **2 -CP     )/2. +PO          *(C*(DF/YA)**2 +CK)*SIN(P)**2
             W = WF(Y)
             U = UF(Y)
             TR = TRF(Y)
             SM (N) = W*R*R
             SM1(N) = U*Y**CP*R
             SM2(N) = FDF(Y)
          70 S = S + H
             PD = P * 57.2957795
             TD = T * 57.2957795
             SIM  = SIM  + H*(SM (1) + 4.*SM (2) + SM (3))/3.
             SIM1 = SIM1 + H*(SM1(1) + 4.*SM1(2) + SM1(3))/3.
             SIM2 = SIM2 + H*(SM2(1) + 4.*SM2(2) + SM2(3))/3.
             Q = CQ*W*R / SQRT(SIM)
             ZR = 1./ZF(SIM1, R)
             Q1 = COT*Y**CP*U*CF2(ZR)
             Q2 = CQR*FNF(Y)/SIM2**0.2
             REYS = URM*Y**CQ*U*S
             REYM = CREM*W/( Y**(Q*CM)*Q)
             WRITE(6, 616) S, X, PD, TD, R, Y, REYM, REYS, Q, Q1, Q2
             SM (1) = SM (3)
             SM1(1) = SM1(3)
             SM2(1) = SM2(3)
             IF (X .GE. XJ) GO TO 400
          90 IF (DF.LE. CM    ) GO TO 92
          92 RNU = RNUQ + DELQ        - ATAN(DF)
             CALL CELLAR (GAM, G, RMQ, RNL, PM)
             WRITE (6, 606)
             WRITE (6, 620) DF, PM, RNU, Y
             NN = NN - L
             DO 98 L = 1, NN
             DO 95 N = 2, 3
             CALL RUN3   (X, P, T, R, TB, PT,PM, XA,PA,TA,RA,TBA,PTA,PMA)
             X = X + XA
             P = P + PA
             T = T + TA
             R = R + RA
             TB = TB + TBA
             PT = PT + PTA
             PM = PM + PMA
             DF = (1. - X)/SQRT(2.*X - X*X)
             YA = SQRT(1. + DF*DF)
```

```
12065          T  C  TAI                   FORTRAN SOURCE LIST MAIN
   ISN        SOURCE STATEMENT

   332        CP = COS(P)
   333        Y               = (C*((DF*CA+SA)/YA)**2 +CK)*(CP    **2 + CP    )/2.
             1 + PT*(CP    **2 - CP    )/2. + PO            *PM*SIN(P)**2
   334        W = WF(Y)
   335        U = UF(Y)
   336        TR = TRF(Y)
   337        SM (N) = W*R*R
   340        SM1(N) = U*Y**CP*R
   341        SM2(N) = FDF(Y)
   342     95 S = S + H
   344        PD = P * 57.2957795
   345        TD = T * 57.2957795
   346        SIM  = SIM  + H*(SM (1) + 4.*SM (2) + SM (3))/3.
   347        SIM1 = SIM1 + H*(SM1(1) + 4.*SM1(2) + SM1(3))/3.
   350        SIM2 = SIM2 + H*(SM2(1) + 4.*SM2(2) + SM2(3))/3.
   351        C = CQ*W*R / SQRT(SIM)
   352        ZR = 1./ZF(SIM1, R)
   353        C1 = CCT*Y**CP*U*CF2(ZR)
   354        C2 = CCR*FNF(Y)/SIM2**0.2
   355        REYS = URM*Y**CG*U*S
   356        REYM = CREM*W/( Y**(G*CM)*Q)
   357        WRITE(6, 616) S, X, PD, TD, R, Y, REYM, REYS, C, C1, C2
   360        SM (1) = SM (3)
   361        SM1(1) = SM1(3)
   362        SM2(1) = SM2(3)
   363        IF (X .GE. XJ) GO TO 400
   366     98 IF ( DF .LE. CE ) GO TO 100
   372    100 RNU = RNUC + DELC -AL   - ATAN(DF)
   373        CALL COLLAR (GAM, G, RMC, RNU, PB)
   374        WRITE (6, 608)
   375        WRITE (6, 620) DF, PB, RNU, Y
   376        NN = NN - L
   377        DO 108 L = 1, NN
   400        DO 105 N = 2, 3
   401        CALL RUN4   (X, P, T, R, TB, PT,PM,PB,XA,PA,TA,RA,TBA,PTA,PMA,PBA)
   402        X = X + XA
   403        P = P + PA
   404        T = T + TA
   405        R = R + RA
   406        TB = TB + TBA
   407        PT = PT + PTA
   410        PM = PM + PMA
   411        PB = PB + PBA
   412        CP = COS(P)
   413        Y                  = 0.5*(( PB+PT)*CP     **2 + (PB-PT)*CP     ) +
             1 PO*PM*SIN(P)**2
   414        W = WF(Y)
   415        U = UF(Y)
   416        TR = TRF(Y)
   417        SM (N) = W*R*R
   420        SM1(N) = U*Y**CP*R
   421        SM2(N) = FDF(Y)
   422    105 S = S + H
   424        PD = P * 57.2957795
   425        TD = T * 57.2957795
```

```
12065          T  C  TAI                    FORTRAN SOURCE LIST MAIN
  ISN       SOURCE STATEMENT

  426       SIM  = SIM  + H*(SM (1) + 4.*SM (2) + SM (3))/3.
  427       SIM1 = SIM1 + H*(SM1(1) + 4.*SM1(2) + SM1(3))/3.
  430       SIM2 = SIM2 + H*(SM2(1) + 4.*SM2(2) + SM2(3))/3.
  431       Q = CQ*W*R / SQRT(SIM)
  432       ZR = 1./ZF(SIM1, R)
  433       Q1 = CQT*Y**GP*U*CF2(ZR)
  434       Q2 = CQR*FNF(Y)/SIM2**0.2
  435       REYS = URM*Y**CG*U*S
  436       REYM = CREM*W/( Y**(G*CM)*Q)
  437       WRITE(6, 616) S, X, PD, TD, R, Y, REYM, REYS, Q, Q1, Q2
  440       SM (1) = SM (3)
  441       SM1(1) = SM1(3)
  442       SM2(1) = SM2(3)
  443   108 IF ( X .GE. XJ ) GO TO 400
  447   400 H = H*FACTOR
  450       DF = DFJ
  451       WRITE (6, 610) H, BD
  452   460 DO 465 L = 1, 800
  453       DO 463 N = 2, 3
  454       CALL RUN5   (X, P, T, R, TB,     XA,PA,TA,RA,TBA,Y)
  455       X = X + XA
  456       P = P + PA
  457       T = T + TA
  460       R = R + RA
  461       TB = TB + TBA
  462       W = WF(Y)
  463       U = UF(Y)
  464       TR = TRF(Y)
  465       SM (N) = W*R*R
  466       SM1(N) = U*Y**GP*R
  467       SM2(N) = FDF(Y)
  470   463 S = S + H
  472       PD = P * 57.2957795
  473       TD = T * 57.2957795
  474       SIM  = SIM  + H*(SM (1) + 4.*SM (2) + SM (3))/3.
  475       SIM1 = SIM1 + H*(SM1(1) + 4.*SM1(2) + SM1(3))/3.
  476       SIM2 = SIM2 + H*(SM2(1) + 4.*SM2(2) + SM2(3))/3.
  477       Q = CQ*W*R / SQRT(SIM)
  500       ZR = 1./ZF(SIM1, R)
  501       Q1 = CQT*Y**GP*U*CF2(ZR)
  502       Q2 = CQR*FNF(Y)/SIM2**0.2
  503       REYS = URM*Y**CG*U*S
  504       REYM = CREM*W/( Y**(G*CM)*Q)
  505       WRITE(6, 616) S, X, PD, TD, R, Y, REYM, REYS, Q, Q1, Q2
  506       SM (1) = SM (3)
  507       SM1(1) = SM1(3)
  510       SM2(1) = SM2(3)
  511   465 IF (X .GE. XED .OR. PD .GE. PED ) GO TO 490
  515   490 CONTINUE
  517       GO TO 10
  520   501 FORMAT ( 7F10.8, E10.4)
  521   505 FORMAT (I10)
  522   601 FORMAT (1H1,8HM(CC) = , F5.2, 3X, 12HGAMMA BAR = , F4.2, 3X,
           1 8HP(CC) = , F6.2, 3X, 8HT(CC) = , F6.2, 3X, 5HPR = , F4.2, 3X,
           2 8HTW/TO = , F4.2, 3X, 9HMU(CC) = , E10.4// 1X, 8HALPHA = , F4.1,
```

```
12065          T  C  TAI                    FORTRAN SOURCE LIST MAIN
  ISN         SOURCE STATEMENT

             3 3X, 5HXO = , F8.6, 3X, 5HRS = , F8.6, 5X, 5HFO = , F8.6, 3X,
             4 6HDFO = , F9.6, 3X, 7HDDFO = ,F11.6, 3X, 4HA = , F8.6//
             5 1X, 6HCR1 = , F4.2, 3X, 6HCR2 = , F4.2, 3X, 5HRE = , F4.2,
             6 3X, 8HOMEGA = , F4.2//)
   523     602 FORMAT (1X, 33HK, MO, PO, DELO, NUO, TMD, XJ, FJ)
   524     604 FORMAT (1X,51HLEEWARD    LINE IS IN P-M REGION   DF, PT, NU, P/PC)
   525     606 FORMAT (1X,51HZERO ALPHA LINE IS IN P-M REGION   DF, PM, NU, P/PC)
   526     608 FORMAT (1X,51HWINDWARD   LINE IS IN P-M REGION   DF, PB, NU, P/PC)
   527     610 FORMAT (/1X, 12HSTEP SIZE = , F7.4, 3X, 7HBETA = , F6.2/)
   530     612 FORMAT (1H1, 37X,
             1 58HCALCULATION OF STREAMLINE, SCALE FACTORS AND HEATING RATES//
             2 3X, 1HS,  9X, 1HX, 13X, 3HPHI, 11X, 5HTHETA, 10X, 1HH, 8X,
             3 4HP/PO, 4X, 6HREY(M), 2X, 11HREYNOLDS NO, 6X, 7HQ/QO(L), 6X,
             4 8HQ/QO(T1), 5X, 8HQ/QO(T2)/)
   531     616 FORMAT (1X, F7.4, 2X, F9.6, 4X, F10.6, 5X, F10.6, 3X,F10.6, 2X,
             1 F8.6, 2X, F6.2, 1X, E13.6, 5X, F8.6, 5X, F8.6, 5X, F8.6)
   532     620 FORMAT (1X, 8E16.8/)
   533     633 FORMAT(35H RECOV, CL, URM, CO, COT, COR, CREM/7E18.8)
   534    1000 STOP
   535         END
```

```
312065          T  C  TA1                    FORTRAN SOURCE LIST
  ISN       SOURCE STATEMENT

    0 $IBFTC RUN1
    1       SUBROUTINE RUN1   (X, P, T, R, TB, XA, PA, TA, RA, TBA)
    2       COMMON C,CK,CA,SA,GAM,G,F,PC, XJ, FJ, DFJ
    3       DIMENSION DX(6), DP(6), DT(6), DR(6), DTB(6)
    4       EXTERNAL NOLMUN
    5       FF(X) = SQRT(2.*X - X*X)
    6       FTB(                   R,TB) = -DF*  CT    *TB/(F*YA) + R*(    ST
           1 **2* (F*DDF-DF*DF*YA*YA)/ (F*YA*YA)**2 - TS*(TS+DF*ST/(F*YA)))
           2 +((YE*CT +YF*ST)*TB - R*(YH*ST*ST+YK*CT*CT/F) +R*ST*CT*(YI/F +YJ)
           3 -YL*(YE*ST - YF*CT)/YG)/YG
    7       DATA DX(1), DP(1), DT(1), DR(1), DTB(1) /5*0.0/
   10       DO 700 N = 2, 5
   11       ST =  SIN(T+DT(N-1)/2.)
   12       CT =  COS(T+DT(N-1)/2.)
   13       SP =  SIN(P+DP(N-1)/2.)
   14       CP =  COS(P+DP(N-1)/2.)
   15       F = FF      (X+DX(N-1)/2.)
   16       DF = (1. - (X+DX(N-1)/2.))/F
   17       DDF = -1./F**3
   20       DDDF = 3.  *DF/F**4
   21       YA =  SQRT(1.  +DF*DF)
   22       YB = DF*CA + SA*CP
   23       YC = CA - DF*SA*CP
   24       YD = C*YB*YB + CK*YA*YA
   25       YE = 2.  *C*DDF*YB*YC/(YA**2*YD)
   26       YF    = -2.  *C*SA* SP     *YB/(F*YD)
   27       YG = 2.  *((YA**2/YD)**G -1.   )/G
   30       YH     = DDF*YE*(DDDF/DDF**2 + CA/YB - SA* CP      /YC - 2.   *(C*YB*
           1  CA + CK*DF)/YC - 3.  *DF/YA**2)/YA
   31       YI     = YE*SA* SP     *(-1.  /YB +DF/YC + 2.   *C*YB/YD)
   32       YJ = YF*(DDF*CA/YB -DF/F -2.   *DDF*(C*YB*CA+CK*DF)/YD)/YA
   33       YK     = YF*( CP     / SP      +SA* SP     *(2.   *C*YB/YD-1.   /YB))
   34       YL       = 4.      *(YA**2/YD)**G* (DDF*ST*(YA**2*(C*YB*CA +CK*DF)/YD
           1 - DF)/YA**3 + C*YE*SA* SP     *CT/(F*YD)) *(R+DR(N-1)/2.)
   35       TS = (YE*ST - YF*CT)/YG - DF*ST/(F*YA)
   36       DX(N) = H*CT/YA
   37       DP(N) = H*ST/F
   40       DT(N)   TS*H
   41       DR(N) =H* (TB+DTB(N-1)/2.   + (R+DR(N-1)/2.)*DF*CT/(F*YA))
   42   700 DTB(N)=H*FTB( R+DR(N-1)/2., TB+DTB(N-1)/2.)
   44       XA  = ( DX(2) + ( DX(3) +  DX(4))*2. +  DX(5)) / 6.
   45       PA  = ( DP(2) + ( DP(3) +  DP(4))*2. +  DP(5)) / 6.
   46       TA  = ( DT(2) + ( DT(3) +  DT(4))*2. +  DT(5)) / 6.
   47       RA  = ( DR(2) + ( DR(3) +  DR(4))*2. +  DR(5)) / 6.
   50       TBA = (DTB(2) + (DTB(3) + DTB(4))*2. + DTB(5)) / 6.
   51       RETURN
   52       END
```

```
$12005               T  C  TAI                           FORTRAN SOURCE LIST
   ISN         SOURCE STATEMENT

     0 $IBFTC RUN2
     1         SUBROUTINE RUN2   (X, P, T, R, TB, PT,XA,PA,TA,RA,TBA, PTA)
     2         COMMON C,CK,CA,SA,GAM,G,H,PC
     3         DIMENSION DX(6), DP(6), DT(6), DR(6), DTB(6), DPT(6)
     4         EXTERNAL NCLFUN
     5          ZB(  PT) = DDF/YA**2* ((CA-DF*SA       )/YA**2 *C*(DF*CA+SA) *
              1 (CP     **2 +CP      ) + GAM   *RMT    /SQRT(RMT    - 1.)* PT*(CP     **
              2 2 - CP     )/2.+2.*C*DF*PD               /YA**2 *SP     **2)
     6          ZC(  PT)=SP    *(2.*PC              *(C*DF*DF/YA**2 +CK)* CP    -(CK+
              1 C*((DF*CA+SA)/YA)**2)*(2.*CP      +1.)/2. + PT*(1.- 2.*CP    )/2.)
     7          ZD(  PT)=(C*((DF*CA+SA)/YA)**2+CK)*(CP     **2 +CP     )/2. +   PT*
              1 (CP     **2 -CP      )/2. +PD               *(C*(DF/YA)**2 +CK)*SP    **2
    10          ZH(  PT    ) = (YB*(DDDF- 3.*DF*(DDF/YA)**2)/DDF + (DDF/YA**2)**2
              1 *( C*( 2.*CA*CA -1. -2.*DF*SA*CA - 2.*DF*(DF*CA+SA)*(CA-DF*SA)/
              2 YA**2) *(CP     **2 + CP      ) + GAM*RMT*PT* (GAM*RMT- (2.- RMT/(
              3 RMT-1.))/PT**G)*(CP     **2 - CP     )/(2.*(RMT-1.))
              4 +2.*C*PD               * (1.-DF*DF)/YA**2*SP     **2
              5                                     ) - YB*YB/YD )/(YA*YA*YD)
    11          ZI(  PT)=DDF*SP     /YA**2*(4.*C*DF*PD                 * CP     /YA**2 -(CA
              1 - DF*           SA)/YA**2 *C*(DF*CA+SA)*(2.*CP      +1. ) + GAM*RMT
              2 /SQRT(RMT    -1.)* PT*(0.5 -CP      )) - YB*YC/YD
    12          ZK(  PT) = (YC*CP/SP       - SP      **2* (2.*PD              *(C*(DF/YA)
              1 **2 +CK)-(C*((DF*CA+SA)/YA)**2 +CK) - PT) - YC*YC/YD)/ (F*YD)
    13          FRMT( PT)= 2./(GAM - 1.)*(1./ PT**G - 1.)
    14          FPT(PT,RMT) = DDF*CT/YA**3 * GAM*RMT/SQRT(RMT - 1.) *PT
    15          FTB(                    R,TB) = -DF*   CT      *TB/(F*YA) + R*(     ST
              1 **2* (F*DDF-DF*DF*YA*YA)/ (F*YA*YA)**2 - TS*(TS+DF*ST/(F*YA)))
              2 +((YE*CT +YF*ST)*TB - R*(YH*ST*ST+YK*CT*CT/F) +R*ST*CT*(YI/F +YJ)
              3 -YL*(YE*ST - YF*CT)/YG)/YG
    16          DATA DX(1), DP(1), DT(1), DR(1), DTB(1) /5*0.0/
    17          DO 701 N = 2, 5
    20          F = SQRT(2.*(X+DX(N-1)/2.) - (X+DX(N-1)/2.)**2)
    21          DF = (1. - (X+DX(N-1)/2.))/F
    22          DDF = -1./F**3
    23          DDDF = 3.   *DF/F**4
    24          ST =   SIN(T+DT(N-1)/2.)
    25          CT =   COS(T+DT(N-1)/2.)
    26          SP =   SIN(P+DP(N-1)/2.)
    27          CP =   COS(P+DP(N-1)/2.)
    30          RMT =  FRMT(PT+DPT(N-1)/2.)
    31          YA =   SQRT(1.   +DF*DF)
    32          YB = ZB(                 PT+DPT(N-1)/2.)
    33          YC = ZC(                 PT+DPT(N-1)/2.)
    34          YD = ZD(                 PT+DPT(N-1)/2.)
    35          YE = YB/(YA*YD)
    36          YF = YC/(F*YD)
    37          YG = 2.   *(1./YD**G - 1.)/G
    40          YH = ZH(                 PT+DPT(N-1)/2.)
    41          YI = ZI(               PT+DPT(N-1)/2.) / (YA*YD)
    42          YJ = YI/F - YC*DF/(F*F*YA*YD)
    43          YK = ZK(                 PT+DPT(N-1)/2.)
    44          YL    = 2.   /YD**(1. + G)*(YE*ST/YA - YC*CT/F)* (R+DR(N-1)/2.)
    45          TS = (YE*ST - YF*CT)/YG - DF*ST/(F*YA)
    46          DX(N) = H*CT/YA
    47          DP(N) = H*ST/F
```

```
12065              T  C  TAI                    FORTRAN SOURCE LIST RUN2
   ISN          SOURCE STATEMENT

                DT(N) = TS*H
                DR(N) =H* (TB+DTB(N-1)/2.  + (R+DR(N-1)/2.)*DF*CT/(F*YA))
                DTB(N)=H*FTB( R+DR(N-1)/2., TB+DTB(N-1)/2.)
           701  DPT(N)=H*FPT(PT+DPT(N-1)/2., RMT)
                XA  = (DX (2) + (DX (3) + DX (4))*2. + DX (5)) / 6.
                PA  = (DP (2) + (DP (3) + DP (4))*2. + DP (5)) / 6.
                TA  = (DT (2) + (DT (3) + DT (4))*2. + DT (5)) / 6.
                RA  = (DR (2) + (DR (3) + DR (4))*2. + DR (5)) / 6.
                TBA = (DTB(2) + (DTB(3) + DTB(4))*2. + DTB(5)) / 6.
                PTA = (DPT(2) + (DPT(3) + DPT(4))*2. + DPT(5)) / 6.
                RETURN
                END
```

```
  ISN      SOURCE STATEMENT

  C $IBFTC RUN3
   1        SUBROUTINE RUN3   (X, P, T, R, TB, PT,PM,XA,PA,TA,RA,TBA,PTA,PMA)
   2        COMMON C,CK,CA,SA,GAM,G,H,PO
   3        DIMENSION DX(6), DP(6), DT(6), DR(6), DTB(6), DPT(6), DPM(6)
   4        EXTERNAL NOLFUN
   5        ZB(  PT,PM) = DDF/YA**2* (C*(DF*CA+SA)*(CA -DF*SA)*(CP     **2 +
          1 CP     )/YA**2 + GAM*RMT*PT*(CP      **2 - CP      )/(2.*SQRT(RMT-1.))
          2 + PO              * GAM*RMM*PM* SP      **2 /SQRT(RMM -1.))
   6        ZC(  PT,PM) = SP      * (PT*(0.5- CP       ) + 2.*PO            *PM*
          1 CP       - (C*((DF*CA+SA)/YA)**2 +CK)* (0.5 +CP      ))
   7        ZD(  PT,PM) = (C*((DF*CA+SA)/YA)**2 +CK)*(CP        **2 + CP      )/2.
          1 + PT*(CP      **2 - CP      )/2. + PO               *PM*SP      **2
  10        ZH(  PT,PM) = (YB*(DDDF- 3.*DF*(DDF/YA)**2)/DDF + (DDF/YA**2)**2
          1 *( C*( 2.*CA*CA -1. -2.*DF*SA*CA - 2.*DF*(DF*CA+SA)*(CA-DF*SA)/
          2 YA**2) *(CP      **2 + CP      ) + GAM*RMT*PT* (GAM*RMT- (2.- RMT/(
          3 RMT-1.))/PT**G)*(CP      **2 - CP      )/(2.*(RMT-1.))+PO
          4 *GAM*RMM*PM*(GAM*RMM -(2. -RMM/(RMM-1.))/PM**G)*SP      **2/(RMM-1.
          5 ) ) - YB*YB/YD )/(YA*YA*YD)
  11        ZI(  PT,PM) = DDF*SP      /YA**2 * (GAM*RMT*PT*(0.5-CP      )/SQRT(RMT
          1 -1.) + 2.*PO              *GAM*RMM*PM*CP      /SQRT(RMM-1.) - C*(DF*CA
          2 +SA)*(CA -DF*SA)*(2.*CP        +1.)/YA**2 ) - YB*YC/YD
  12        ZK(  PT,PM) = (YC*CP/SP      + (PT - 2.*PO              *PM + C*((DF*CA
          1 +SA)/YA)**2 + CK)*SP **2 - YC*YC/YD )/ (F*YD)
  13        FRMT( PT)= 2./(GAM - 1.)*(1./ PT**G - 1.)
  14        FPT(PT,RMT) = DDF*CT/YA**3 * GAM*RMT/SQRT(RMT - 1.) *PT
  15        FTB(                     R,TB) = -DF*  CT    *TB/(F*YA) + R*(     ST
          1 **2* (F*DDF-DF*DF*YA*YA)/ (F*YA*YA)**2 - TS*(TS+DF*ST/(F*YA)))
          2 +((YE*CT +YF*ST)*TB - R*(YH*ST*ST+YK*CT*CT/F) +R*ST*CT*(YI/F +YJ)
          3 -YL*(YE*ST - YF*CT)/YG)/YG
  16        DATA DX(1), DP(1), DT(1), DR(1), DTB(1), DPT(1), DPM(1) /7*0.0/
  17        DO 702 N = 2, 5
  20        F = SQRT(2.*(X+DX(N-1)/2.) - (X+DX(N-1)/2.)**2)
  21        DF = (1. - (X+DX(N-1)/2.))/F
  22        DDF = -1./F**3
  23        DDDF = 3.  *DF/F**4
  24        ST =  SIN(T+DT(N-1)/2.)
  25        CT =  COS(T+DT(N-1)/2.)
  26        SP =  SIN(P+DP(N-1)/2.)
  27        CP =  COS(P+DP(N-1)/2.)
  30        RMT = FRMT(PT+DPT(N-1)/2.)
  31        RMM = FRMT(PM+DPM(N-1)/2.)
  32        YA =  SQRT(1.  +DF*DF)
  33        YB = ZB(                PT+DPT(N-1)/2., PM+DPM(N-1)/2.)
  34        YC = ZC(                PT+DPT(N-1)/2., PM+DPM(N-1)/2.)
  35        YD = ZD(                PT+DPT(N-1)/2., PM+DPM(N-1)/2.)
  36        YE = YB/(YA*YD)
  37        YF = YC/(F*YD)
  40        YG = 2.  *(1./YD**G - 1.)/G
  41        YH = ZH(                PT+DPT(N-1)/2., PM+DPM(N-1)/2.)
  42        YI = ZI(                PT+DPT(N-1)/2., PM+DPM(N-1)/2.)/ (YA*YD)
  43        YJ = YI/F - YC*DF/(F*F*YA*YD)
  44        YK = ZK(                PT+DPT(N-1)/2., PM+DPM(N-1)/2.)
  45        YL     = 2.  /YD**(1. + G)*(YB*ST/YA - YC*CT/F)* (R+DR(N-1)/2.)
  46        TS = (YE*ST - YF*CT)/YG - DF*ST/(F*YA)
  47        DX(N) = R*CT/YA
```

```
12065            T  C  TAI                    FORTRAN SOURCE LIST RUN3
   ISN         SOURCE STATEMENT

    50         DP(N) = H*ST/F
    51         DT(N) = TS*H
    52         DR(N) =H* (TB+DTB(N-1)/2.  + (R+DR(N-1)/2.)*DF*CT/(F*YA))
    53         DTB(N)=H*FTB( R+DR(N-1)/2., TB+DTB(N-1)/2.)
    54         DPT(N)=H*FPT(PT+DPT(N-1)/2., RMT)
    55     702 DPM(N)=H*FPT(PM+DPM(N-1)/2., RMM)
    57         XA  = (DX (2) + (DX (3) + DX (4))*2. + DX (5)) / 6.
    60         PA  = (DP (2) + (DP (3) + DP (4))*2. + DP (5)) / 6.
    61         TA  = (DT (2) + (DT (3) + DT (4))*2. + DT (5)) / 6.
    62         RA  = (DR (2) + (DR (3) + DR (4))*2. + DR (5)) / 6.
    63         TBA = (DTB(2) + (DTB(3) + DTB(4))*2. + DTB(5)) / 6.
    64         PTA = (DPT(2) + (DPT(3) + DPT(4))*2. + DPT(5)) / 6.
    65         PMA = (DPM(2) + (DPM(3) + DPM(4))*2. + DPM(5)) / 6.
    66         RETURN
    67         END
```

```
12065          T  C  TAI                    FORTRAN SOURCE LIST
  ISN       SOURCE STATEMENT

    0 $IBFTC RUN4
    1       SUBROUTINE RUN4   (X, P, T, R, TB, PT,PM,PB,XA,PA,TA,RA,TBA,PTA,
          1 PMA, PBA)
    2       COMMON C,CK,CA,SA,GAM,G,H,PC
    3       DIMENSION DX(6), DP(6), DT(6), DR(6), DTB(6), DPT(6),DPM(6),DPB(6)
    4       EXTERNAL NOLMUN
    5       ZB(  PT,PM,PB) = GAM*DDF/YA**2 *(RMB*PB*(CP     **2 +CP     )/(2.*
          1 SQRT(RMB-1.)) + RMT*PT*(CP     **2 -CP     )/(2.*SQRT(RMT-1.)) +
          2 PC*RMM*PM*SP     **2/SQRT(RMM-1.) )
    6       ZC(  PT,PM,PB) = SP     * (PT*(0.5-CP     ) + 2.*PC*PM*CP -
          1 PB*(0.5+CP     ))
    7       ZD(  PT,PM,PB) = 0.5*(( PB+PT)*CP     **2 + (PB-PT)*CP     ) +
          1 PC*PM*SP     **2
   10       ZH(  PT,PM,PB) = ( YB/DDF*(DDDF -3.*DF*(DDF/YA)**2) + GAM*(DDF/
          1 YA**2)**2 *(RMB*PB* (GAM*RMB -(2.- RMB/(RMB-1.))/ PB**G)*(CP
          2 **2 +CP     ) /(2.*(RMB-1.)) + RMT*PT* (GAM*RMT - (2.-RMT/(RMT-1.)
          3 )/PT**G) *(CP     **2 -CP     )/(2.*(RMT-1.)) +  PC*RMM*PM* (GAM*RMM
          4-(2.-RMM/(RMM-1.))/PM**G)*SP     **2/(RMM-1.))-YB*YB/YD)/(YA*YA*YD)
   11       ZI(  PT,PM,PB) = GAM*DDF*SP     /YA**2 * ( RMT*PT*(0.5-CP     )/SQRT
          1 (RMT-1.) + 2.*PC*RMM*PM*CP     /SQRT(RMT-1.) - RMB*PB*(0.5+CP     )
          2 /SQRT(RMB-1.) ) - YB*YC/YD
   12       ZK(  PT,PM,PB) = (YC*CP/SP     + (PT- 2.*PC*PM+PB)*SP     **2-YC*YC
          1 /YD) / (F*YD)
   13       FRMT( PT)= 2./(GAM - 1.)*(1./ PT**G - 1.)
   14       FPT(PT,RMT) = DDF*CT/YA**3 * GAM*RMT/SQRT(RMT - 1.) *PT
   15       FTB(                  R,TB) = -DF*  CT    *TB/(F*YA) + R*(    ST
          1 **2* (F*DDF-DF*DF*YA*YA)/ (F*YA*YA)**2 - TS*(TS+DF*ST/(F*YA)))
          2 +((YE*CT +YF*ST)*TB - R*(YH*ST*ST+YK*CT*CT/F) +R*ST*CT*(YI/F +YJ)
          3 -YL*(YE*ST - YF*CT)/YG)/YG
   16       DATA DX(1),DP(1),DT(1),DR(1),DTB(1),DPT(1),DPM(1),DPB(1)/8*0.0/
   17       DO 703 N = 2, 5
   20       F = SQRT(2.*(X+DX(N-1)/2.) - (X+DX(N-1)/2.)**2)
   21       DF = (1. - (X+DX(N-1)/2.))/F
   22       DDF = -1./F**3
   23       DDDF = 3.   *DF/F**4
   24       ST =   SIN(T+DT(N-1)/2.)
   25       CT =   COS(T+DT(N-1)/2.)
   26       SP =   SIN(P+DP(N-1)/2.)
   27       CP =   COS(P+DP(N-1)/2.)
   30       RMT = FRMT(PT+DPT(N-1)/2.)
   31       RMM = FRMT(PM+DPM(N-1)/2.)
   32       RMB = FRMT(PB+DPB(N-1)/2.)
   33       YA =   SQRT(1.   +DF*DF)
   34       YB=ZB(               PT+DPT(N-1)/2.,PM+DPM(N-1)/2.,PB+DPB(N-1)/2.)
   35       YC=ZC(               PT+DPT(N-1)/2.,PM+DPM(N-1)/2.,PB+DPB(N-1)/2.)
   36       YD=ZD(               PT+DPT(N-1)/2.,PM+DPM(N-1)/2.,PB+DPB(N-1)/2.)
   37       YE = YB/(YA*YD)
   40       YF = YC/(F*YD)
   41       YG = 2.   *(1./YD**G - 1.)/G
   42       YH=ZH(               PT+DPT(N-1)/2.,PM+DPM(N-1)/2.,PB+DPB(N-1)/2.)
   43       YI=ZI(               PT+DPT(N-1)/2.,PM+DPM(N-1)/2.,PB+DPB(N-1)/2.)
          1 /(YA*YD)
   44       YJ = YI/F - YC*DF/(F*F*YA*YD)
   45       YK=ZK(               PT+DPT(N-1)/2.,PM+DPM(N-1)/2.,PB+DPB(N-1)/2.)
   46       YL    = 2.   /YD**(1. + G)*(YD*ST/YA - YC*CT/F)*  (R+DR(N-1)/2.)
```

```
2065            T   C   TAI                         FORTRAN SOURCE LIST RUN4
  ISN           SOURCE STATEMENT

   47           TS = (YE*S) - YF*CT)/YC - DF*ST/(F*YA)
   50           DX(N) = H*CT/YA
   51           DP(N) = H*ST/F
   52           DT(N) = TS*H
   53           DR(N) =H* (TB+DTB(N-1)/2.  + (R+DR(N-1)/2.)*DF*CT/(F*YA))
   54           DTB(N)=H*FTB( R+DR(N-1)/2., TB+DTB(N-1)/2.)
   55           DPT(N)=H*FPT(PT+DPT(N-1)/2., RMT)
   56           DPM(N)=H*FPT(PM+DPM(N-1)/2., RMM)
   57       703 DPB(N)=H*FPT(PB+DPB(N-1)/2., RMB)
   61           XA  = (DX (2) + (DX (3) + DX (4))*2. + DX (5)) / 6.
   62           PA  = (DP (2) + (DP (3) + DP (4))*2. + DP (5)) / 6.
   63           TA  = (DT (2) + (DT (3) + DT (4))*2. + DT (5)) / 6.
   64           RA  = (DR (2) + (DR (3) + DR (4))*2. + DR (5)) / 6.
   65           TBA = (DTB(2) + (DTB(3) + DTB(4))*2. + DTB(5)) / 6.
   66           PTA = (DPT(2) + (DPT(3) + DPT(4))*2. + DPT(5)) / 6.
   67           PMA = (DPM(2) + (DPM(3) + DPM(4))*2. + DPM(5)) / 6.
   70           PBA = (DPB(2) + (DPB(3) + DPB(4))*2. + DPB(5)) / 6.
   71           RETURN
   72           END
```

```
12065          T  C  TAI                      FORTRAN SOURCE LIST
  ISN        SOURCE STATEMENT

   C $IBFTC RUN5
   1          SUBROUTINE RUN5   (X, P, T, R, TE, XA, PA, TA, RA, TBA, Y)
   2          DIMENSION DX(6), DP(6), DT(6), DR(6), DTB(6)
   3          EXTERNAL NOLMUN
   4          COMMON C,CK,CA,SA,GAM,G,H,PC,XJ,FJ,DFJ /BBC/BC1,BC2,BC3,
             1 B1,B2,B3,C1,C2,C3
   5          DATA DX(1), DP(1), DT(1), DR(1), DTB(1) /5*0.0/
   6          FTB(                    R,TE) = -DF*  CT   *TE/(F*YA) + R*(    ST
             1 **2* (      -DF*DF*YA*YA)/ (F*YA*YA)**2 - TS*(TS+DF*ST/(F*YA)))
             2 +((YE*CT +YF*ST)*TE - R*(YH*ST*ST+YK*CT*CT/F) +R*ST*CT*(YI/F +YJ)
             3 -YL*(YE*ST - YF*CT)/YG)/YG
   7          DF = DFJ
  10          YA = SQRT(1. + DF*DF)
  11          DO 705 N = 2, 5
  12          ST =  SIN(T+DT(N-1)/2.)
  13          CT =  COS(T+DT(N-1)/2.)
  14          SP =  SIN(P+DP(N-1)/2.)
  15          CP =  COS(P+DP(N-1)/2.)
  16          S2P= SIN((P+DP(N-1)/2.)*2.)
  17          C2P= COS((P+DP(N-1)/2.)*2.)
  20          Z = X + DX(N-1)/2. - XJ
  21          F = FJ + Z*DF
  22          E1 = EXP(-C1*Z)
  23          E2 = EXP(-C2*Z)
  24          E3 = EXP(-C3*Z)
  25          A = 0.5*(BC3 - BC1 + B3*E3 - B1*E1)
  26          B = 0.25 * (BC1 + 2.*BC2 + BC3 + B1*E1 + 2.*B2*E2 + B3*E3)
  27          E = B - BC2 - B2*E2
  30          DA =-0.5 * (B3*C3*E3 - B1*C1*E1)
  31          DB =-.25*(B1*C1*E1 + 2.*B2*C2*E2 + B3*C3*E3)
  32          DE = DB + B2*C2*E2
  33          DDA = 0.5 * (B3*C3*C3*E3 - B1*C1*C1*E1)
  34          DDB = 0.25*(B1*C1*C1*E1 + 2.*B2*C2*C2*E2 + B3*C3*C3*E3)
  35          DDE = DDB - B2*C2*C2*E2
  36          YB = DA*CP + DB + DE*C2P
  37          YC = -A*SP - 2.*E*S2P
  40          YD = A*CP + B + E*C2P
  41          YE = YB/(YA*YD)
  42          YF = YC/(YD*(F+H*CT/YA*DF))
  43          YG = 2.  *(1./YD**G - 1.)/G
  44          YH = (DDA*CP + DDB + DDE*C2P - YB*YB/YD) / (YA*YA*YD)
  45          YI = -(DA*SP + 2.*DE*S2P + YB*YC/YD) / (YA*YD)
  46          YJ = YI/F - YC*DF/(F*F*YA*YD)
  47          YK = -(A*CP + 4.*E*C2P + YC*YC/YD) / (F*YD)
  50          YL    = 2.   /YD**(1. + G)*(YF*ST/YA - YC*CT/F)* (R+DR(N-1)/2.)
  51          TS = (YE*ST - YF*CT)/YG - DF*ST/(F*YA)
  52          DX(N) = H*CT/YA
  53          DP(N) = H*ST/(F+H*CT/YA*DF)
  54          DT(N) = TS*H
  55          DR(N) =H* (TB+DTB(N-1)/2.  + (R+DR(N-1)/2.)*DF*CT/(F*YA))
  56      705 DTB(N)=H*FTB( R+DR(N-1)/2., TB+DTB(N-1)/2.)
  60          XA  = ( DX(2) + ( DX(3) +  DX(4))*2. +  DX(5)) / 6.
  61          PA  = ( DP(2) + ( DP(3) +  DP(4))*2. +  DP(5)) / 6.
  62          TA  = ( DT(2) + ( DT(3) +  DT(4))*2. +  DT(5)) / 6.
  63          RA  = ( DR(2) + ( DR(3) +  DR(4))*2. +  DR(5)) / 6.
```

ISN SOURCE STATEMENT

```
TBA = (DTB(2) + (DTB(3) + DTB(4))*2. + DTB(5)) / 6.
Z = X + XA - XJ
E1 = EXP(-C1*Z)
E2 = EXP(-C2*Z)
E3 = EXP(-C3*Z)
A = 0.5*(BO3 - BO1 + B3*E3 - B1*E1)
B = 0.25 * (BO1 + 2.*BO2 + BO3 + B1*E1 + 2.*B2*E2 + B3*E3)
B = B - BO2 - B2*E2
Y = A*COS(P+PA) + B + B*COS(2.*(P+PA))
RETURN
END
```

```
12065            T  C  TAI                        FORTRAN SOURCE LIST
   ISN         SOURCE STATEMENT

     0 $IBFTC COLLAR
     1         SUBROUTINE COLLAR (GAM, G, RMQ, RNU, PT)
     2         RMO = RMQ*RMQ
     3         DO 60 I = 1, 20
     4         RM = 6./COS((RNU + ARCOS(1./SQRT(RMO))) / SQRT(6.))**2 - 5.
     5         IF ( ABS((RM-RMO)/RMO) .LE. 0.0001) GO TO 70
    10      60 RMO = RM
    12      70  PT = (2./(2.+ (GAM - 1.)*RM ))**(1./G)
    13         RETURN
    14         END
```

X. REFERENCES

1. Lees, Lester, "Laminar Heat Transfer over Blunted-Nosed Bodies at Hypersonic Flight Speeds," Jet Propulsion, Vol. 26, No. 4, pp. 259-269 and p. 274, April, 1956.

2. Rose, P. H., Probstein, R. F. and Adams, M. C., "Turbulent Heat Transfer through a Highly Cooled, Partially Dissociated Boundary Layer," J. A. S. Vol. 25, No. 12, pp. 751-760, December, 1958.

3. Ferri, A., Kuchemann, D., and Stearne, L. H. G., editors, "Progress in Aeronautical Sciences," Vol. 2, Pergamon Press, 1962.

4. Sasman, P. K. and Cresci, R. J., "Compressible Turbulent Boundary Layer with Pressure Gradient and Heat Transfer," AIAA Journal Vol. 4, No. 1, pp. 19-29, January, 1966.

5. Bradley, R. G., "Approximate Solutions for Compressible Turbulent Boundary Layers in Three-Dimensional Flow," AIAA Journal Vol. 6, No. 5, pp. 859-864, May, 1968.

6. DeJarnette, F. R. and Davis, R. M., "A Simplified Method for Calculating Heat Transfer over Bodies at an Angle of Attack," NASA TN D-4720, August, 1968.

7. Beckwith, I. E., "Similarity Solutions for Small Cross Flows in Laminar Compressible Boundary Layers," NASA TR R-107, 1961.

8. Cooke, J. C., "An Axially Symmetry Analogue for General Three-Dimensional Boundary Layers," ARC R & M No. 3200 (London), June, 1959.

9. Vaglio-Laurin, R., "Turbulent Heat Transfer on Blunt-Nosed Bodies in Two-Dimensional and General Three-Dimensional Hypersonic Flow," J. A. S. Vol. 27, No. 1, pp. 27-36, January, 1960.

10. Vaglio-Laurin, R., "Laminar Heat Transfer on Three-Dimensional Blunt Nosed Bodies in Hypersonic Flow," ARS Journal, Vol. 29, No. 2, pp. 123-129, February, 1959.

11. Davis, R. T. and Flugge-Lotz, I., "Second-Order Boundary-Layer Effects in Hypersonic Flow Past Axisymmetric Blunt Bodies," J. Fluid Mech. Vol. 20, No. 4, pp. 593-623, December, 1964.

12. Cresci, R. J., Mackenzie, D. A. and Libby, P. A., "An Investigation of Laminar, Transitional and Turbulent Heat Transfer on Blunt-Nosed Bodies in Hypersonic Flow," J. A. S. Vol. 27, No. 6, June, 1960.

13. Zakkay, V., "Pressure and Laminar Heat Transfer Results in Three-Dimensional Hypersonic Flow," WADC TN 58-182, ASTIA Document No. AD 155-679, September, 1958.

14. Zakkay, V. and Callahan, C. J., "Laminar, Transitional, and Turbulent Heat Transfer to a Cone-Cylinder-Flare Body at Mach 8.0," J. A. S. Vol. 29, No. 12, December, 1962.

15. Mager, A., "Transformation of the Compressible Turbulent Boundary Layer," J. A. S. Vol. 25, No. 5, pp. 305-331, May, 1958.

16. Von Karman, T., "The Problem of Resistance in Compressible Fluids," Volta Kongress Rome, pp. 222-277, 1935.

17. Eckert, E. R. G., "Engineering Relations for Friction and Heat Transfer to Surfaces in High Velocity Flow," J. A. S. Vol. 22, No. 8, pp. 585-587, August, 1955.

18. Van Driest, E. R., "The Turbulent Boundary Layer in Compressible Flow," J. A. S. Vol. 18, No. 3, pp. 145-160, March, 1951.

19. Reshotko, E. and Tucker, M., "Approximate Calculation of Compressible Turbulent Boundary Layer with Heat Transfer and Arbitrary Pressure Gradient," NACA TN 4154, 1957.

20. Cohen, N. B., "A Method for Computing Turbulent Heat Transfer in the Presence of a Streamwise Pressure Gradient for Bodies in High-Speed Flow," NASA MEMO 1-2-59 L, 1959.

21. Harris, E. L., "Determination of Streamlines on a Sphere-Cone at Angles of Attack from the Measured Surface Pressure Distribution," NOL TR 63-37, Naval Ordnance Lab., White Oak, Maryland, February 18, 1963.

22. Maikapar, G. I., "Calculation of Streamlines with a Known Pressure Distribution on the Surface of a Rigid Body," J. of App. Math & Mach., January, 1965.

23. Fannelop, T. K., "A Method of Solving the Three-Dimensional Laminar Boundary-Layer Equations with Application to a Lifting Re-Entry Body," AIAA Journal Vol. 6, No. 6, pp. 1075-1084, June, 1968.

24. Kurfman, II, L. G., "Pressure Estimation Techniques for Hypersonic Flows over Blunt Bodies," J. of Astronautical Sciences, Vol. X, No. 2, pp. 35-41, Summer, 1963.

25. Knox, E. C. and Lewis, C. H., "A Comparison of Experimental and Theoretically Predicted Pressure Distributions and Force and Stability Coefficients for a Spherically Blunted Cone at $M_\infty = 18$ and Angle of Attack," ARO Inc., AEDC-TR-65-234, February, 1966.

26. Wayne, C. E., "Heat Transfer over Axisymmetric Bodies at Angles of Attack in Hypersonic Flow," M.S. thesis, Virginia Polytechnic Institute, Blacksburg, Virginia, 1967.

27. Cleary, J. W., "Effects of Angle of Attack and Nose Bluntness on the Hypersonic Flow over Cones," AIAA Paper No. 66-414, June, 1966.

28. Hughes, W. F. and Gaylord, E. W., "Basic Equations of Engineering Science," Schaum Publishing Company, New York, 1964.

29. Schlichting, H., "Boundary Layer Theory," Fourth English Edition, McGraw-Hill, 1962.

30. Dorrance, W. H., "Viscous Hypersonic Flow," McGraw-Hill, 1962.

31. Stetson, K. F., "Boundary Layer Transition on Blunt Bodies with Highly Cooled Boundary Layers," J. A. S. Vol. 27, No. 2, pp. 81-91, February, 1960.

32. Bloxsom, D. E., Jr., "Transition of Air Laminar Boundary Layers," AIAA Journal, Vol. 3, No. 5, pp. 982-984, May, 1965.

33. Ames Research Staff, "Equation, Tables and Charts for Compressible Flow," NACA Report 1135, 1953.

34. Eggers, A. J., Savin, R. C. and Syvertson, C. A., "The Generalized Shock-Expansion Method and Its Application to Bodies Traveling at High Supersonic Air Speeds," J. A. S. Vol. 22, No. 4, pp. 231-238 and p. 248, April, 1955.

35. Kaattari, G. E., "Pressure Distribution of Forward Face of Blunt Bodies at Angle of Attack," J. of Spacecraft, Vol. 4, No. 8, pp. 1110-1112, August, 1967.

36. Syvertson, C. A. and Dennis, D. H., "Second-Order Shock Expansion Method Applicable to Bodies of Revolution Near Zero Lift," NACA Report 1328, 1957.

37. Eggers, A. J., Jr. and Savin, R. C., "Approximate Methods for Calculating the Flow about Nonlifting Bodies of Revolution at High Supersonic Airspeeds," NACA TN 2579, 1952.

38. Kopal, Z., "Tables of Supersonic Flow around Cones," Massachusetts Institute of Technology, Tech. Report, No. 1, 1947.

39. Kuby, W., Foster, R. M. and Byron, S. R., "Symmetrical, Equilibrium Flow Past a Blunt Body at Superorbital Re-Entry Speeds," AIAA Journal, Vol. 5, No. 4, April, 1967.

40. Southworth, R. W. and Deleeuw, S. L., "Digital Computation and Numerical Methods," McGraw-Hill, 1965.

41. Hayes, W. D. and Probstein, R. F., "Hypersonic Flow Theory, Second Edition, Vol. I, Inviscid Flows," Academic Press, New York, 1966.

42. Collar, A. R., "An Iteration Process for the Solution of the Prandtl-Meyer Expansion," J. of Roy. Aero. Society, Vol. 65, pp. 357-360, May, 1961.

43. Fay, J. A. and Riddel, F. R., "Theory of Stagnation Point Heat Transfer in Dissociated Air," J. A. S. Vol. 25, No. 2, pp. 73-85, February, 1958.

44. Rietz, H. L., Reilly, J. F. and Woods, R., "Plane and Spherical Trigonometry," Third Edition, MacMillan, 1950.

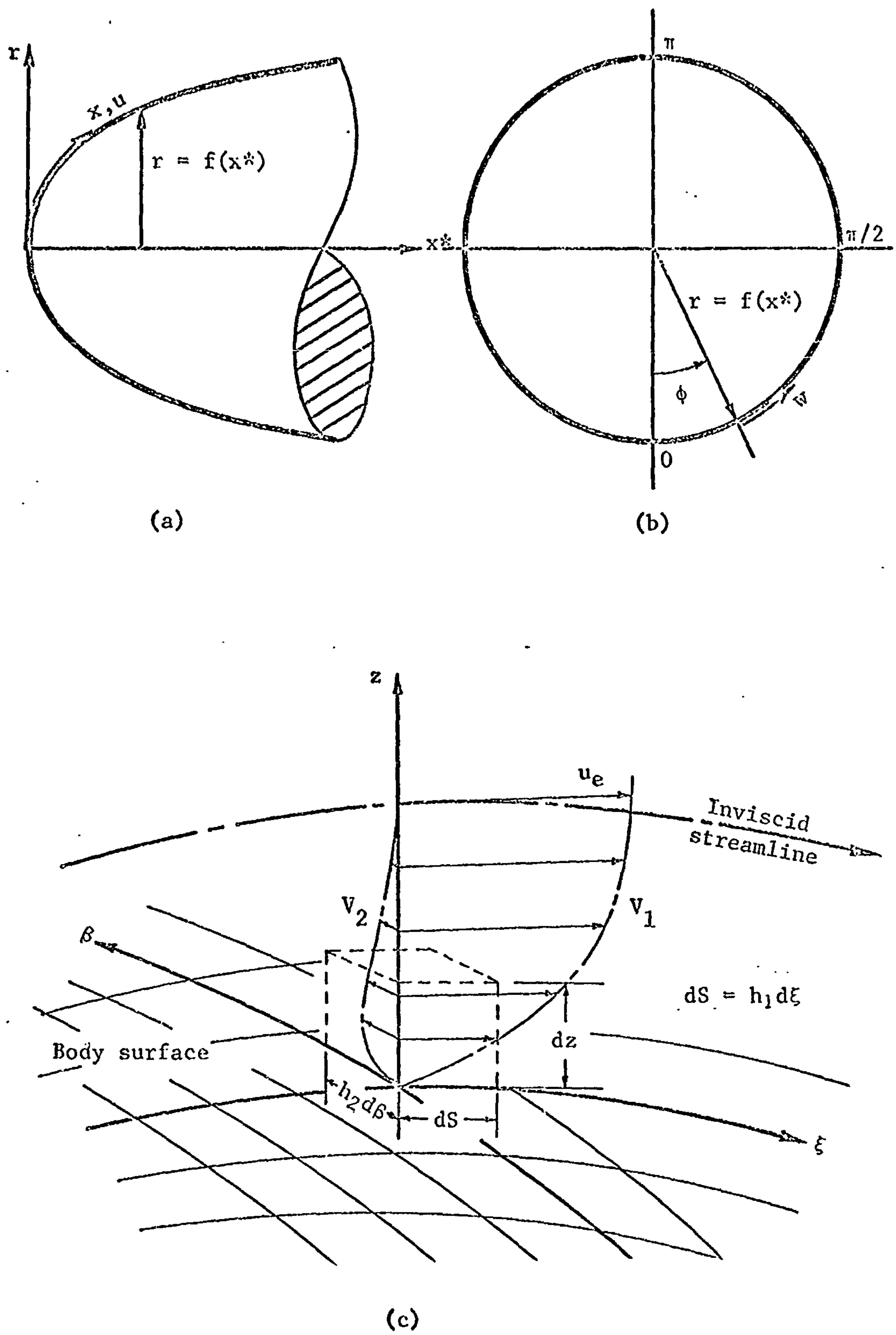

(c)

Fig. 1 Body geometry and coordinate system

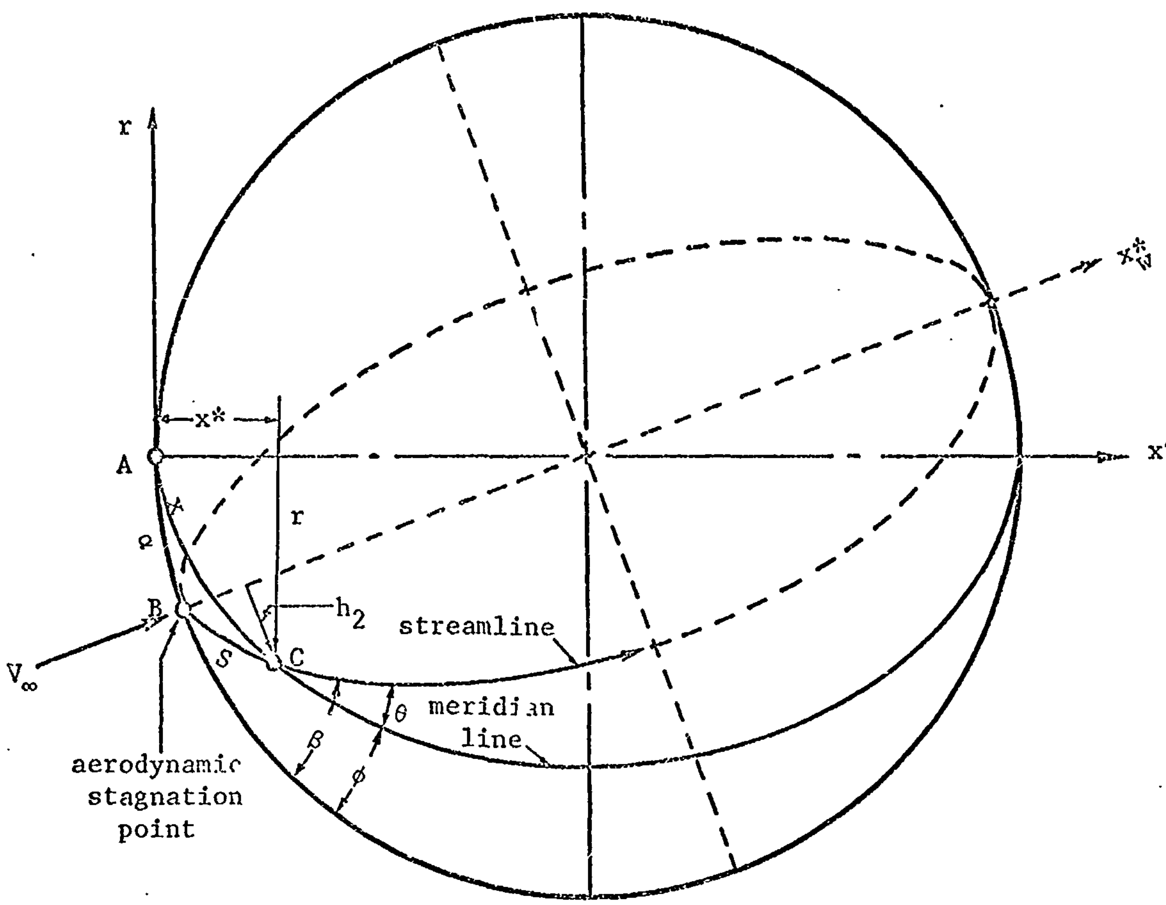

Fig. 2 Streamline geometry over a sphere

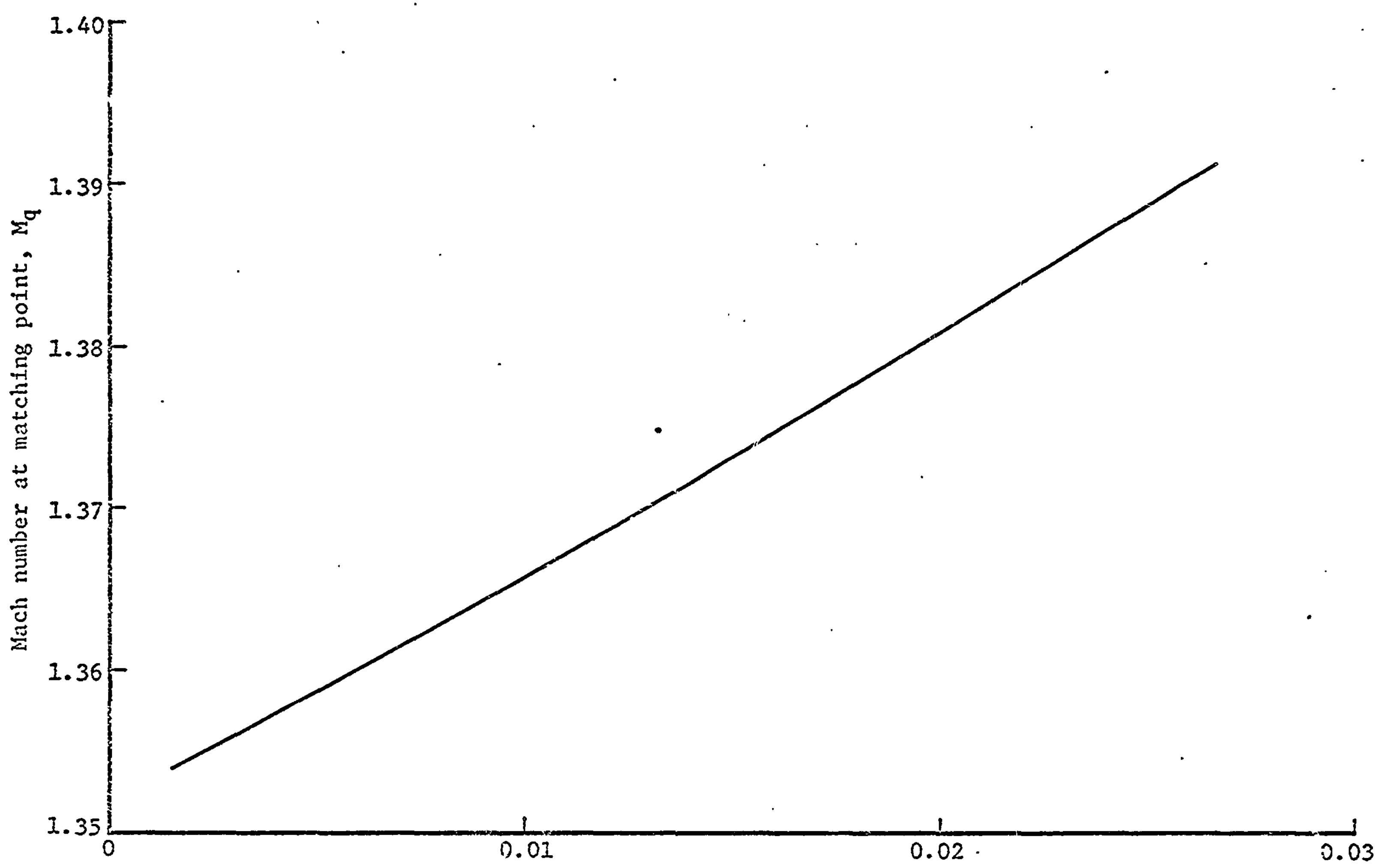

Fig. 3 Variation of Mach number at "matching point" versus freestream to stagnation pressure ratio

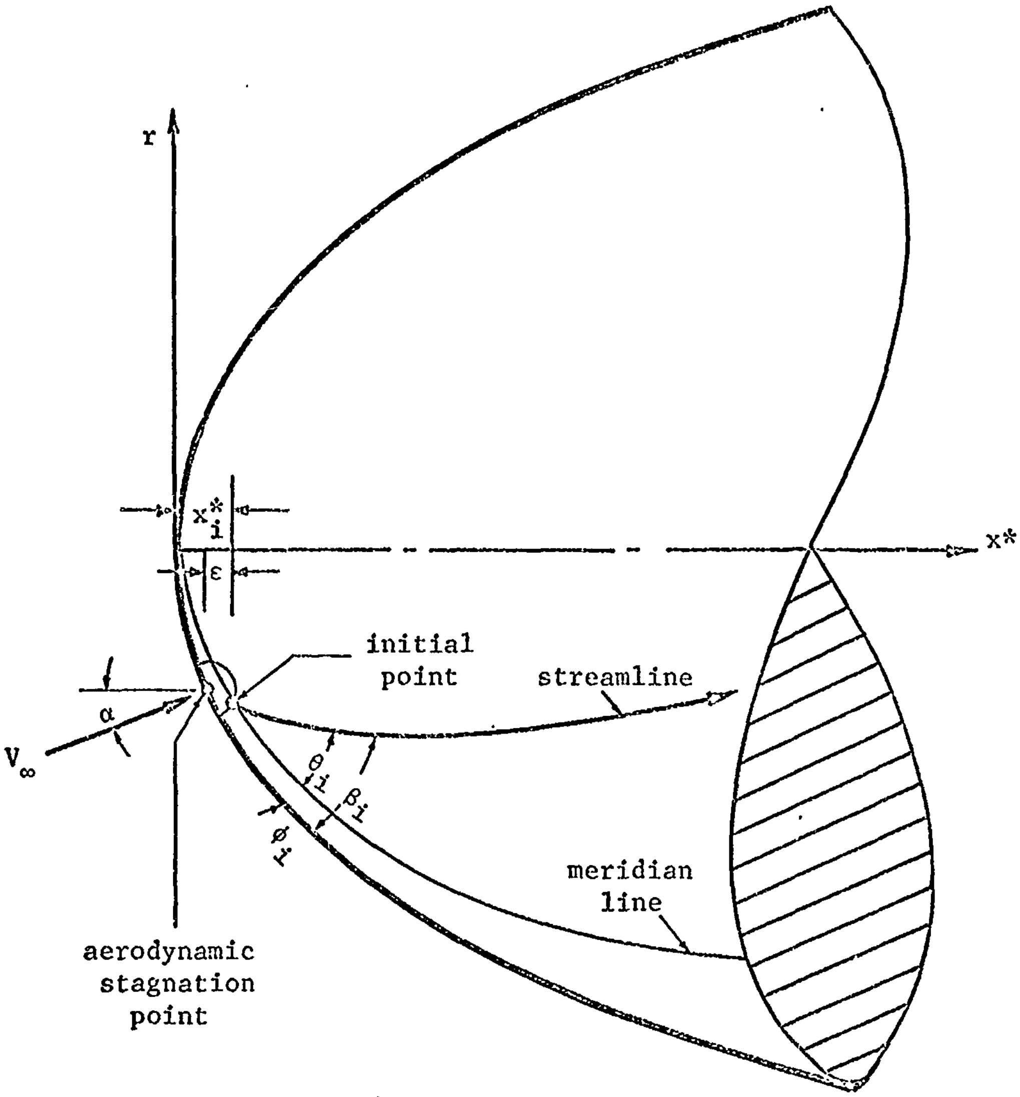

Fig. 4 Evaluation of initial conditions for a body of revolution at an angle of attack

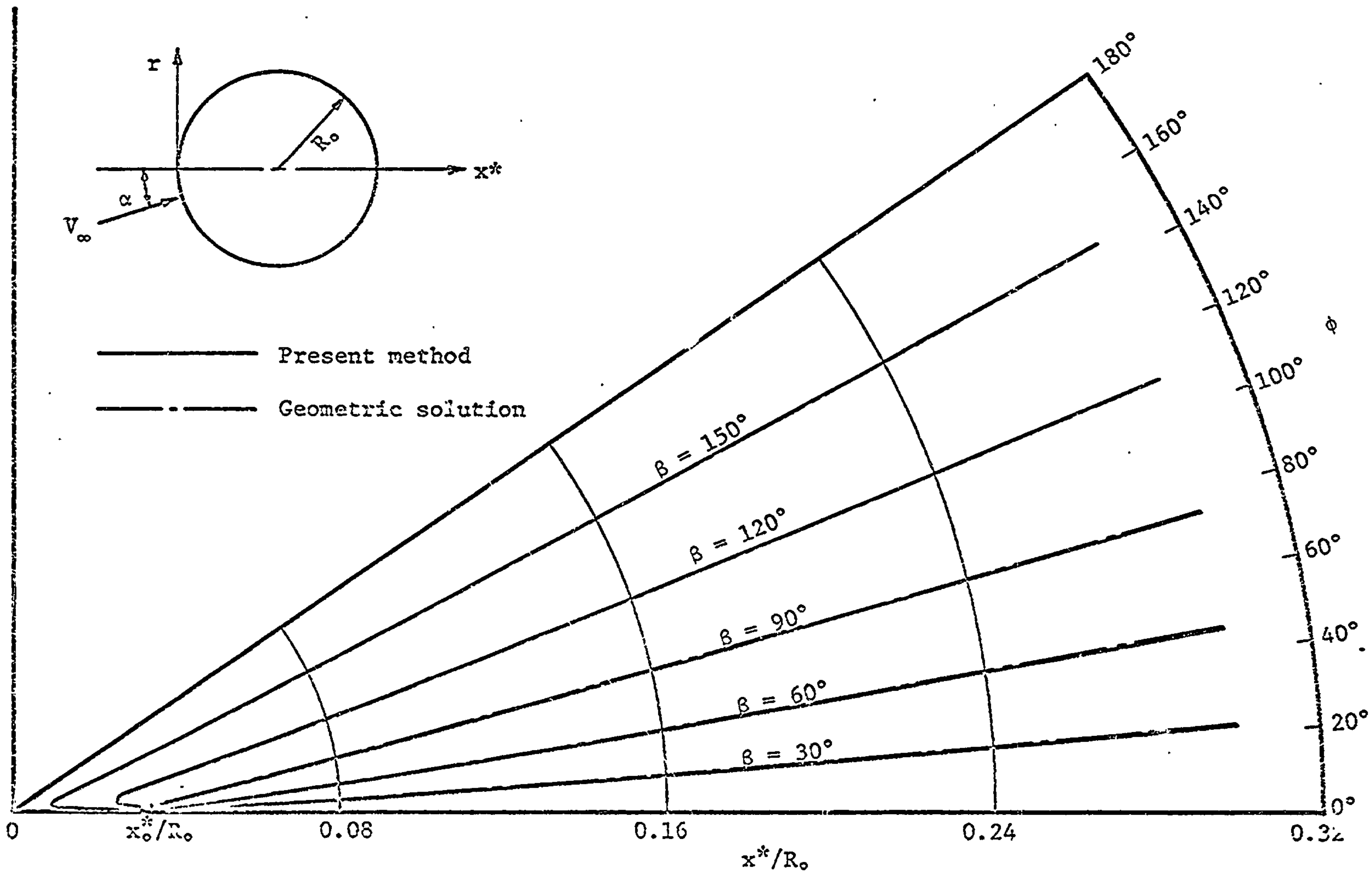

Fig. 5 Streamline patterns for a sphere at $\alpha = 15°$ and $M_\infty = 8.0$

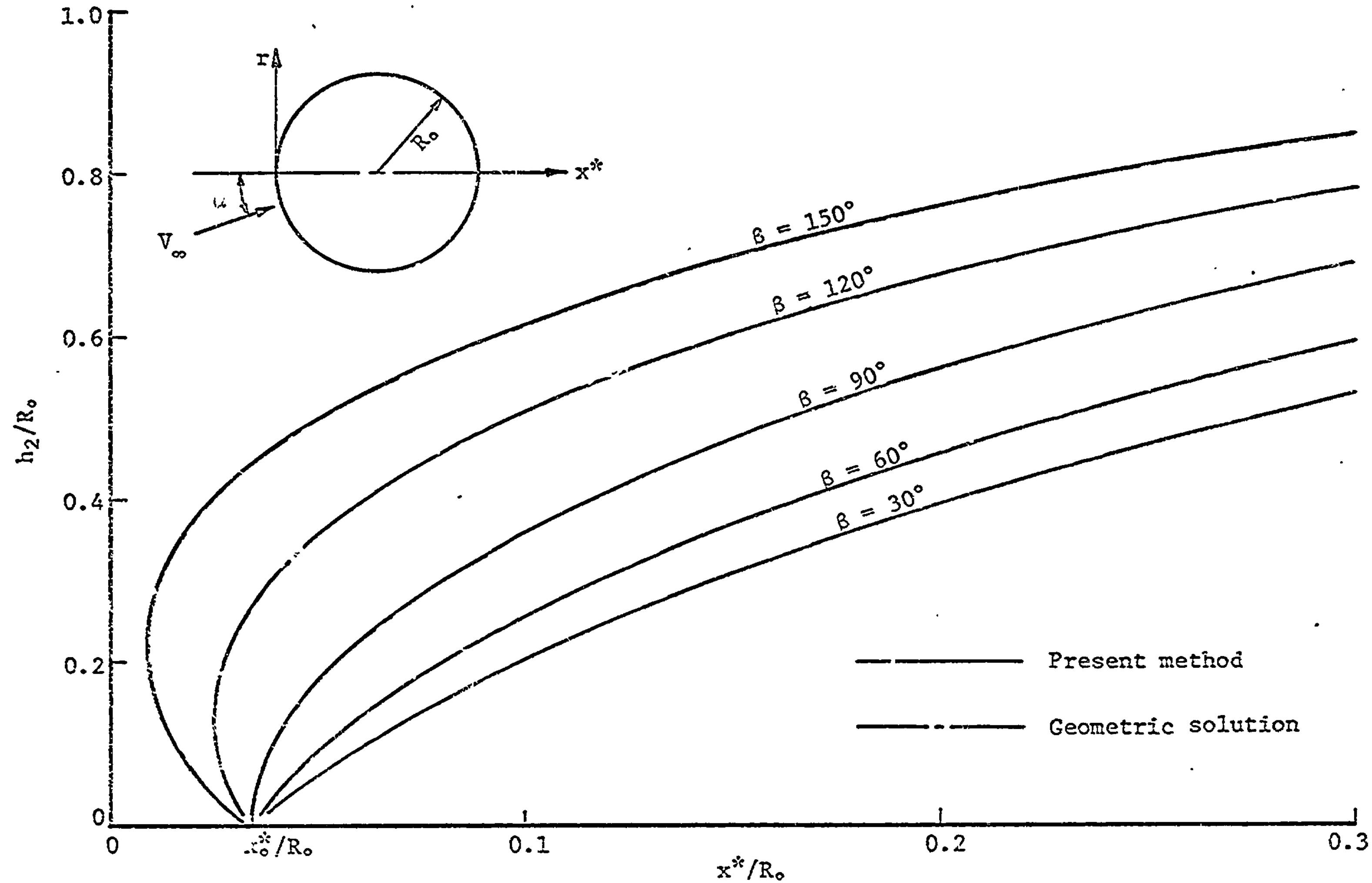

Fig. 6 Scale factors for a sphere at α = 15° and M_∞ = 8.0

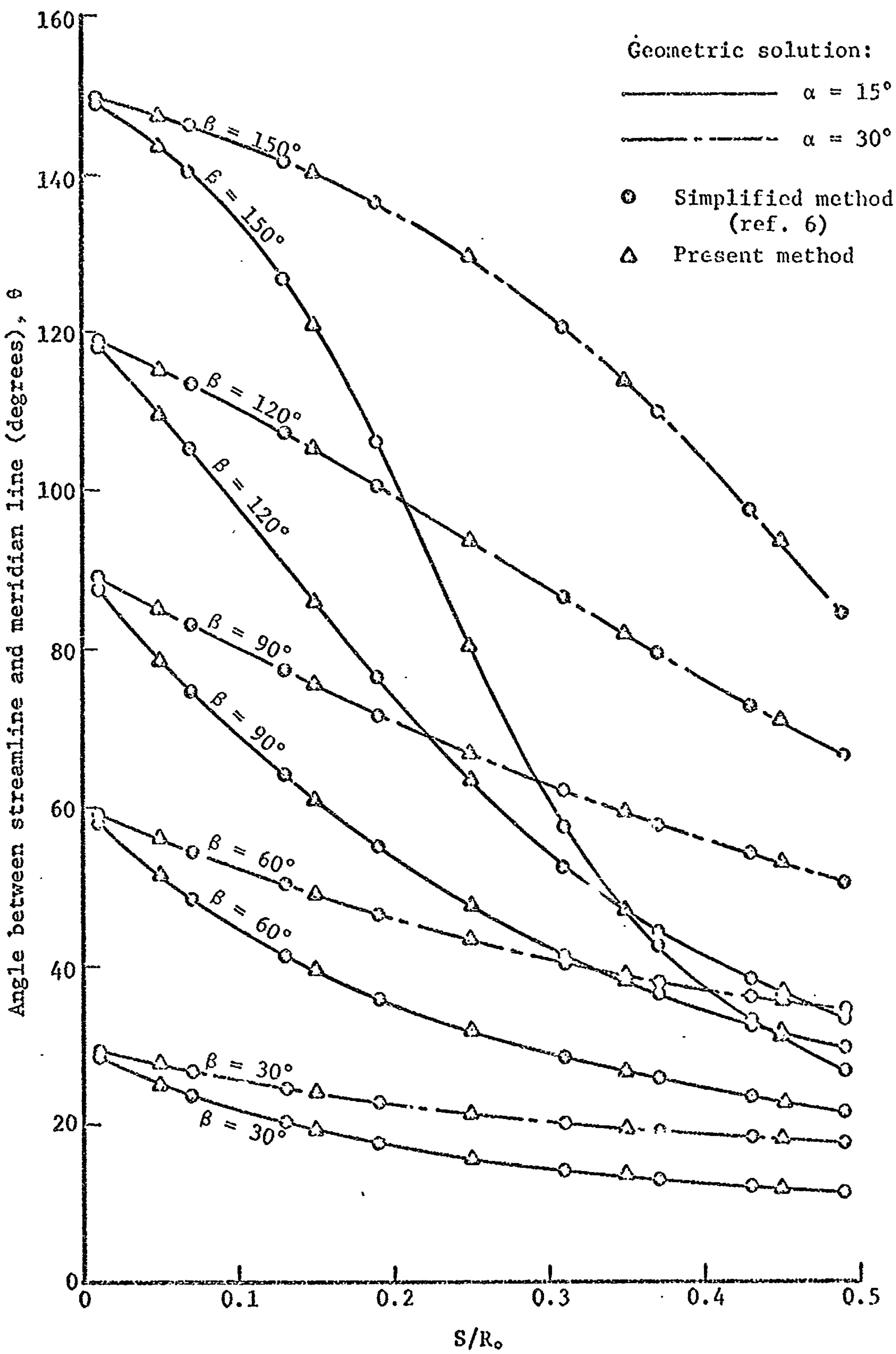

Fig. 7 Streamline direction over a sphere at $\alpha = 15°$ and $30°$ and $M_\infty = 8.0$

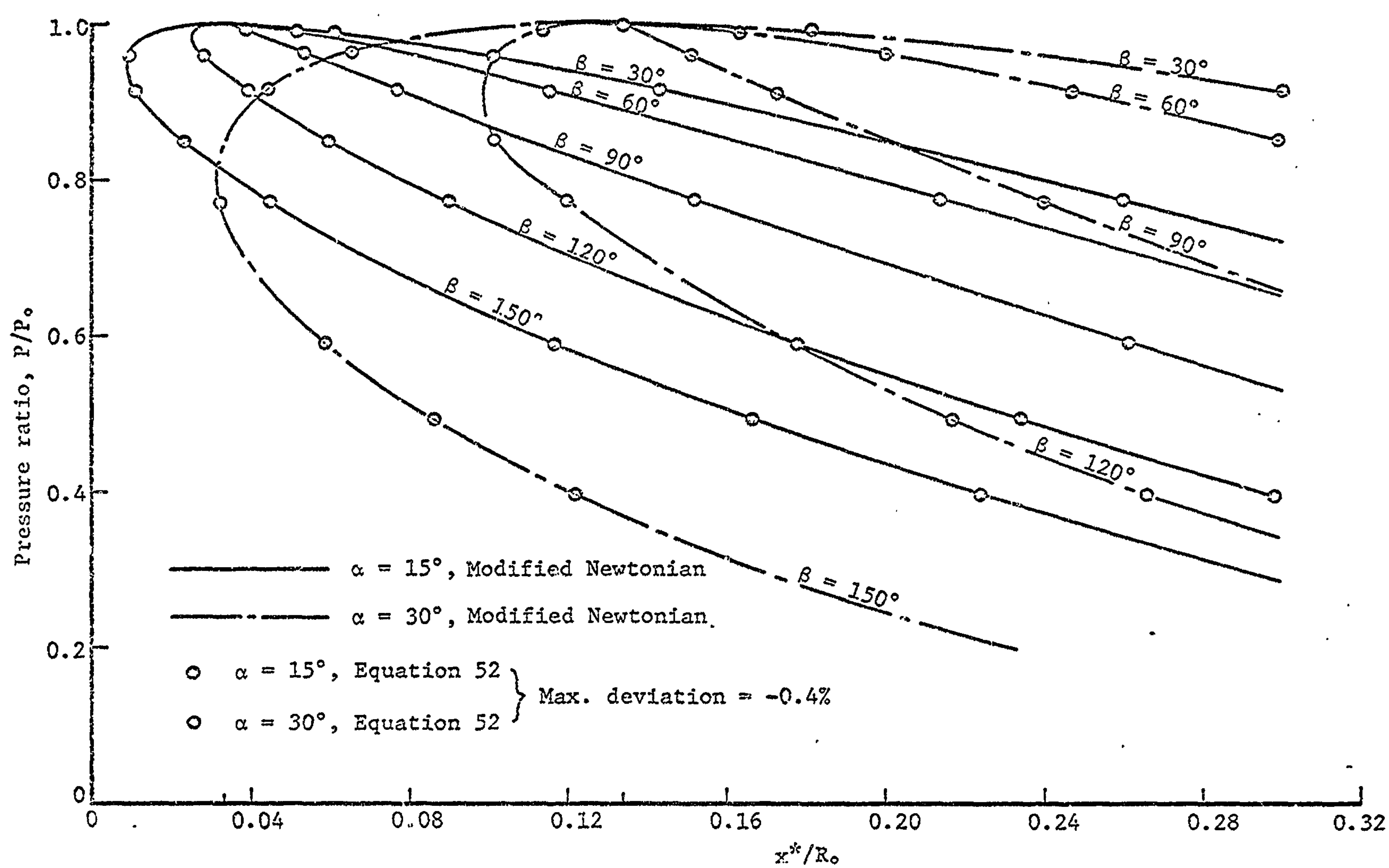

Fig. 8 Pressure distributions over a sphere at α = 15° and 30° and M_{∞} = 8.0

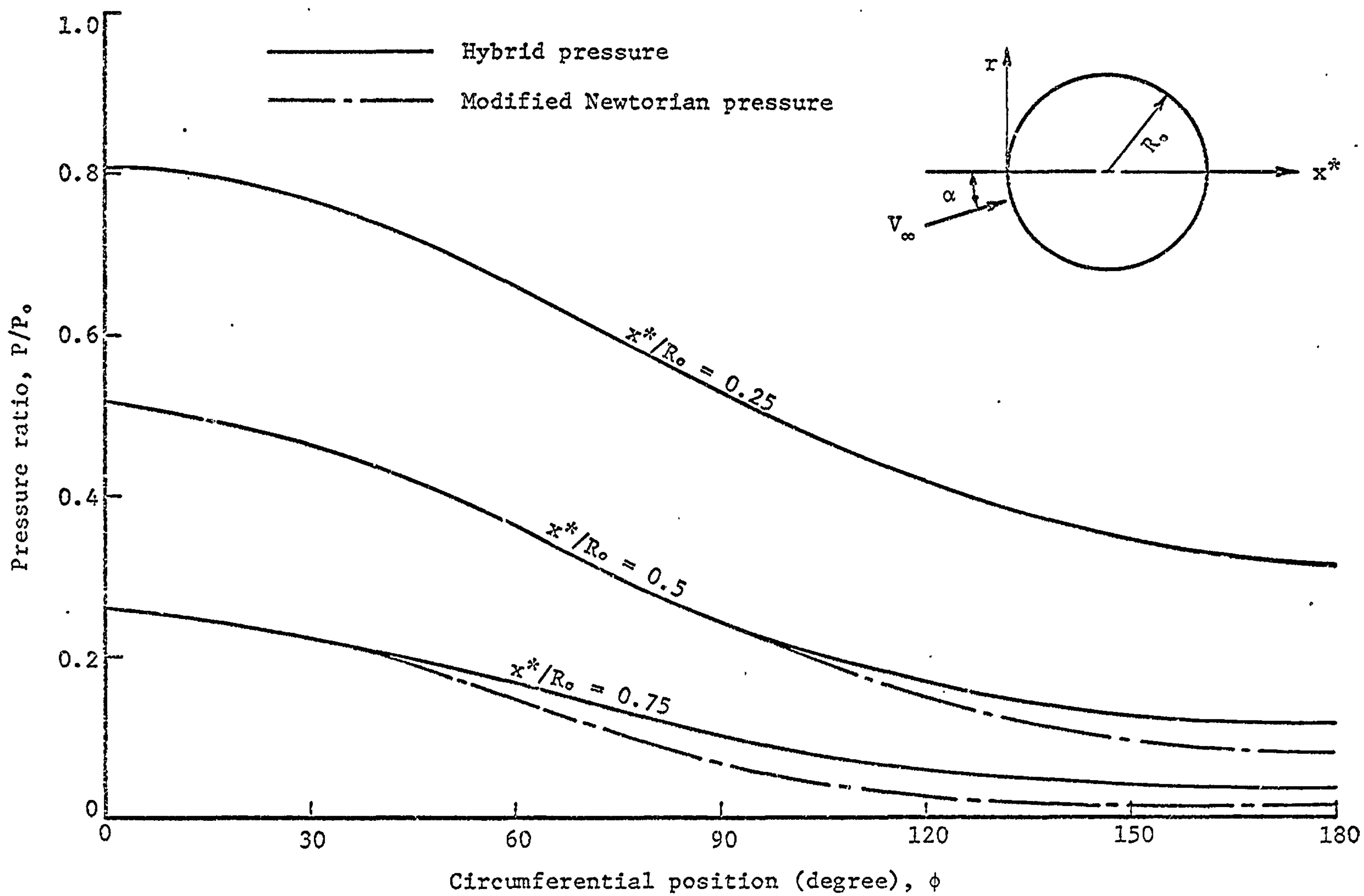

Fig. 9 Circumferential pressure distributions over a sphere at $\alpha = 15°$ and $M_{\infty} = 8.0$

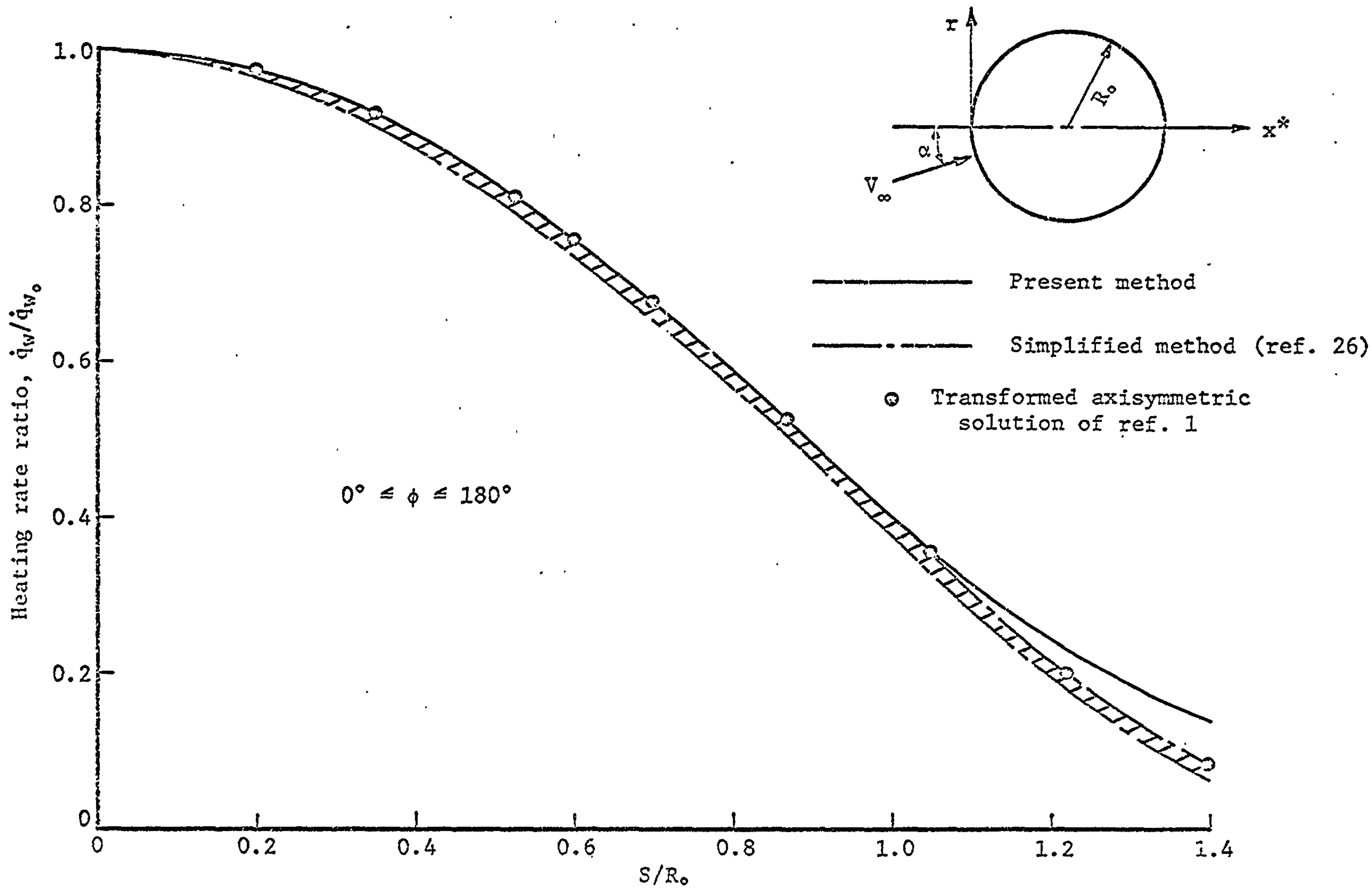

Fig. 10 Longitudinal laminar heat transfer distribution over a sphere at $\alpha = 15°$ and $M_\infty = 8.0$

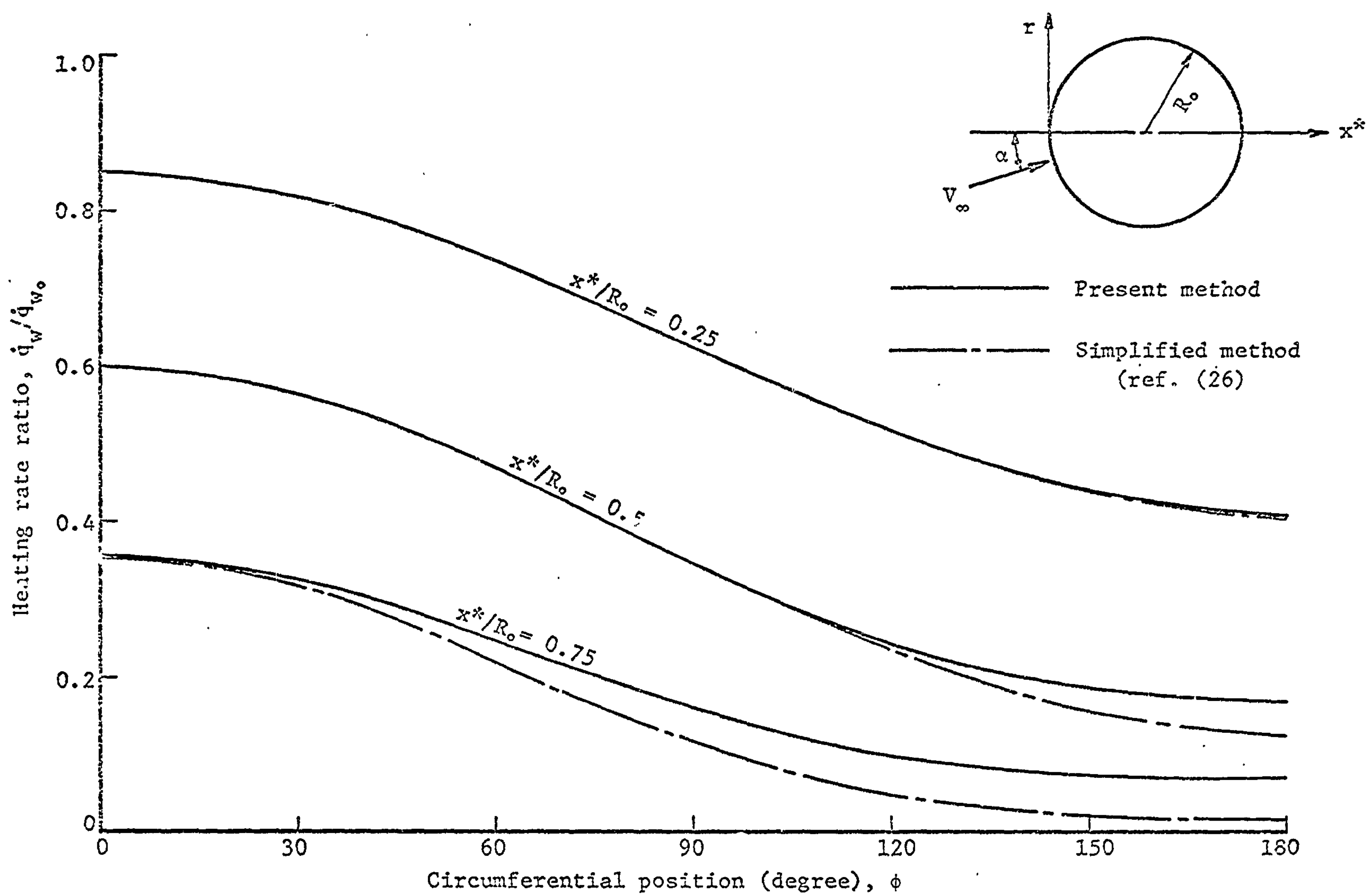

Fig. 11 Circumferential laminar heat transfer distribution over a sphere at $\alpha = 15°$ and $M_\infty = 8.0$

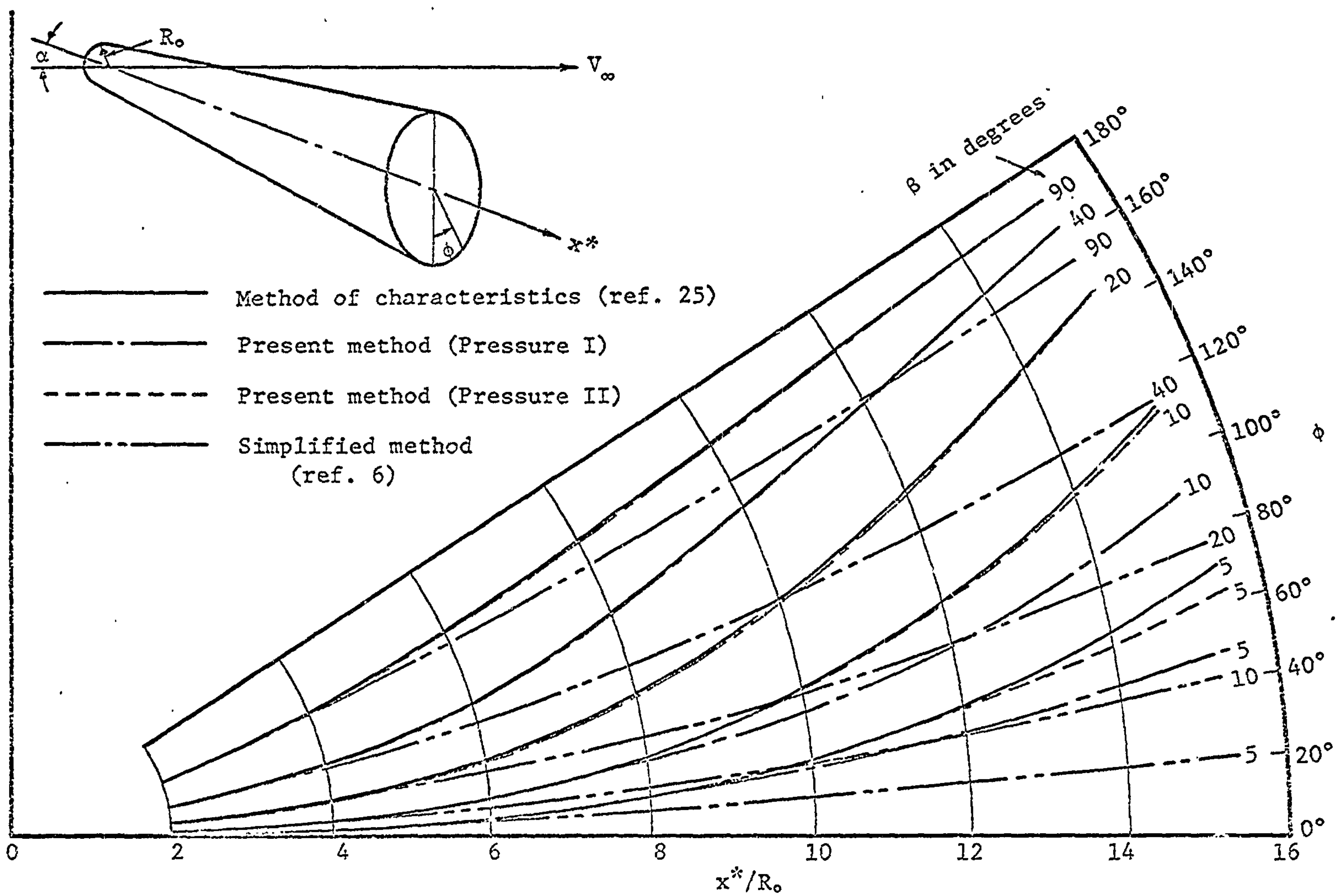

Fig. 12 Streamline patterns for a 9° half-angle sphere-cone at $\alpha = 10°$ and $M_\infty = 18$

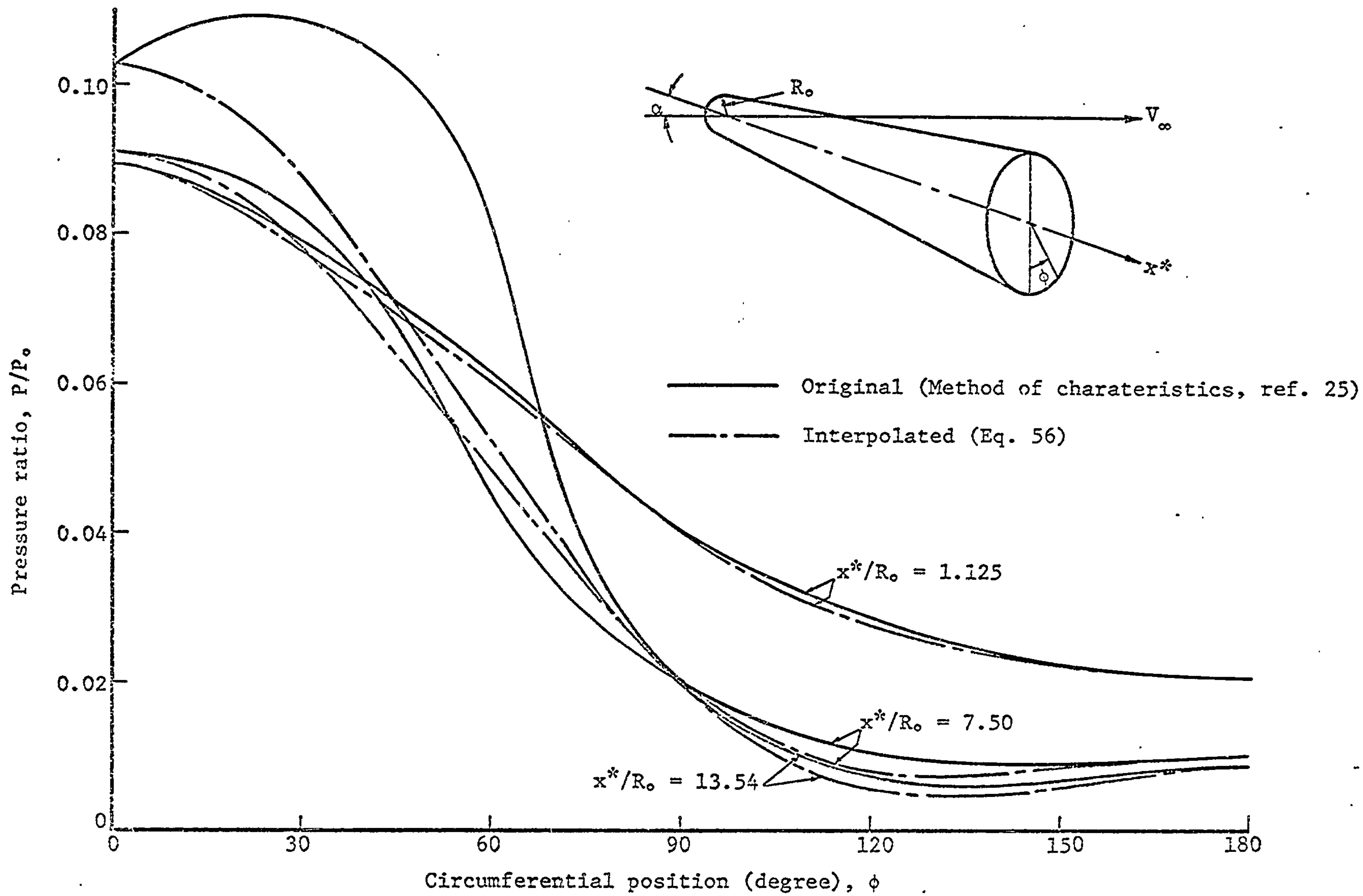

Fig. 13 Circumferential pressure distribution over a 9° half-angle sphere-cone at $\alpha = 10°$ and $M_\infty = 18$

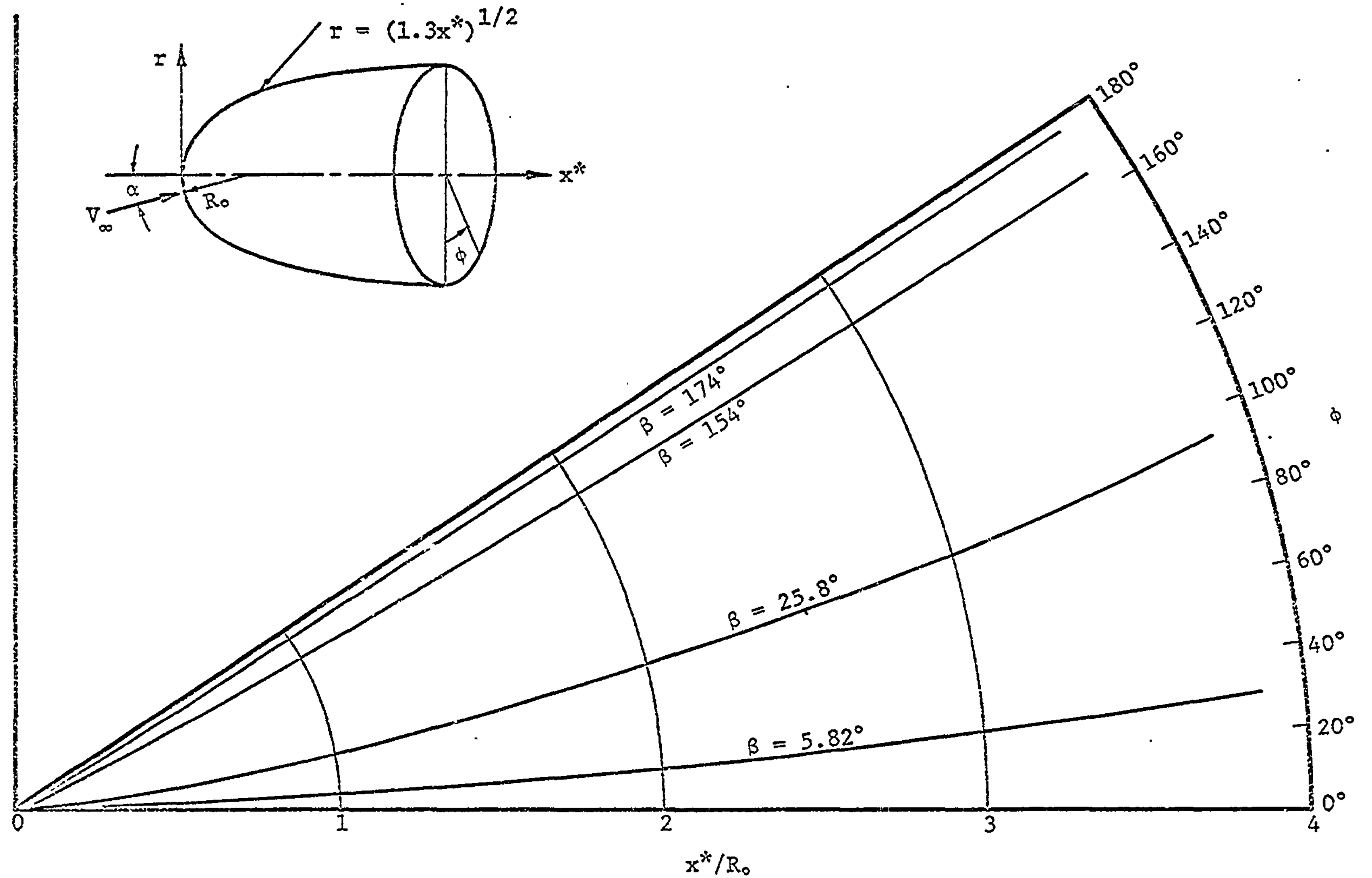

Fig. 14 Streamline patterns for a paraboloid at $\alpha = 15°$ and $M_\infty = 8.0$

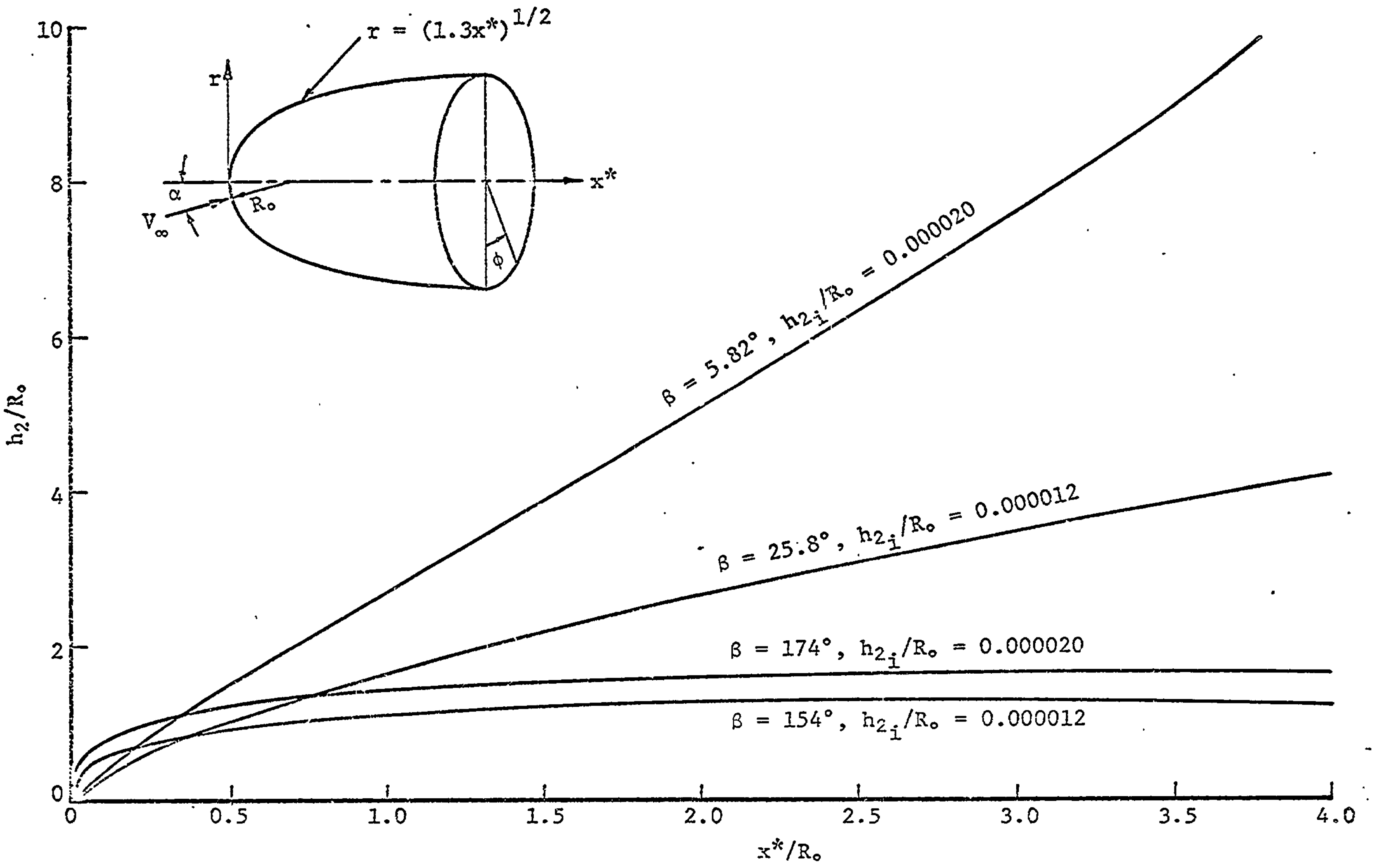

Fig. 15 Scale factors for a paraboloid at $\alpha = 15°$ and $M_\infty = 8.0$

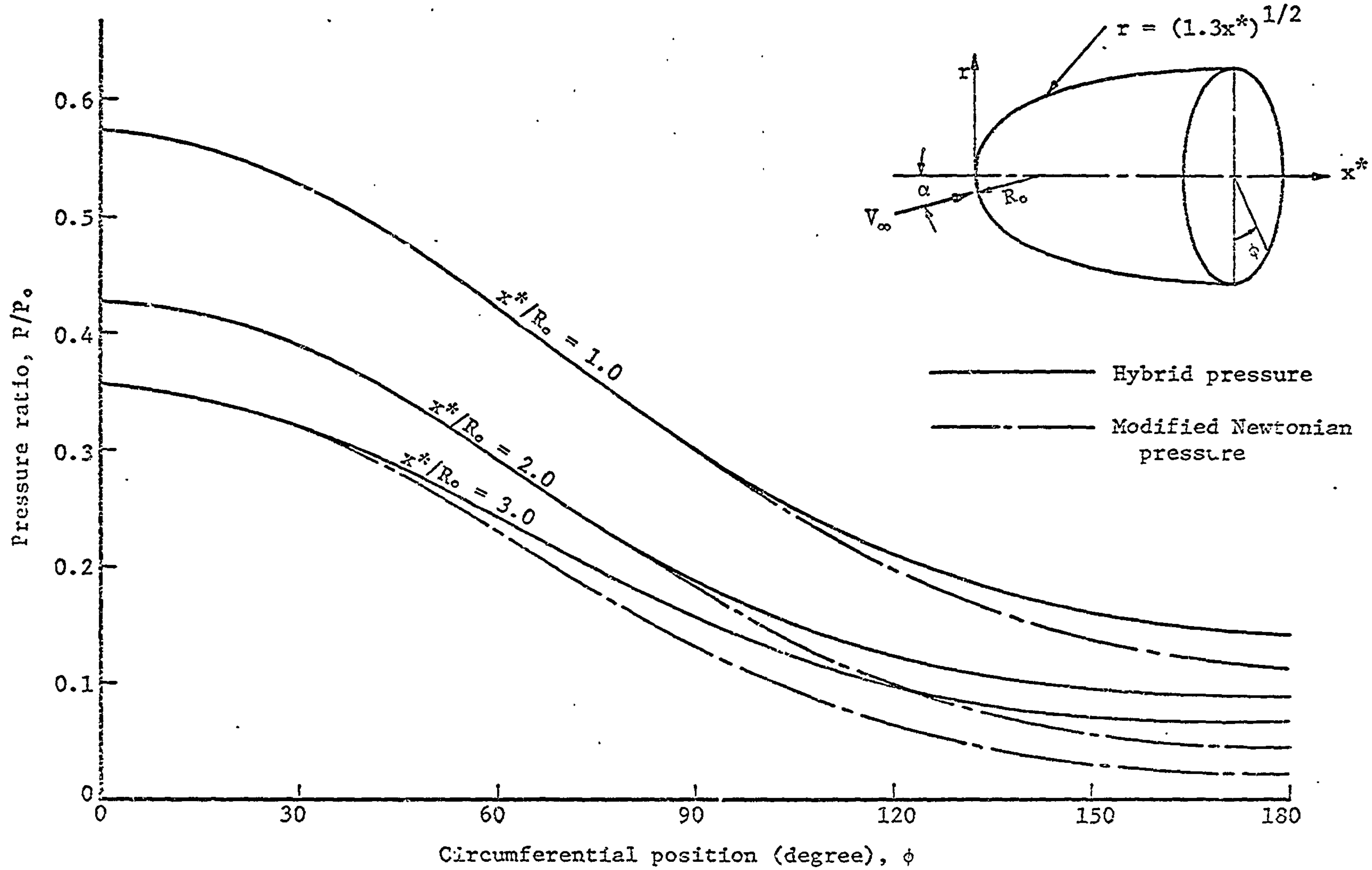

Fig. 16 Circumferential pressure distribution over a paraboloid at $\alpha = 15°$ and $M_\infty = 8.0$

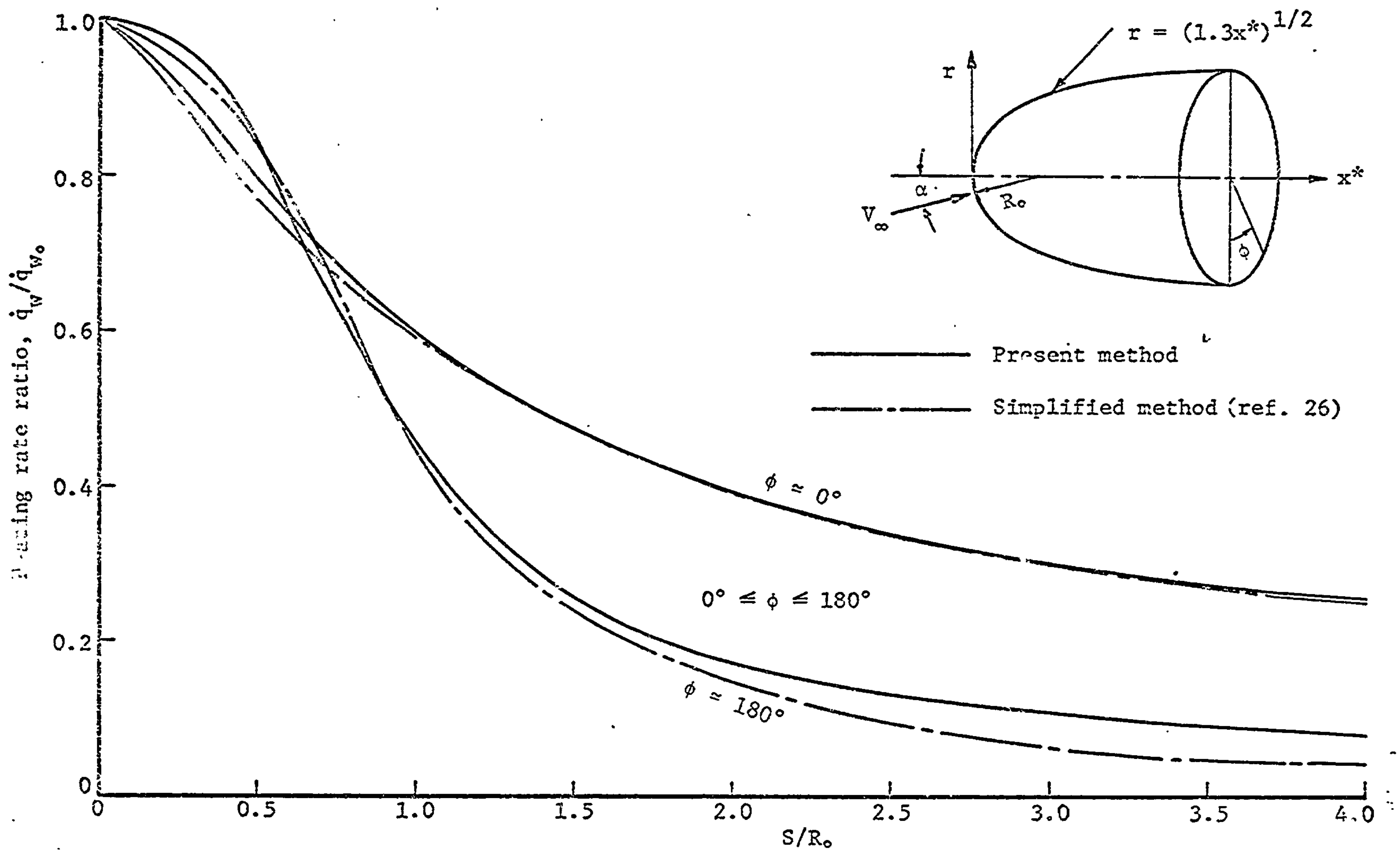

Fig. 17 Longitudinal laminar heat transfer distribution over a paraboloid at α = 15° and M_∞ = 8.0

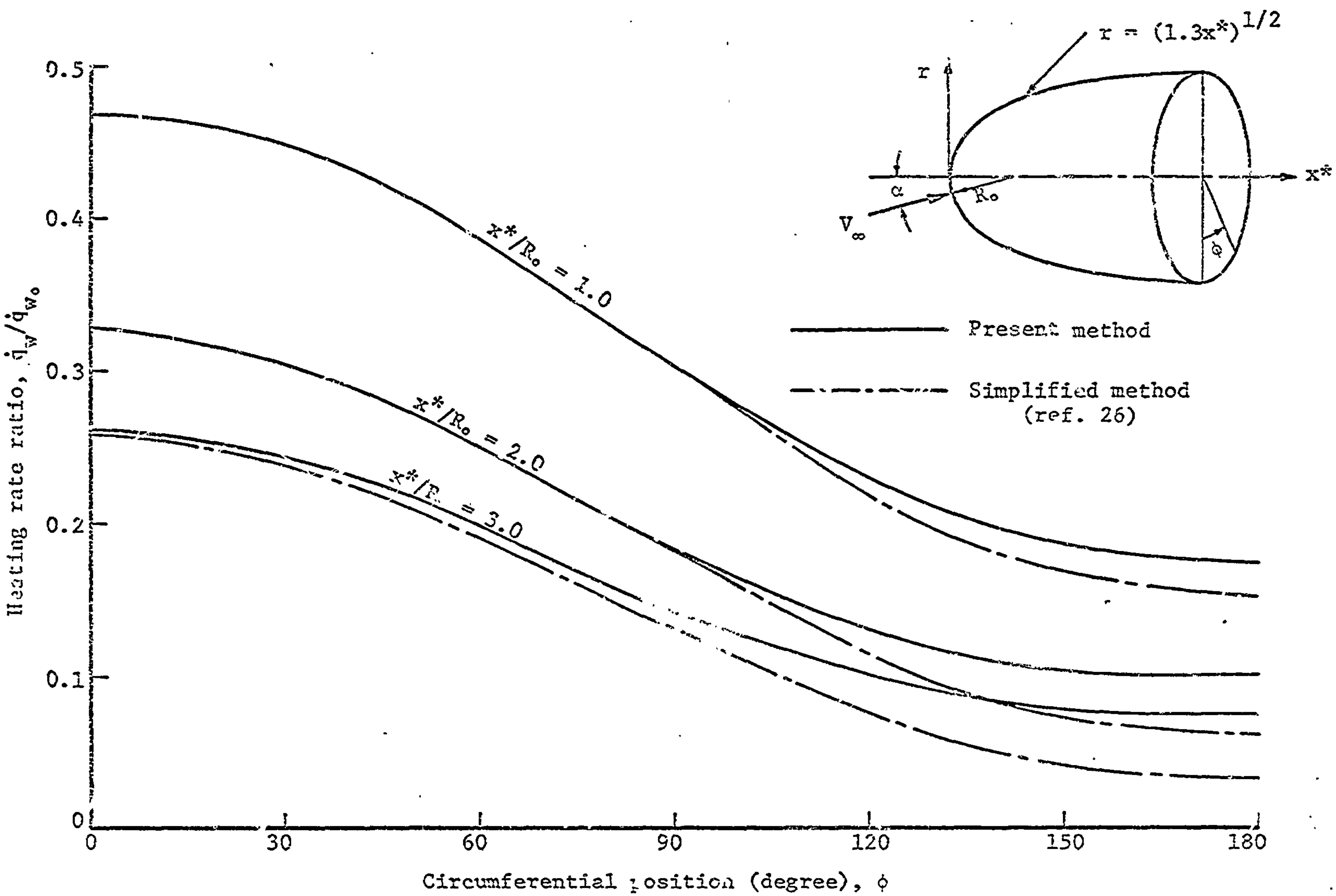

Fig. 18 Circumferential laminar heat transfer distribution over a paraboloid at $\alpha = 15°$ and $M_\infty = 8.0$

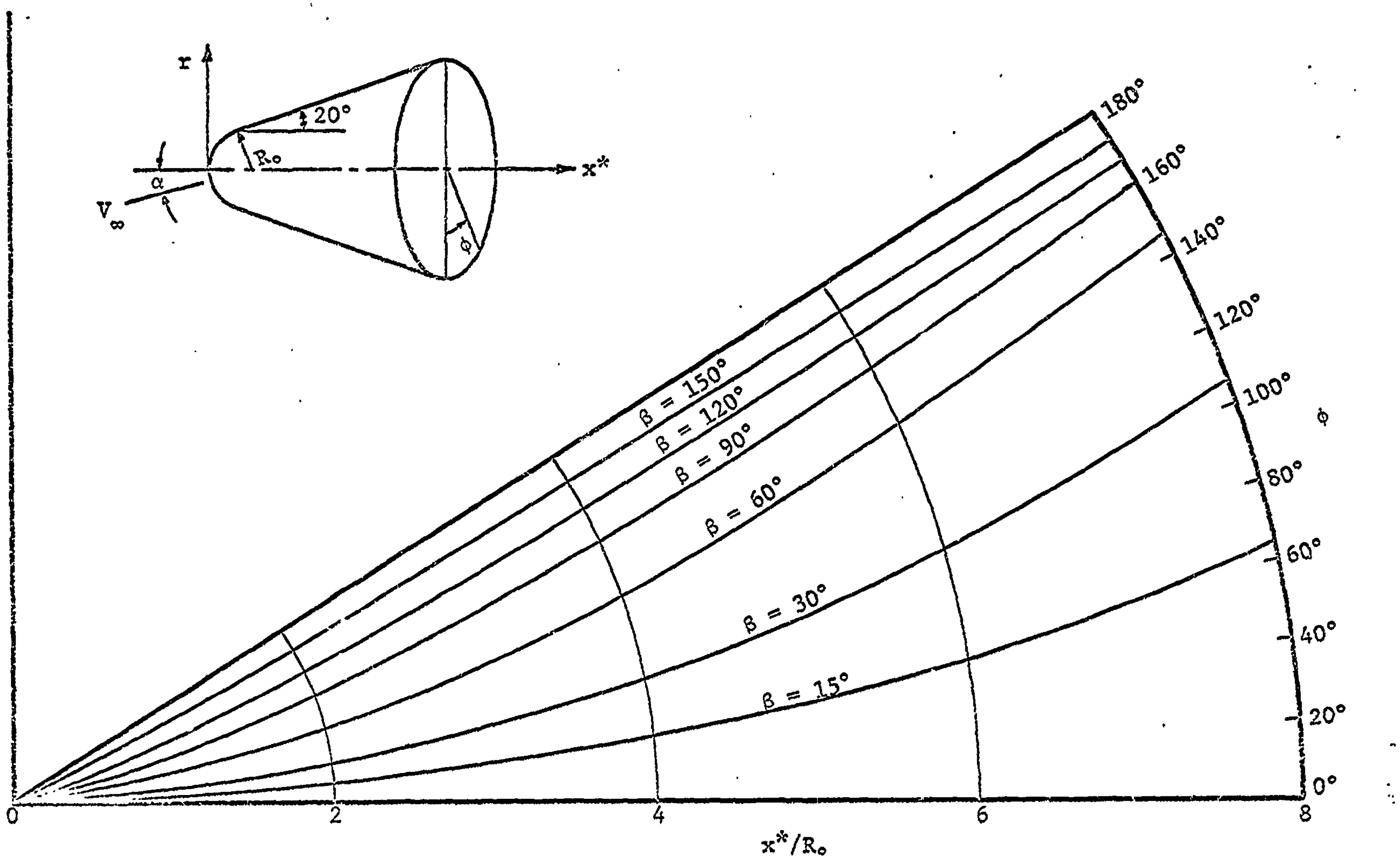

Fig. 19 Streamline patterns for a 20° half-angle sphere-cone at $\alpha = 15°$ and $M_\infty = 6.0$

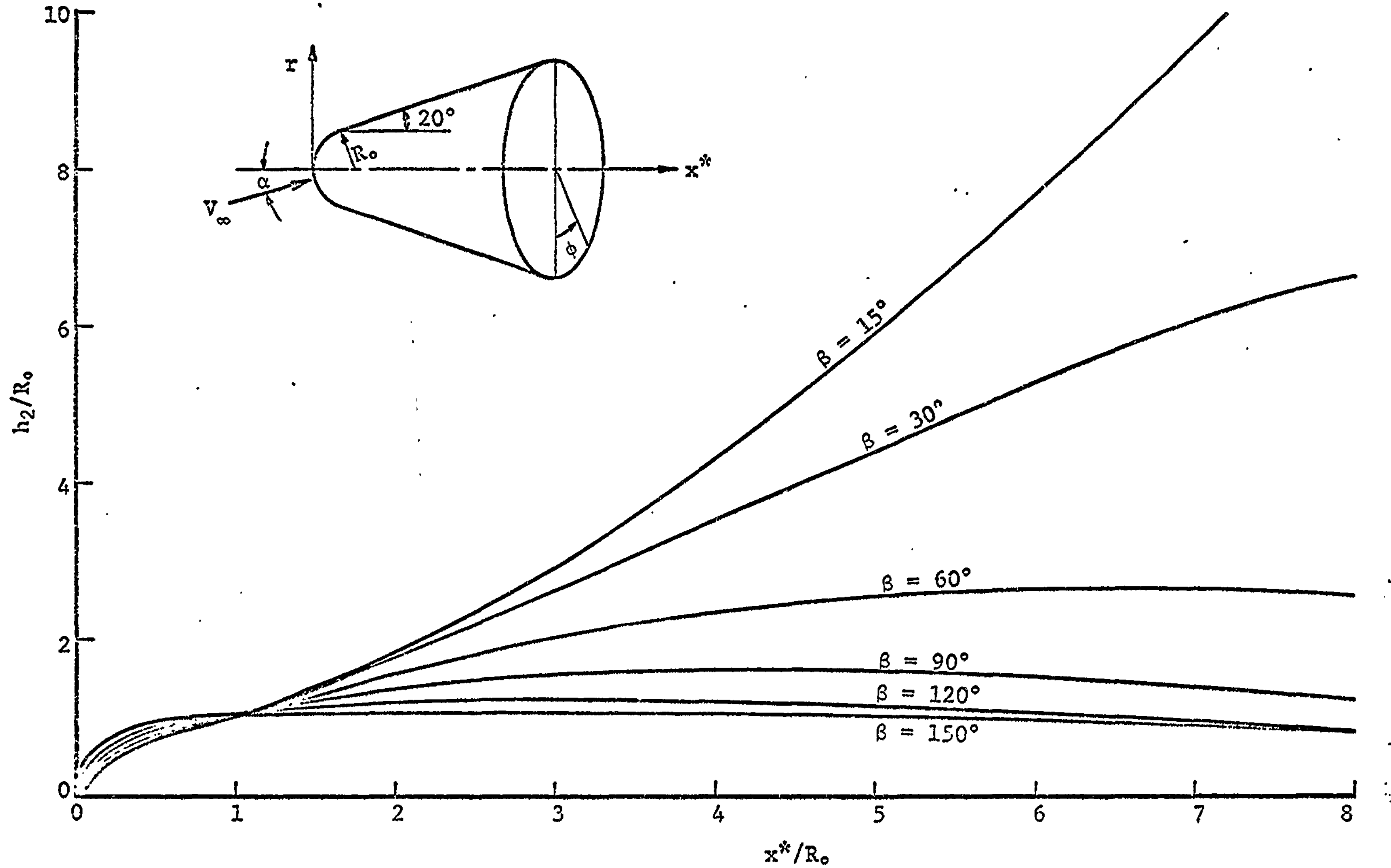

Fig. 20 Scale factors for a 20° half-angle sphere-cone at $\alpha = 15°$ and $M_\infty = 6.0$

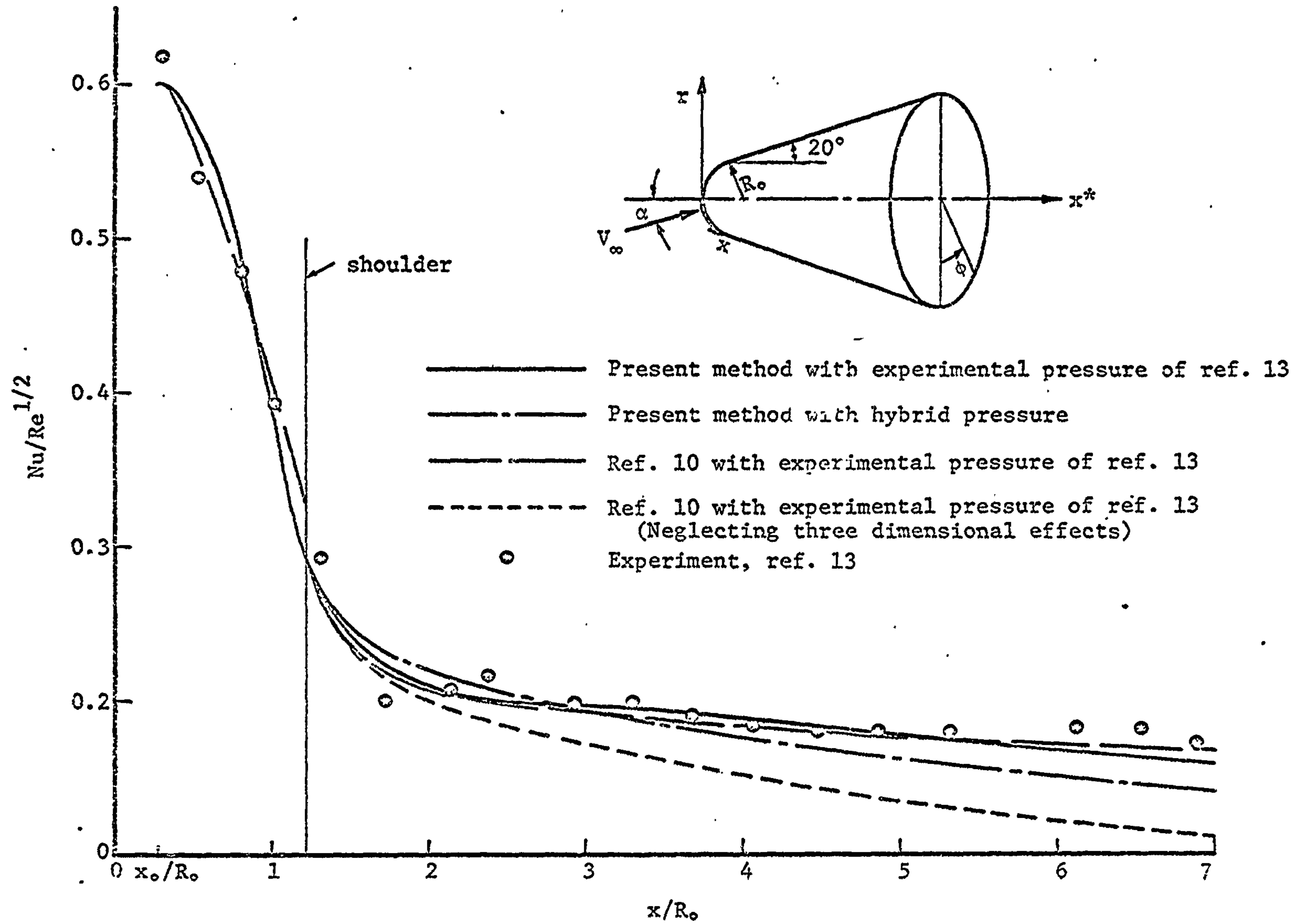

Fig. 21 Laminar heat transfer distribution over a 20° half-angle sphere-cone at $\alpha = 15°$, $M_\infty = 6.0$ and $\phi = 0$

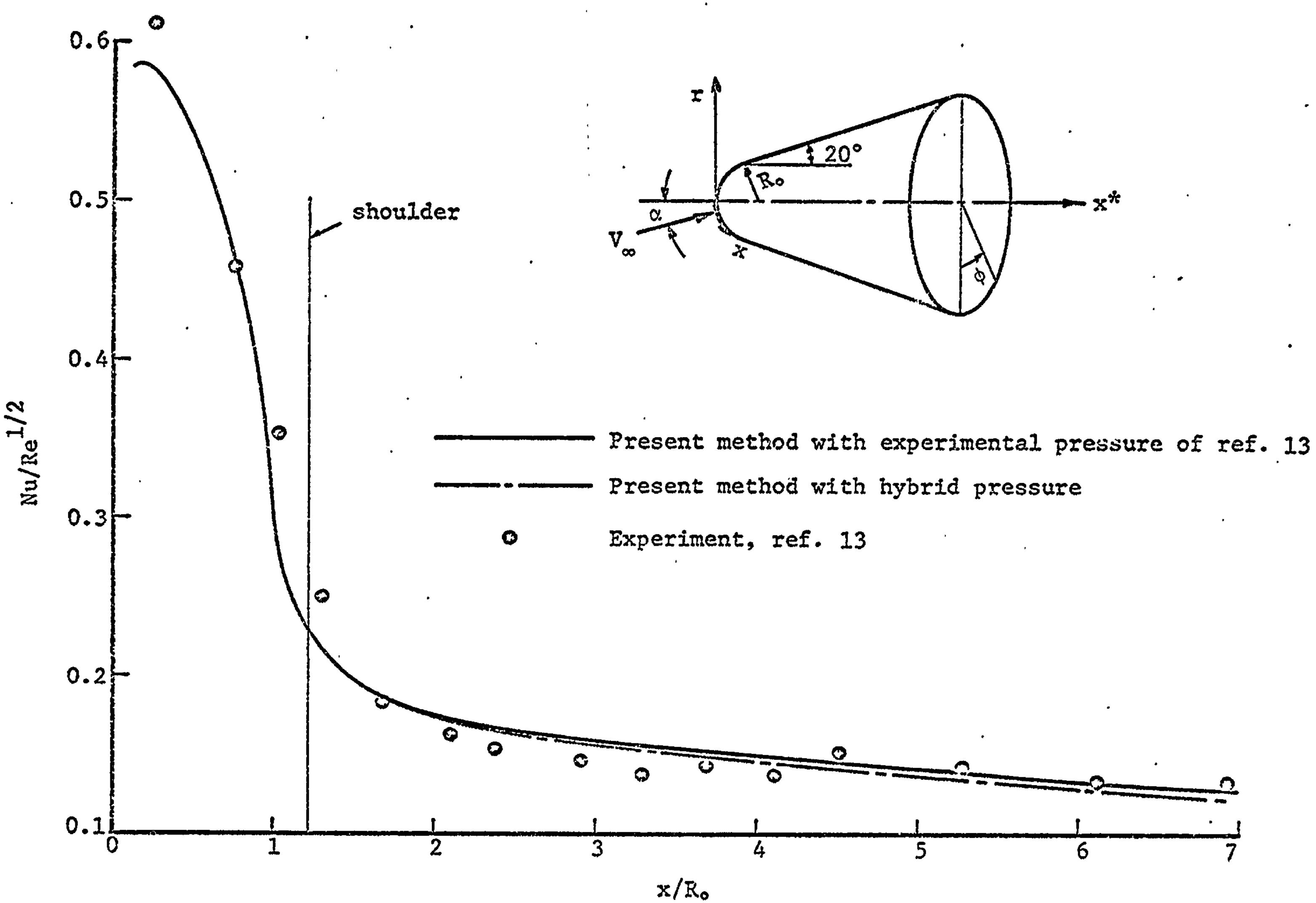

Fig. 22 Laminar heat transfer distribution over a 20° half-angle sphere-cone at $\alpha = 15°$, $M_\infty = 6.0$ and $\phi = 45°$

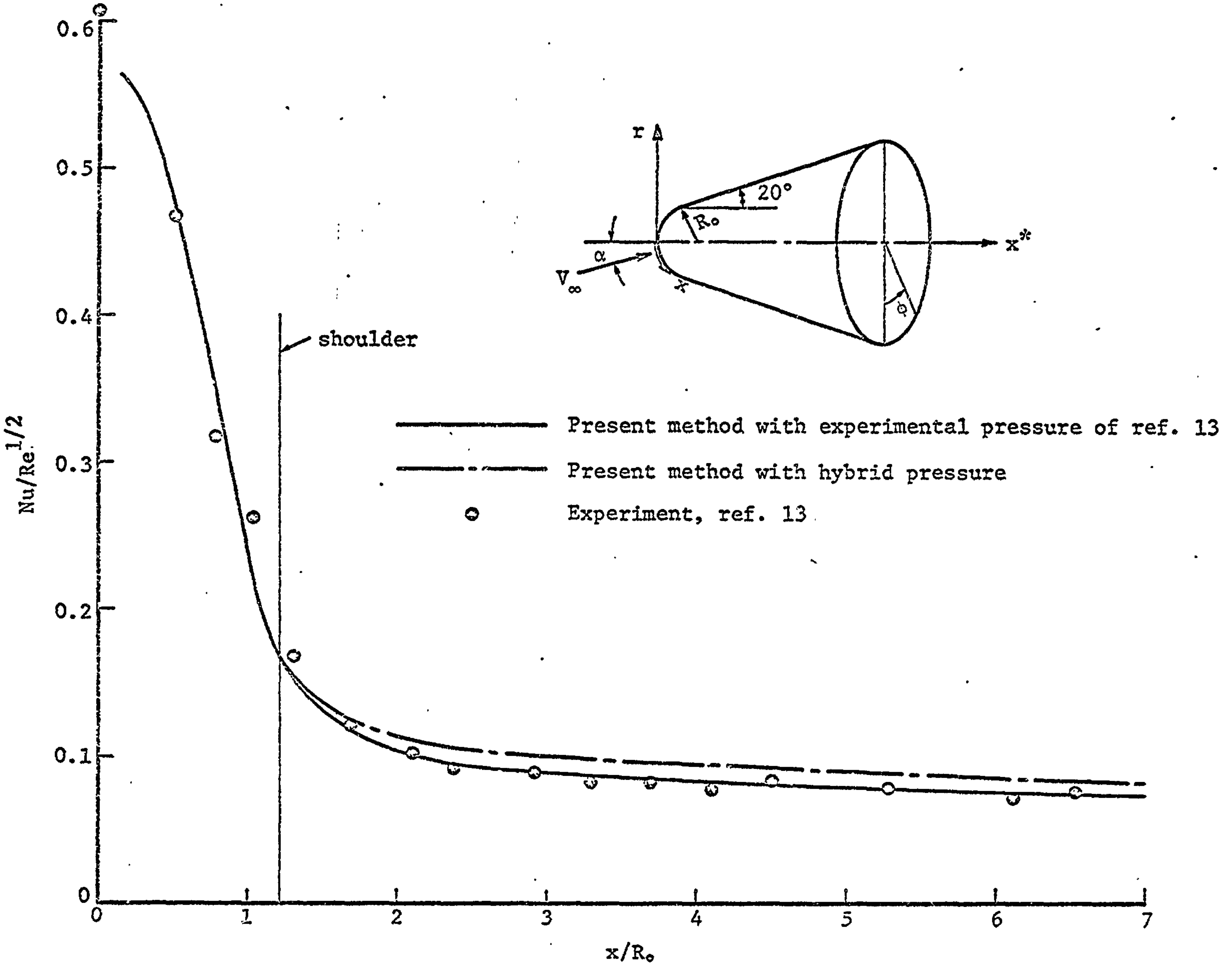

Fig. 23 Laminar heat transfer distribution over a 20° half-angle sphere-cone at $\alpha = 15°$, $M_\infty = 6.0$ and $\phi = 90°$

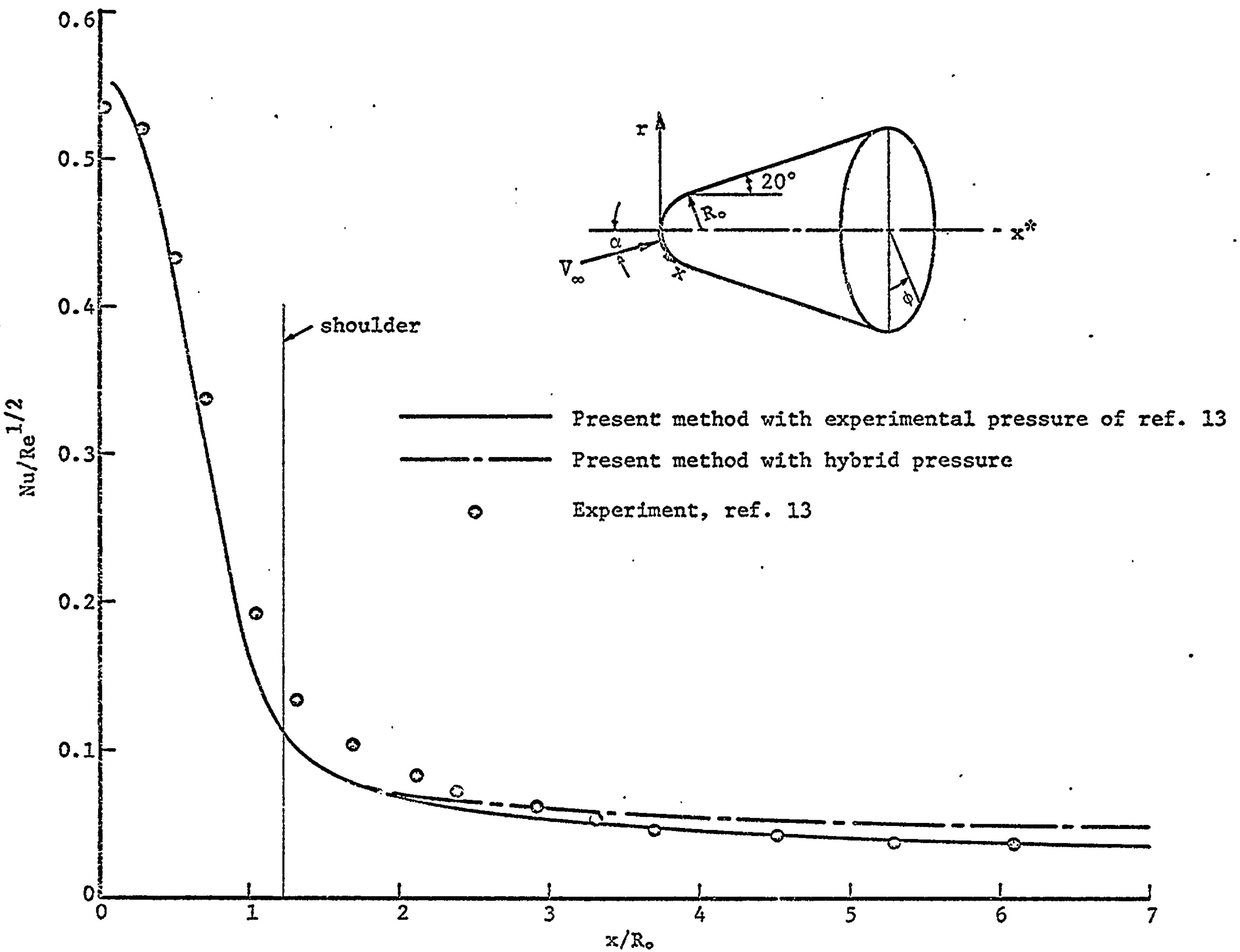

Fig. 24 Laminar heat transfer distribution over a 20° half-angle sphere-cone at $\alpha = 15°$, $M_\infty = 6.0$ and $\phi = 135°$

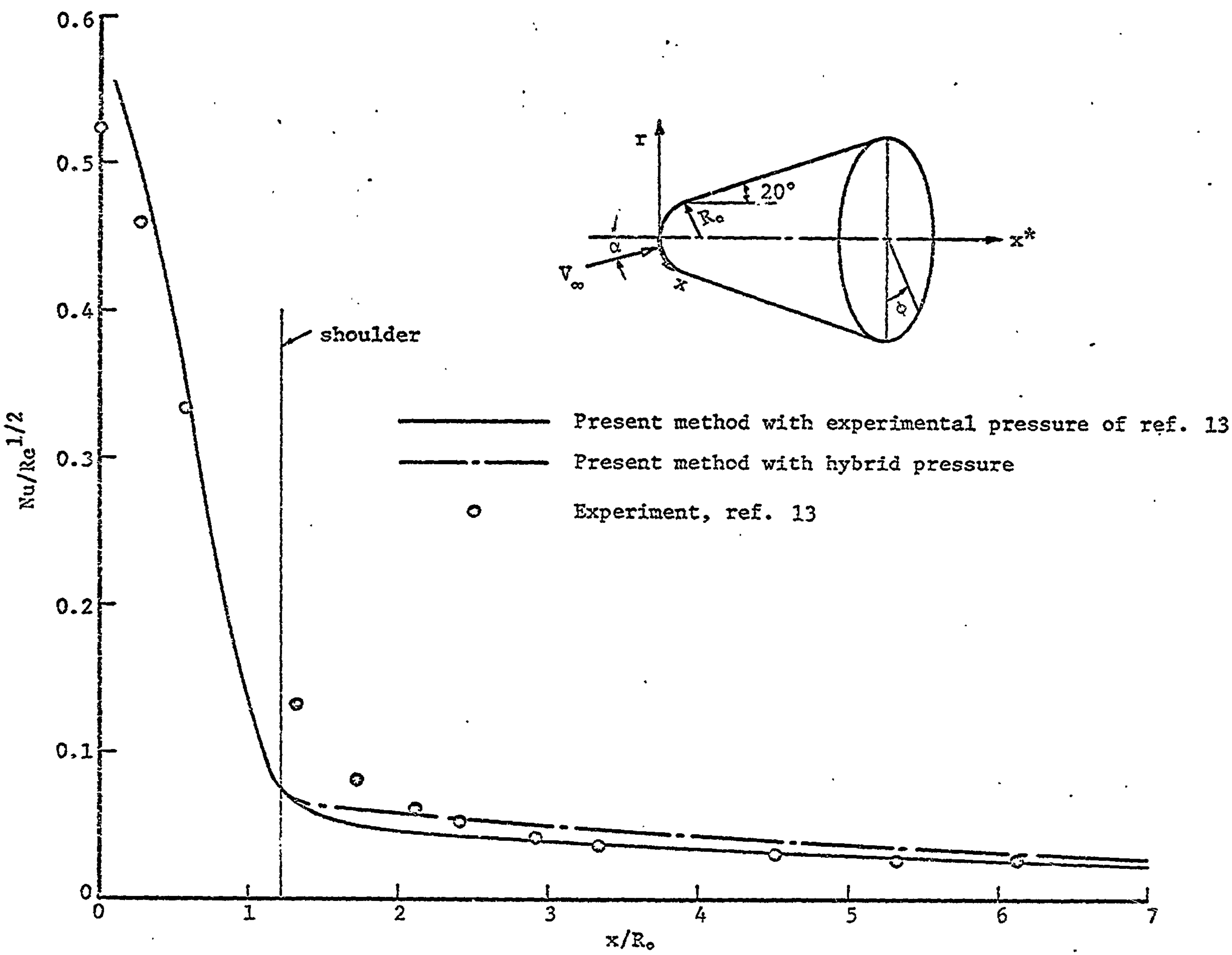

Fig. 25 Laminar heat transfer distribtuion over a 20° half-angle sphere-cone at $\alpha = 15°$, $M_\infty = 6.0$ and $\phi = 180°$

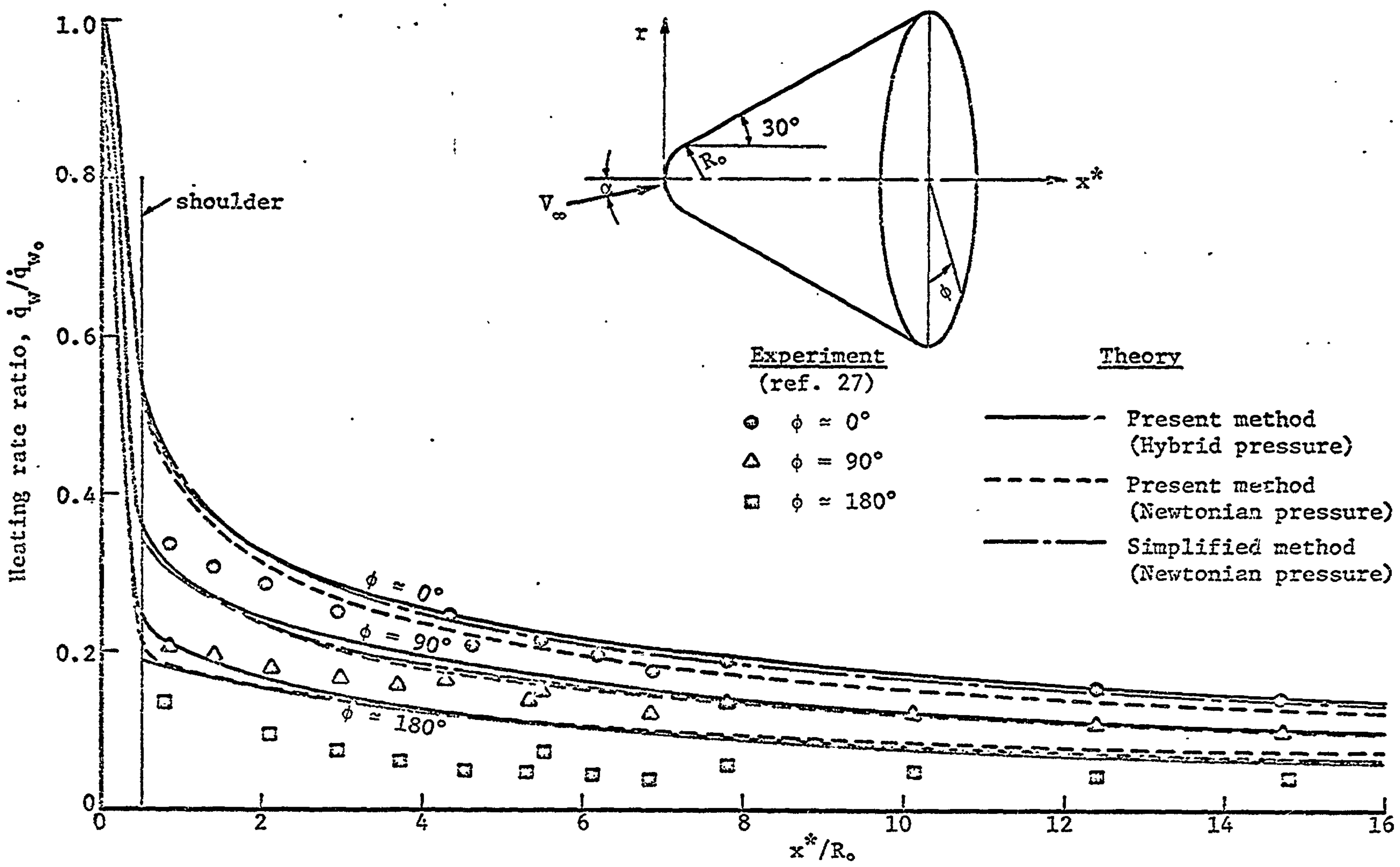

Fig. 26 Laminar heat transfer distribution over a 30° half-angle sphere-cone at $\alpha = 10°$ and $M_\infty = 10.6$

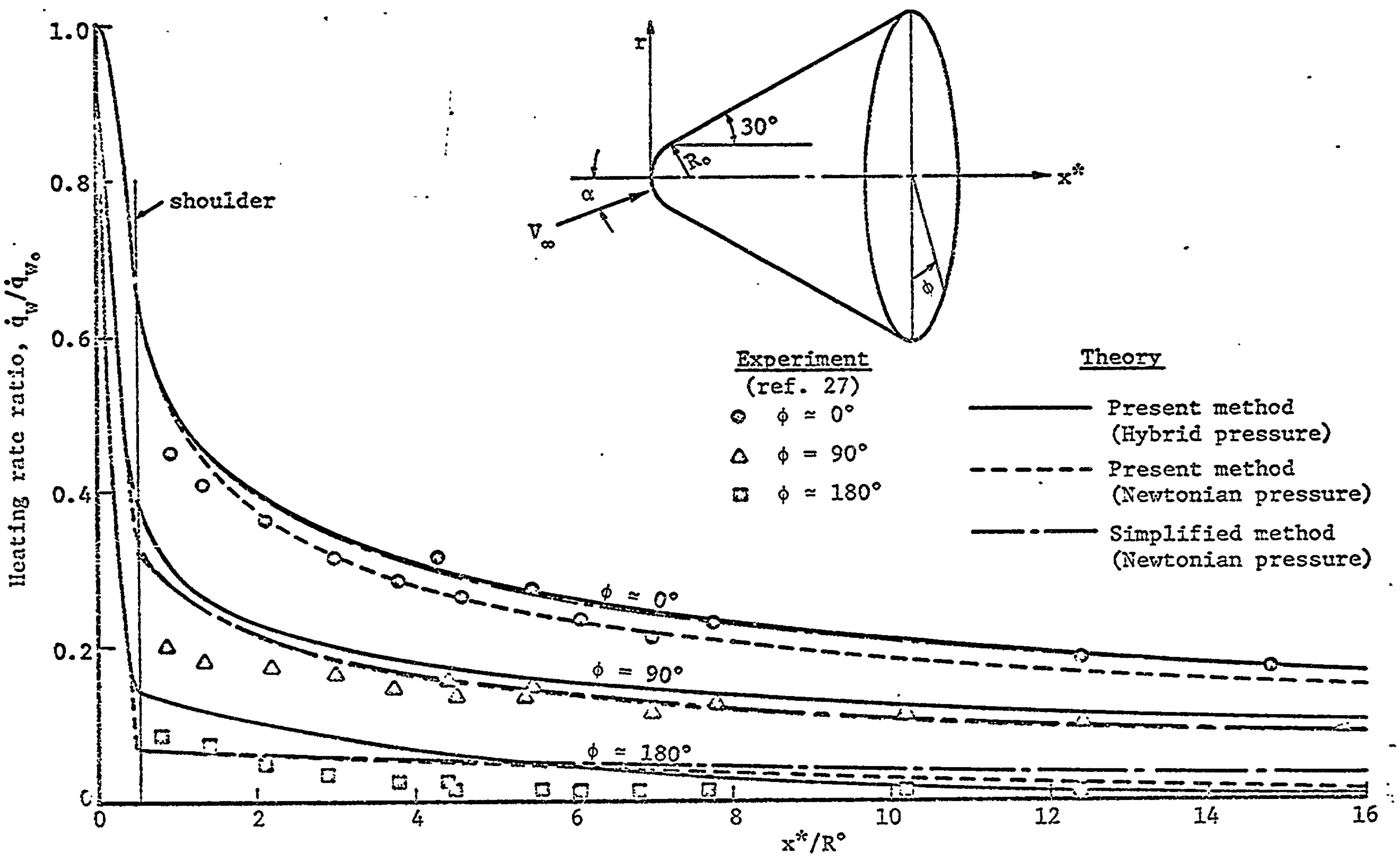

Fig. 27 · Laminar heat transfer distribution over a 30° half-angle sphere-cone at $\alpha = 20°$ and $M_\infty = 10.6$

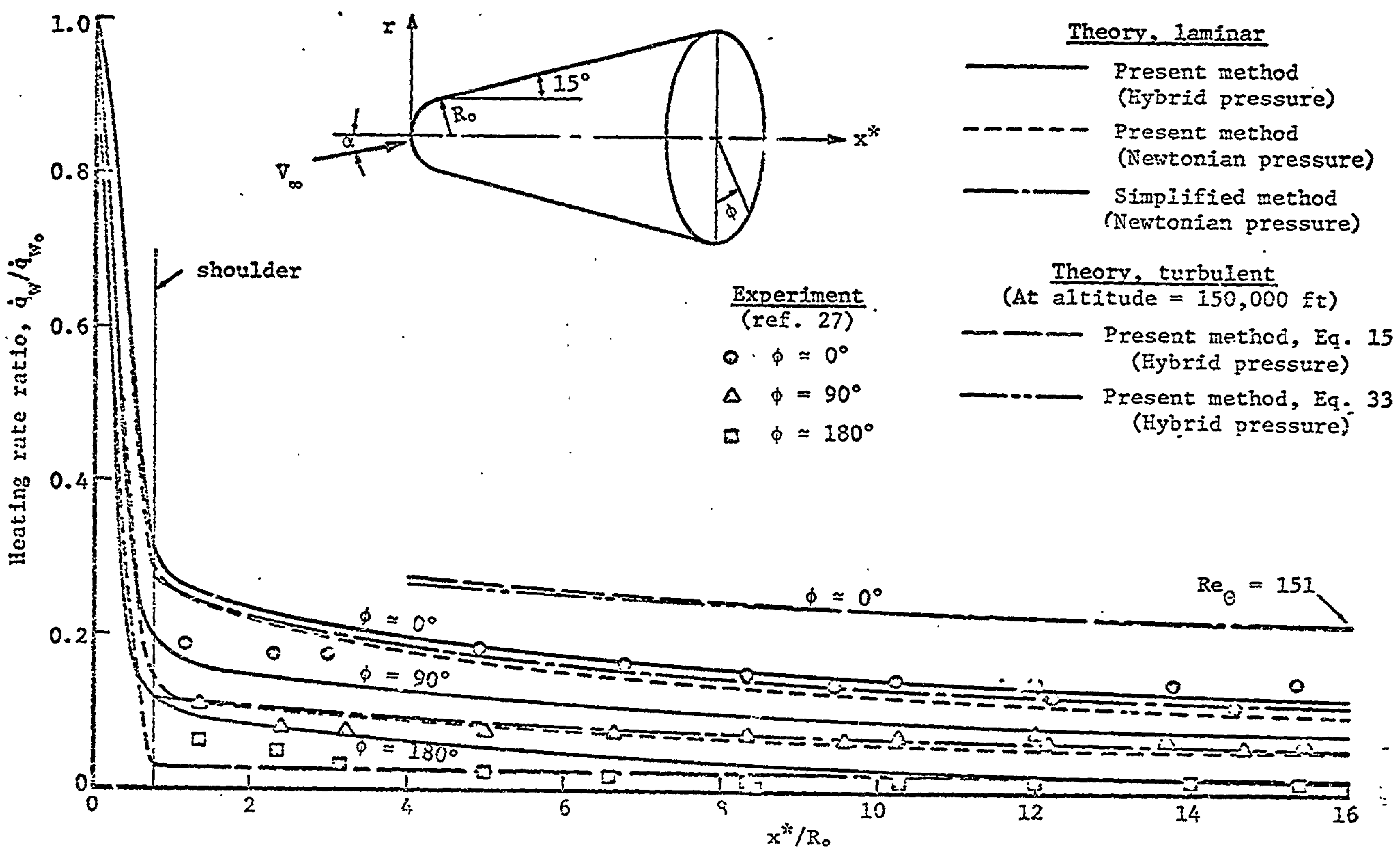

Fig. 28 Laminar and turbulent heat transfer distribution over a 15° half-angle sphere-cone at $\alpha = 10°$ and $M_\infty = 10.6$

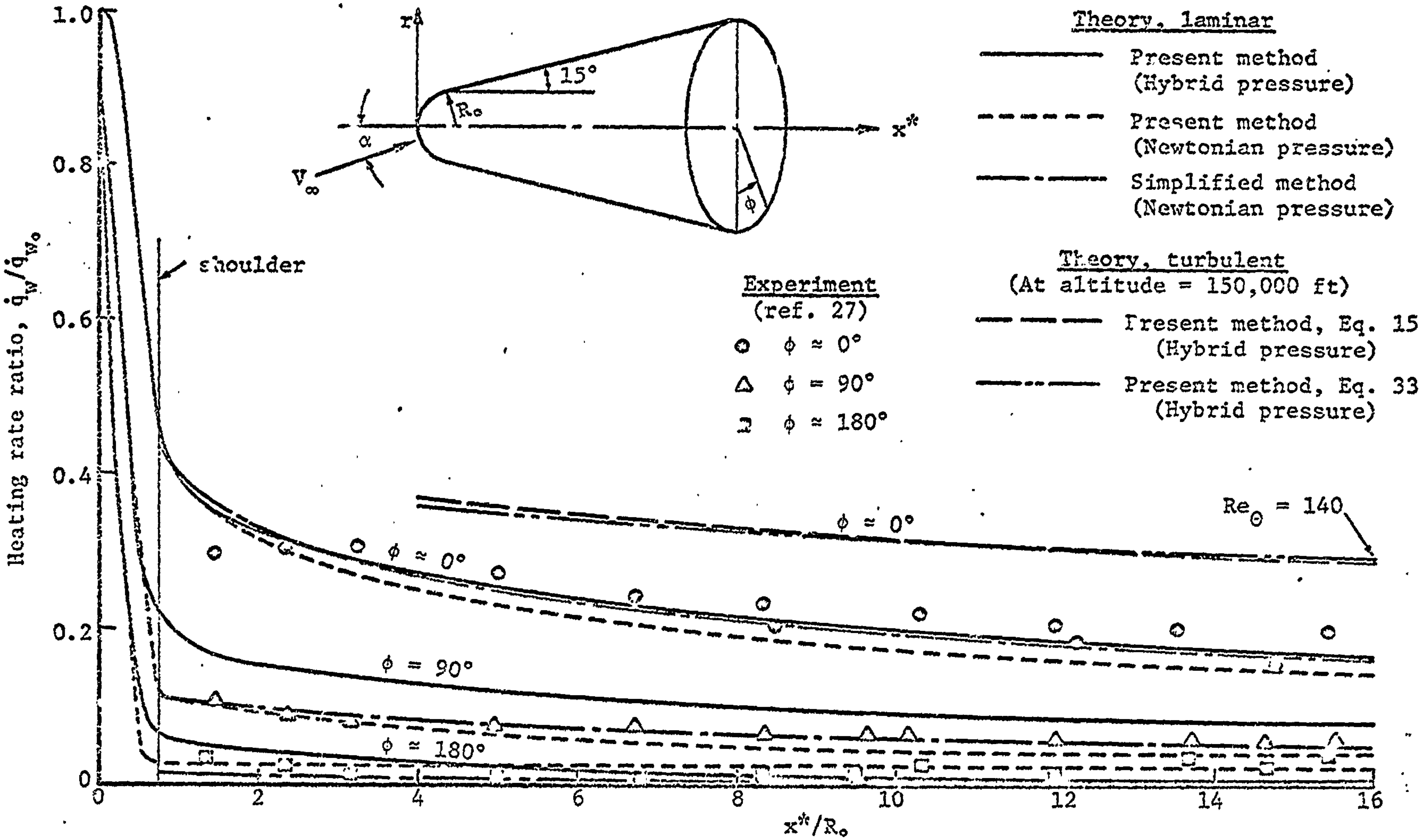

Fig. 29 Laminar and turbulent heat transfer distribution over a 15° half-angle sphere-cone at α = 20° and M_∞ = 10.6

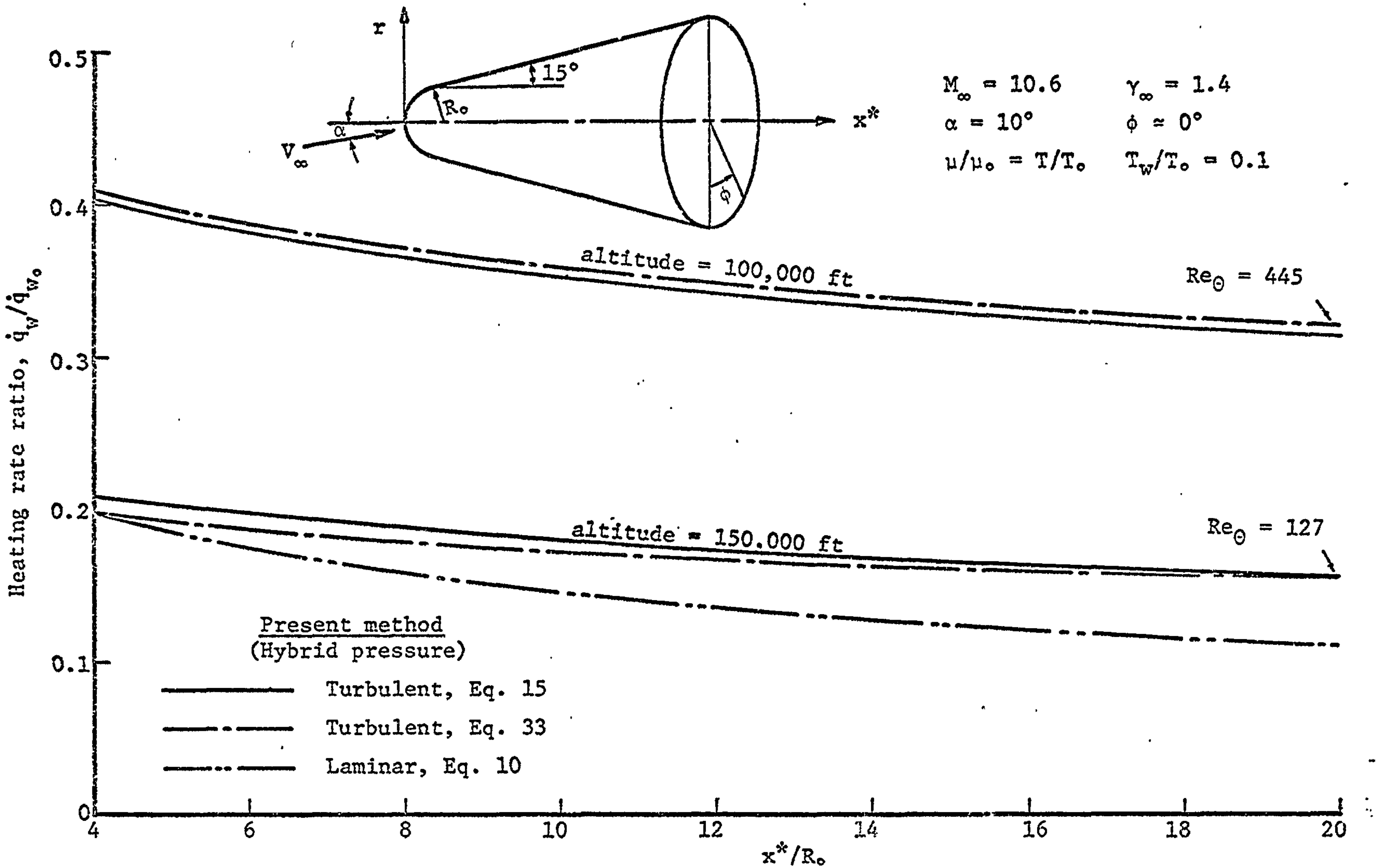

Fig. 30 Effect of altitude on normalized turbulent heat transfer distribution

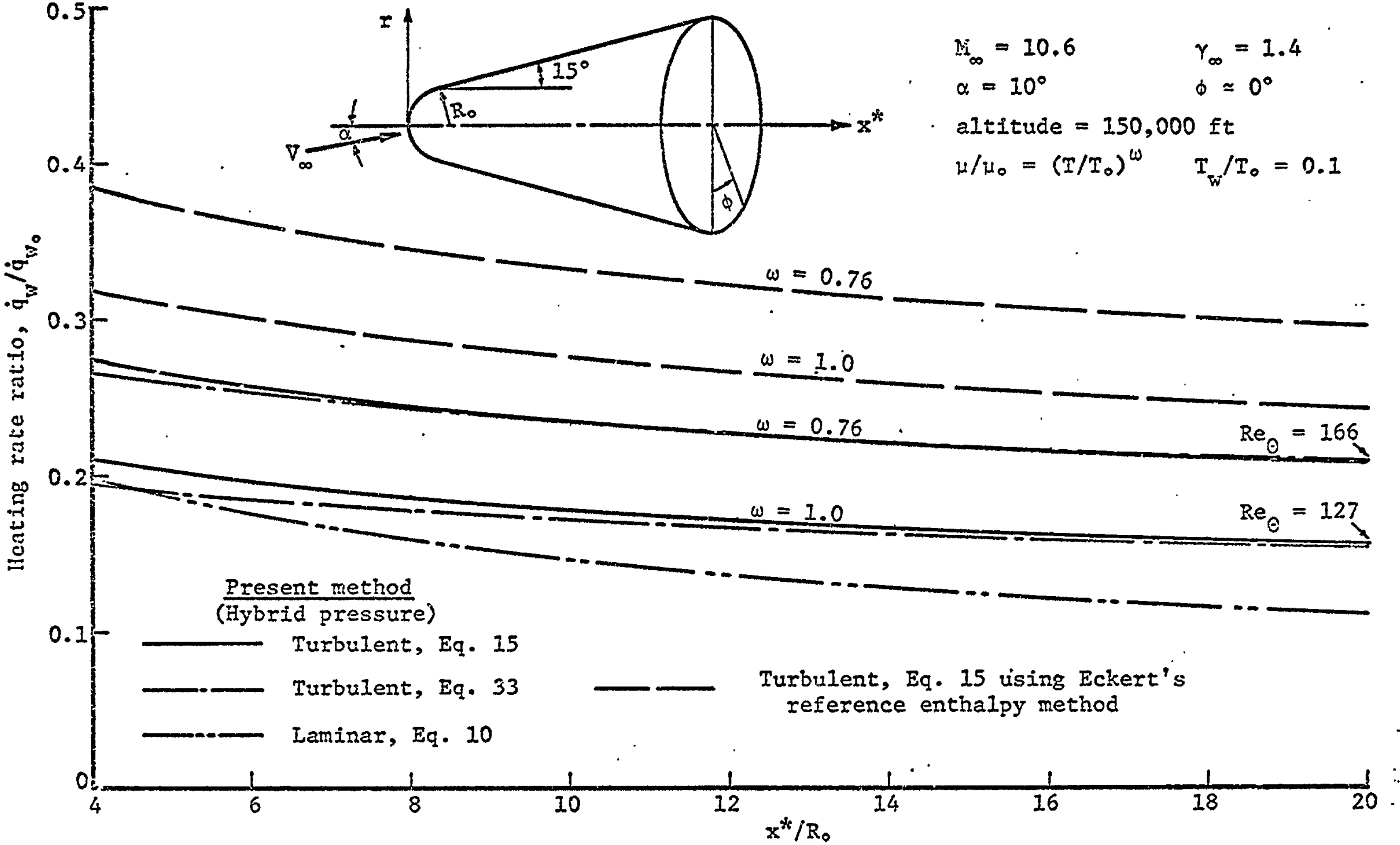

Fig. 31 Effect of viscosity-temperature relation and reference condition on normalized turbulent heat transfer distribution

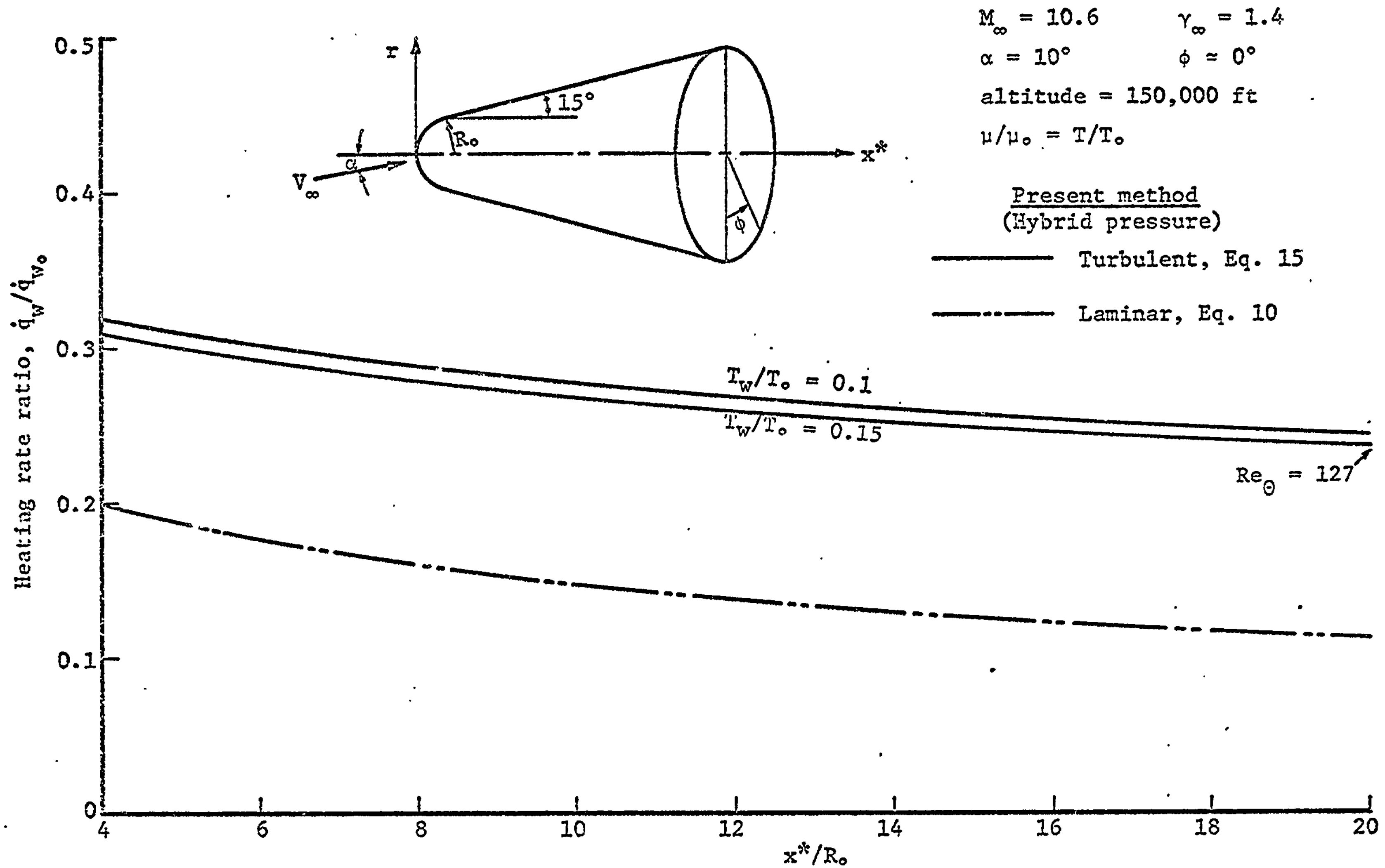

Fig. 32 Effect of wall temperature on normalized turbulent heat transfer distribution

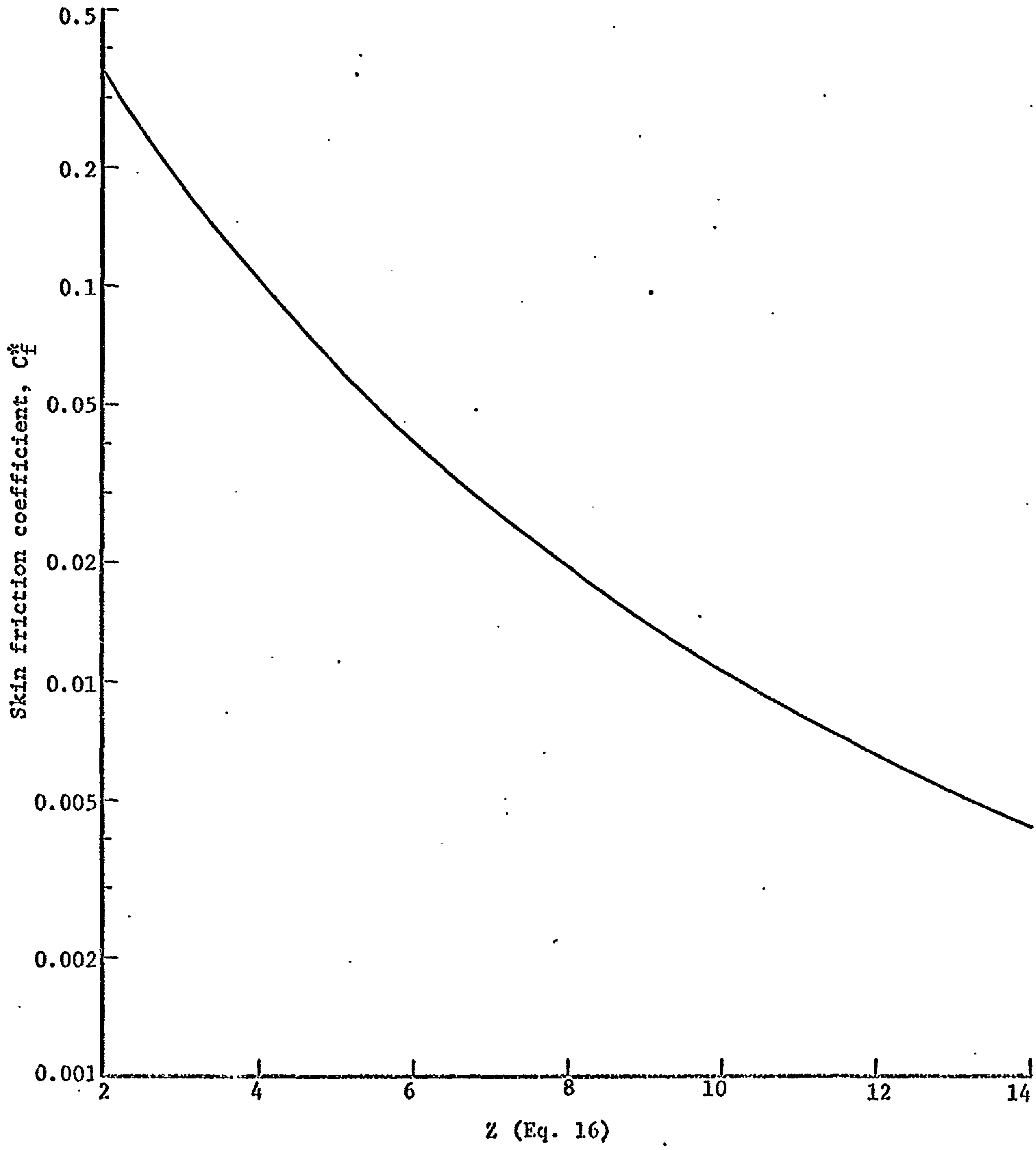

Fig. 33 Variation of skin friction coefficient versus integral Z

Table I Accuracy of initial conditions for a sphere

α	β	A_∞	$\varepsilon \times 10^6$	x_i^*/R_o			ϕ_i			$(h_{2_i}/R_o) \times 10^5$		
				Present method	Geometric solution	Error %	Present method	Geometric solution	Error %	Present method	Geometric solution	Error %
10°	149°	20	2	0.015194	0.015194	0	0.002292	0.002302	-0.52	1.34369	1.34495	-0.09
20°	113°	20	2	0.060309	0.060309	0	0.002292	0.002293	-0.04	1.48637	1.48783	-0.10
30°	101°	20	2	0.133977	0.133977	0	0.002292	0.002292	0	2.03760	2.03962	-0.10
after integration for 20 step sizes			S/R_o	x^*/R_o			ϕ			$(h_{2_i}/R_o) \times 10^2$		
α	β	A_∞		Present method	Geometric solution	Error %	Present method	Geometric solution	Error %	Present method	Geometric solution	Error %
10°	149°	20	0.01101	0.016888	0.016888	0	1.783090	1.784368	-0.07	1.10034	1.10132	-0.09
20°	113°	20	0.01015	0.061844	0.061844	0	1.676743	1.676631	0.01	1.10033	1.10147	-0.10
30°	101°	20	0.01020	0.135107	0.135107	0	1.233647	1.233616	0.003	1.10091	1.10202	-0.10

$M_\infty = 8.0 \qquad \gamma_\infty = 1.4 \qquad \phi = A_\infty|\varepsilon|^{a_o} \qquad a_o = -\dfrac{f_o''}{1 + f_o'^2}$

XI. ACKNOWLEDGEMENTS

The authors wish to thank the Research Division of Virginia Polytechnic Institute and the National Aeronautics and Space Administration for providing funds for this study.